



Search for heavy diboson resonances in semileptonic final states in pp collisions at $\sqrt{s} = 13$ TeV with the ATLAS detector

ATLAS Collaboration*

CERN, 1211 Geneva 23, Switzerland

Received: 30 April 2020 / Accepted: 13 October 2020 / Published online: 17 December 2020
© CERN for the benefit of the ATLAS collaboration 2020

Abstract This paper reports on a search for heavy resonances decaying into WW , ZZ or WZ using proton–proton collision data at a centre-of-mass energy of $\sqrt{s} = 13$ TeV. The data, corresponding to an integrated luminosity of 139 fb^{-1} , were recorded with the ATLAS detector from 2015 to 2018 at the Large Hadron Collider. The search is performed for final states in which one W or Z boson decays leptonically, and the other W boson or Z boson decays hadronically. The data are found to be described well by expected backgrounds. Upper bounds on the production cross sections of heavy scalar, vector or tensor resonances are derived in the mass range 300–5000 GeV within the context of Standard Model extensions with warped extra dimensions or including a heavy vector triplet. Production through gluon–gluon fusion, Drell–Yan or vector-boson fusion are considered, depending on the assumed model.

Contents

1	Introduction	1
2	Detector and data sample	2
3	Simulation of signal and background processes	3
3.1	Signal models and simulation	3
3.2	Background process simulation	4
4	Object reconstruction and identification	4
4.1	Leptons	4
4.2	Jets	5
4.3	Overlap removal	6
4.4	Missing transverse quantities	6
5	Event classification and selections	6
5.1	Categorisation of production processes	6
5.2	Reconstruction and identification of the $V \rightarrow qq$ decay	7
5.3	Event selections for individual leptonic channels	8
5.3.1	0-lepton: $ZV \rightarrow \nu\nu qq$	8
5.3.2	1-lepton: $WV \rightarrow \ell\nu qq$	9
5.3.3	2-lepton: $ZV \rightarrow \ell\ell qq$	10

5.4	Signal region definitions	11
5.5	Reconstruction of invariant and transverse resonance mass	11
5.6	Signal efficiencies and mass resolutions	11
6	Background estimations	12
6.1	Control regions for W +jets, Z +jets, and $t\bar{t}$	12
6.2	Multijet background	12
7	Systematic uncertainties	14
7.1	Experimental uncertainties	14
7.2	Theoretical uncertainties	15
7.3	Impact of systematic uncertainties	15
8	Results and interpretations	16
8.1	Statistical procedure	16
8.2	Data and background comparisons	16
8.3	Limits on the production of heavy resonances	20
8.3.1	Limits on the production of RS radions	20
8.3.2	Limits on the production of HVT resonances	21
8.3.3	Limits on the production of RS gravitons	22
8.4	Comparisons of the limits	23
9	Summary	23
	References	24

1 Introduction

Many extensions to the Standard Model (SM) predict the existence of heavy resonances that decay into pairs of vector bosons (WW , WZ , and ZZ , collectively referred to as VV with $V = W, Z$). These theoretically well-motivated extensions include the two-Higgs-doublet model [1], composite Higgs models [2,3], technicolour [4–6] models, and warped extra dimensions [7,8]. The Large Hadron Collider (LHC), as the world’s highest-energy proton–proton (pp) collider, is a unique facility for the search for these heavy resonances. Indeed, both the ATLAS and CMS collaborations have reported searches for diboson resonances in various production modes and in a variety of decay final states of the vector bosons [9–16].

* e-mail: atlas.publications@cern.ch (corresponding author)

Depending on the assumed model, the predicted diboson resonances can be produced through gluon–gluon fusion (ggF), Drell–Yan (DY), or vector-boson fusion (VBF) processes. Representative Feynman diagrams of these processes are shown in Fig. 1.

This paper reports on a search for heavy resonances X in the mass range 300 GeV to 5 TeV in the $X \rightarrow VV$ diboson decay in pp collisions at $\sqrt{s} = 13$ TeV. Three types of diboson resonances are considered in the search. The first is a neutral scalar resonance, the radion (R) [17, 18] which appears in some Randall–Sundrum (RS) models and which can decay into WW or ZZ . The second is the heavier versions of the SM W and Z bosons, W' and Z' bosons, as parameterised in the Heavy Vector Triplet (HVT) framework [19], which can decay through $W' \rightarrow WZ$ and $Z' \rightarrow WW$. The third diboson resonance is a spin-2 graviton (G_{KK}) of the first Kaluza–Klein (KK) excitation in a bulk RS model [7, 20, 21] and decays into WW or ZZ .

Semileptonic VV final states in which one vector boson decays leptonically ($V_\ell: W \rightarrow \ell\nu, Z \rightarrow \ell\ell$ or $Z \rightarrow \nu\nu$) while the other decays hadronically ($V_h: V \rightarrow qq$) are considered, leading to three distinct channels: $ZV \rightarrow \nu\nu qq$ (0-lepton), $WV \rightarrow \ell\nu qq$ (1-lepton), and $ZV \rightarrow \ell\ell qq$ (2-lepton). Here ℓ denotes either an electron (e) or a muon (μ). The hadronic $V \rightarrow qq$ decays are reconstructed either as two separate small-radius jets (small- R jet, or j) or as one large-radius jet (large- R jet, or J) depending on the transverse momentum (p_T) of the boson. The reconstructed transverse mass (m_T) of the VV system for the 0-lepton channel and VV invariant mass (m_{VV}) for the 1-lepton and 2-lepton channels are used for signal–background discrimination via maximum-likelihood fits to their observed distributions.

Compared with previous searches in these final states [22, 23], the current search is performed with a data set approximately four times larger. Several improvements are made which include utilising a multivariate technique to identify and distinguish production processes, using tracking information in the large- R jet reconstruction, and introducing b -quark jet tagging for large- R jets.

2 Detector and data sample

The ATLAS experiment [24, 25] at the LHC is a multipurpose particle detector with a forward–backward symmetric cylindrical geometry and a near 4π coverage in solid angle.¹ It consists of an inner tracking detector surrounded by a thin

superconducting solenoid providing a 2 T axial magnetic field, electromagnetic and hadron calorimeters, and a muon spectrometer.

The inner tracking detector (ID) covers the pseudorapidity range $|\eta| < 2.5$. It consists of silicon pixel, silicon microstrip, and transition radiation tracking detectors. Lead/liquid-argon (LAr) electromagnetic calorimeters (ECAL) provide electromagnetic (EM) energy measurements with high granularity. A steel/scintillator-tile hadron calorimeter (HCAL) covers the central pseudorapidity range ($|\eta| < 1.7$). The endcap and forward regions are instrumented with LAr calorimeters for EM and hadronic energy measurements up to $|\eta| = 4.9$. The muon spectrometer (MS) surrounds the calorimeters and is based on three large air-core toroidal superconducting magnets with eight coils each. The field integral of the toroids ranges between 2.0 and 6.0 Tm across most of the detector. The muon spectrometer includes a system of precision tracking chambers and fast detectors for triggering. A two-level trigger system [26] selects events to be recorded at a reduced rate. The first level is a hardware implementation aiming to reduce the rate to around 100 kHz, while the software-based high-level trigger provides the remaining rate reduction to approximately 1 kHz.

This search uses the pp collision data at $\sqrt{s} = 13$ TeV recorded by the ATLAS detector during the data-taking between 2015 and 2018 with a total integrated luminosity of $139.0 \pm 2.4 \text{ fb}^{-1}$ [27].

A combination of multiple single-lepton and missing transverse momentum (E_T^{miss}) triggers with varying thresholds, as well as lepton quality and isolation requirements is used [26, 28]. During data-taking, as the instantaneous luminosity increased, the thresholds for unprescaled single-lepton triggers with tight isolations were increased in stages: the electron transverse energy (E_T) threshold was increased from 24 to 26 GeV, and the muon transverse momentum (p_T) threshold was increased from 20 to 26 GeV. Similarly, the threshold of the E_T^{miss} triggers increased from 70 to 110 GeV. Lepton triggers with tight isolations were complemented by those with looser isolations but higher E_T or p_T thresholds. The search uses the E_T^{miss} triggers in the 0-lepton channel and single-lepton triggers in the 2-lepton channel. The trigger efficiencies are greater than 90% for signal events targeted by these two channels, independent of the resonance mass. For the 1-lepton channel, the single-electron triggers were used in the electron case, but the single-muon triggers were used only for $p_T(\mu\nu) < 150$ GeV in the muon case. For $p_T(\mu\nu) > 150$ GeV, since the calculation of E_T^{miss} at the trigger level does not account for the presence of mini-

¹ ATLAS uses a right-handed coordinate system with its origin at the nominal interaction point (IP) in the centre of the detector and the z -axis along the beam pipe. The x -axis points from the IP to the centre of the LHC ring, and the y -axis points upwards. Cylindrical coordinates (r, ϕ) are used in the transverse plane, ϕ being the azimuthal angle

Footnote 1 continued
around the z -axis. The pseudorapidity is defined in terms of the polar angle θ as $\eta = -\ln \tan(\theta/2)$. Angular distance is measured in units of $\Delta R \equiv \sqrt{(\Delta\eta)^2 + (\Delta\phi)^2}$.

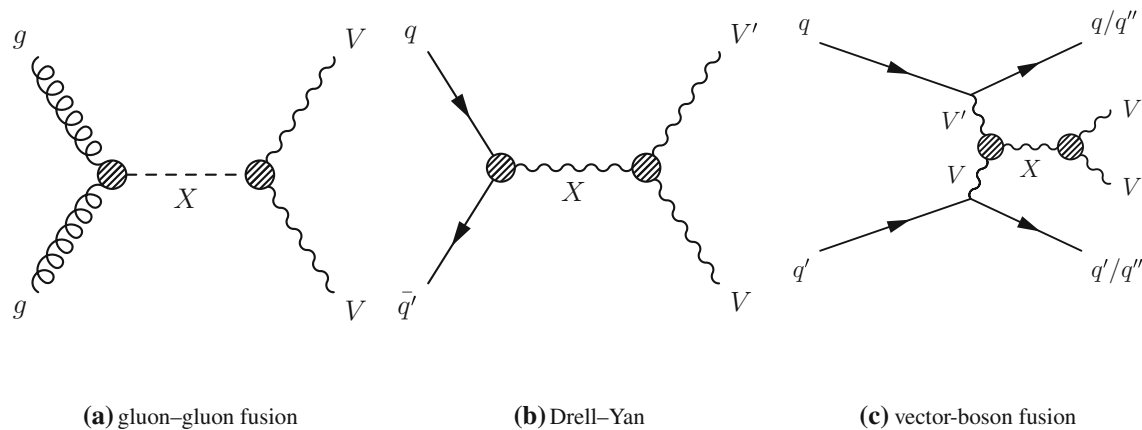


Fig. 1 Representative Feynman diagrams for the production of heavy resonances X with their decays into a pair of vector bosons. The hashed circles represent direct or effective couplings

imum ionising muons, the E_T^{miss} triggers were used instead. Using the unrescaled E_T^{miss} triggers minimises the impact of the efficiency loss from the limited geometric coverage of the muon triggers. The trigger efficiency for the 1-lepton channel increases from approximately 80% at 300 GeV to be above 90% at a resonance mass of 500 GeV.

Events were retained for analysis if they were recorded with all detector systems operating normally and pass data-quality requirements [29]. Collision vertices are formed from tracks with $p_T > 500$ MeV. The vertex candidate with the highest $\sum p_T^2$ of its associated tracks is selected as the primary vertex. All events are required to contain a primary vertex with at least two associated tracks.

3 Simulation of signal and background processes

Monte Carlo (MC) simulations were used for background modellings and estimations, evaluations of signal efficiencies, optimisations of event selections, and estimations of systematic uncertainties. Generated signal and background events were processed through the full ATLAS detector simulation program [30] based on GEANT4 [31]. Multiple overlaid pp collisions (pile-up) were simulated with the soft QCD processes of PYTHIA 8.186 [32] using the A3 set of tuned parameters [33] and the NNPDF2310 parton distribution function (PDF) set [34]. All simulated events are processed with the same trigger and reconstruction algorithm as the data. Scale factors were used to correct differences between the data and simulations.

3.1 Signal models and simulation

Three types of resonances corresponding to different spins are considered in the search. The first one is a scalar neutral radion, introduced in some bulk RS models to stabilise the

radius of the compactified extra dimension r_c [17, 18]. The coupling of the RS radion field to SM fields is inversely proportional to $\Lambda_R = e^{-k\pi r_c} \sqrt{6M_5^3/k}$ [35–37], where M_5 is the five-dimensional Planck mass, and k is the curvature factor. The RS radion events were simulated with $k\pi r_c = 35$ and $\Lambda_R = 3$ TeV [36]. The RS radion couples to SM fermions with a strength proportional to the fermion mass and to SM vector bosons with a strength proportional to the square of the boson mass, similarly to a heavy Higgs boson. However, the RS radion has a much narrower width due to its overall weaker couplings to SM particles. For example, the intrinsic width of a 3 TeV RS radion is approximately 3% of its mass, assuming $\Lambda_R = 3$ TeV. RS radions can be produced through both the ggF and VBF processes at the LHC as shown in Fig. 1.

The second type considered comprises two heavy vector bosons described in the HVT framework [19]: an electrically charged W' boson and an electrically neutral Z' boson produced through the DY and VBF processes. The new heavy vectors couple to the Higgs and the SM gauge bosons via a combination of parameters $g_V c_H$ and to the fermions via the combination $g^2/g_V c_F$. The parameter g_V represents the typical strength of the vector boson interaction, while the parameters c_H and c_F are expected to be of the order of unity in most models. Benchmark Model A [19] ($g_V = 1$) is representative of a model of weakly coupled vector resonances in an extension of the SM gauge group where the HVT bosons have comparable decay branching ratios into SM fermions and vector bosons. Model B [19] with $g_V = 3$, is representative of a composite model scenario where the HVT boson couplings to fermions are suppressed. In Model C, $g_V = c_H = 1$ and the HVT boson coupling to fermions was set to zero, so that only VBF production is possible. The $W' \rightarrow WZ$ and $Z' \rightarrow WW$ decays were considered in this search.

The third benchmark resonance searched for is a spin-2 bulk RS graviton G_{KK} which appears as the first KK excitation of the gravitational field in a bulk RS graviton model [7, 20, 21]. The G_{KK} couplings to light fermions are suppressed and therefore decays into final states involving heavy quarks, Higgs or vector bosons are favoured. The strength of the coupling depends on k/\overline{M}_{Pl} , where k corresponds to the curvature of the warped extra dimension and \overline{M}_{Pl} is the effective four-dimensional Planck scale. The value of k/\overline{M}_{Pl} is typically of $O(1)$, and this and the G_{KK} mass are the only two free parameters. The G_{KK} has a mass-dependent width, which is 3.7% of its mass at 500 GeV and 6.4% at 5 TeV for $k/\overline{M}_{Pl} = 1$. It can be produced through the ggF and VBF processes and decays into WW and ZZ with sizeable branching ratios. The G_{KK} samples were generated with $k/\overline{M}_{Pl} = 1$.

Signal events for the HVT and bulk RS graviton (radion) models were generated with MADGRAPH5_aMC@NLO v2.2.2 (v2.6.1) [38] at leading order (LO) using the NNPDF2310 PDF set. For the production of resonances in the HVT model, both the DY and VBF mechanisms were simulated, and the RS radion and G_{KK} resonances were produced via both the ggF and VBF mechanisms. For all signal models and production mechanisms, the generated events were interfaced to PYTHIA 8.186 (8.230 for the RS radion model) [39] for parton showering, hadronisation, and the underlying event. This interface relied on the A14 set of tuned parameters [40] for events generated with MADGRAPH5_aMC@NLO at LO.

As examples, Table 1 shows the theoretical cross-sections, the diboson decay branching ratios, and the total widths of the resonances for two different mass values.

3.2 Background process simulation

Background processes include W and Z boson production in association with jets (W + jets and Z + jets, collectively denoted by V + jets), top-quark production (both top-quark pair, $t\bar{t}$, and single-top-quark), non-resonant diboson production (WW , WZ and ZZ), and multijet production. MC samples were produced to model these background processes with the exception of multijet production, for which data were used to estimate its contribution.

The production of V +jets was simulated with the SHERPA v2.2.1 [41] generator using the matrix elements (ME) with next-to-leading order (NLO) accuracy for up to two jets, and with leading-order (LO) accuracy for up to four jets, calculated with the Comix [42] and OpenLoops [43, 44] libraries. They were matched with the SHERPA parton shower [45] using the MEPS@NLO prescription [46–49] using the set of tuned parameters developed by the SHERPA authors. The NNPDF30nn10 set of PDFs [50] was used and the samples were normalised to a next-to-next-to-leading-order (NNLO) prediction [51] with a flat K -factor. Simu-

lated V +jets events from MADGRAPH5_aMC@NLO v2.2.2 [38] using LO-accurate ME with up to four final-state partons were used to estimate the possible mismodelling of the SHERPA sample. The ME calculation employed the NNPDF30nn10 set of PDFs [50] or the NNPDF2310 set of PDFs. Events were interfaced to PYTHIA 8.186 for the modelling of the parton shower, hadronisation, and underlying event. The A14 tune [40] of PYTHIA was used with the NNPDF2310 PDF set. The decays of bottom and charm hadrons were performed by EvtGen v1.2.0.

Samples of $t\bar{t}$ and single-top-quark events were generated with POWHEG-BOX [52–55] v2 at NLO with the NNPDF30nn10 PDF set. The parameter h_{damp} , which regulates the high- p_T radiation in the POWHEG, was set to $1.5 m_t$ to obtain good data–MC agreement at high p_T [56], where $m_t = 172.5$ GeV was the top-quark mass used in the simulation. The parton shower, fragmentation, and underlying event were simulated using PYTHIA 8.230 [39] with the NNPDF2310 PDF set and the A14 tune. The decays of bottom and charm hadrons were performed by EvtGen v1.6.0.

Diboson processes were simulated with SHERPA v2.2.1 using the ME at NLO accuracy in QCD for up to one additional parton and at LO accuracy for up to three additional parton emissions, including off-shell effects and Higgs boson contributions. The NNPDF30nn10 PDF set was used. The electroweak $VVjj$ samples were generated by MADGRAPH5_aMC@NLO 2.4.3 [38] and were used, together with the SHERPA diboson sample, for the VBF analysis. The NNPDF3010 PDF set was used. The parton showers and hadronisation were modelled with PYTHIA 8.186 using the A14 tune.

Theoretical cross-sections were used to normalise background contributions. The cross-sections of single-top-quark t - and s -channel production were calculated with the Hathor v2.1 program [57, 58], while the Wt -channel followed the prescriptions from Refs. [59, 60]. Cross-sections for diboson production were calculated at NLO [55, 61]. The normalisations of V + jets and $t\bar{t}$ contributions were estimated from data using the control regions as described in Sect. 6.1.

4 Object reconstruction and identification

Leptons, jets, and E_T^{miss} are basic building blocks for this search. Their identification requirements are summarised briefly in this section.

4.1 Leptons

Electrons are reconstructed from energy clusters that are consistent with EM showers in the ECAL and are matched to tracks in the ID [62]. They are required to have transverse energy $E_T > 7$ GeV and pseudorapidity $|\eta| < 2.47$, exclud-

Table 1 List of benchmark signal models. Predictions of cross-section σ , branching ratio \mathcal{B} into WW , WZ , or ZZ , and intrinsic width divided by the resonance mass Γ/m , for the given hypothetical new particle at $m = 800$ GeV and 3 TeV are summarised

Model		Spin	$m = 800$ GeV			$m = 3$ TeV			
			σ [pb]	\mathcal{B}	Γ/m	σ [fb]	\mathcal{B}	Γ/m	
RS radion ($k\pi r_c = 35$, $\Lambda_R = 3$ TeV)	$R \rightarrow WW$	0	0.54 (ggF)	0.43	2.6×10^{-3}	1.38 (ggF)	0.44	0.032	
	$R \rightarrow ZZ$		1.1×10^{-3} (VBF)	0.21		5.5×10^{-3} (VBF)	0.22		
HVT	Model A	1	$W' \rightarrow WZ$	53	0.024	0.026	79	0.020	0.025
			$Z' \rightarrow WW$	26	0.023		36		
	Model B		$W' \rightarrow WZ$	1.6	0.43	0.040	5.5	0.47	0.031
			$Z' \rightarrow WW$	0.86	0.41		2.5		
	Model C (VBF)		$W' \rightarrow WZ$	4.0×10^{-3}	0.50	3.5×10^{-3}	1.6×10^{-3}	0.50	3.3×10^{-3}
			$Z' \rightarrow WW$	2.7×10^{-3}	0.49		1.0×10^{-3}		
Bulk RS G_{KK} ($k/\overline{M}_{Pl} = 1.0$)	$G_{KK} \rightarrow WW$	2	1.9 (ggF)	0.28	0.051	0.47 (ggF)	0.20	0.062	
	$G_{KK} \rightarrow ZZ$		0.050 (VBF)	0.14		1.6×10^{-2} (VBF)	0.10		

ing the ECAL barrel-endcap transition region: $1.37 < |\eta| < 1.52$. To reduce backgrounds from misidentification and non-prompt sources, electrons must meet a likelihood-based criterion [62]. The likelihood is used to classify electrons as having either *Loose*, *Medium*, or *Tight* quality.

Muons are identified by matching MS tracks with those in the ID and are required to have transverse momentum $p_T > 7$ GeV and pseudorapidity $|\eta| < 2.5$. An identification requirement based on information from the ID and MS systems is applied to reduce backgrounds from misreconstruction and muons originating from hadron decays in flight. Similarly to electrons, muons are classified as having either *Loose*, *Medium*, or *Tight* quality [63].

Leptons are required to have associated tracks satisfying $|d_0/\sigma_{d_0}| < 5$ (3) and $|z_0 \times \sin \theta| < 0.5$ mm for electrons (muons), where d_0 is the transverse impact parameter relative to the beam line, σ_{d_0} is its uncertainty, and z_0 is the distance between the longitudinal position of the track along the beam line at the point where d_0 is measured and the longitudinal position of the primary vertex.

Leptons from W and Z boson decays are required to have $p_T > 30$ GeV. They are expected to be isolated from other energy deposits in the detector. Thus, isolation criteria based on the sum of track p_T , the sum of calorimeter E_T , or both, in small cones around the lepton direction are used to further reduce backgrounds from non-isolated sources. Leptons of *Loose* quality with $p_T < 100$ GeV are required to pass a `FixedCutLoose` isolation requirement and no isolation requirement is applied for $p_T > 100$ GeV so that the leptons from high- p_T $Z \rightarrow \ell\ell$ decays are not removed in the presence of nearby leptons. Details can be found in Refs. [62, 63].

4.2 Jets

Small- R jets are reconstructed from calorimeter energy clusters using the anti- k_t algorithm [64, 65] with a radius param-

eter of $R = 0.4$. Energy- and η -dependent correction factors derived from MC simulations are applied in order to correct jets back to the particle level [66]. Jets are required to have $p_T > 30$ GeV and $|\eta| < 4.5$. To suppress jets from pile-up interactions, a jet vertex tagger [67] is applied to jets with $p_T < 120$ GeV and $|\eta| < 2.5$, based on information about tracks associated with the primary vertex and pile-up vertices. For forward jets, the uncertainty on pileup modelling is taken into account.

A multivariate algorithm for the identification of small- R jets containing b -hadrons (b -tagging) [68] is used. The algorithm is based on information such as track impact-parameter significances and positions of reconstructed secondary decay vertices. The identified jets, called b -jets, are restricted up to $|\eta| < 2.5$ due to the ID coverage. The b -tagging algorithm has an efficiency of 85% for b -hadrons in simulated $t\bar{t}$ events, a light-flavour jet rejection factor of 33 and a c -jet rejection of about 3 [68].

Large- R jets are reconstructed from track-calorimeter clusters [69] with the anti- k_t algorithm, but with the radius parameter increased to $R = 1.0$. The track-calorimeter clusters are formed by combining information from the calorimeter and the ID, utilising the excellent angular resolution of the ID and the improving energy resolution of the calorimeter at high energies. A trimming algorithm [70] is applied to reduce the impact of pile-up and soft radiation overlapping with the jet. The constituents of each jet are reclustered with the k_t algorithm [71] into smaller $R = 0.2$ subjects and those subjects are removed if $p_T^{\text{subject}}/p_T^J < 0.05$, where p_T^{subject} and p_T^J are the transverse momenta of the subject and the large- R jet, respectively. The large- R jets are required to have $p_T > 200$ GeV, $|\eta| < 2.0$, and a jet mass (m_J) greater than 50 GeV.

Variable-radius (VR) jets are used to identify b -jets from boosted hadronic $V \rightarrow qq$ decays that are reconstructed as large- R jets. They are reconstructed from ID tracks associated with large- R jets by using the anti- k_t algorithm with a p_T -dependent radius R parameter between 0.02 and 0.4 and

a ρ -parameter of 30 GeV [72]. They are required to have $p_T > 10$ GeV and $|\eta| < 2.5$. The same b -tagging algorithm which is used for small- R jets is applied to identify variable-radius jets from b -hadrons.

4.3 Overlap removal

An overlap-removal procedure is applied to the selected leptons and jets. If two electrons share the same track, or the separation between their two energy clusters satisfies $|\Delta\eta| < 0.075$ and $|\Delta\phi| < 0.125$, then the lower- p_T electron is discarded. Electrons that fall within $\Delta R = 0.02$ of a selected muon are also discarded. For nearby electrons and small- R jets, the jet is removed if the separation between the electron and jet satisfies $\Delta R < 0.2$; the electron is removed if the separation satisfies $0.2 < \Delta R < 0.4$. For nearby muons and small- R jets, the jet is removed if the separation between the muon and jet satisfies $\Delta R < 0.2$ and if the jet has less than three tracks or the energy and momentum differences between the muon and the jet are small; otherwise the muon is removed if the separation satisfies $\Delta R < 0.4$. To prevent double-counting of energy from an electron inside the large- R jet, the large- R jet is removed if the separation between the electron and the large- R jet satisfies $\Delta R < 1.0$.

4.4 Missing transverse quantities

The missing transverse momentum (\vec{E}_T^{miss}) is calculated as the negative vectorial sum of the transverse momenta of calibrated electrons, muons, small- R jets, and unassociated tracks. Large- R jets are not included in the \vec{E}_T^{miss} calculation to avoid double-counting of energy between the small- R jets and large- R jets. Energy depositions due to the underlying event and other soft radiation are taken into account by constructing a ‘soft term’ from ID tracks associated with the primary vertex but not with any reconstructed object [73]. Similarly, the track-based missing transverse momentum, \vec{p}_T^{miss} , is the negative vectorial sum of the transverse momenta of all good-quality inner-detector tracks that are associated with the primary vertex.

5 Event classification and selections

The search begins with the selection of the leptonically decaying boson V_ℓ . Candidate events are first selected according to the number of *Loose* leptons and assigned to 0-lepton ($V_\ell = Z$, $Z \rightarrow \nu\nu$), 1-lepton ($V_\ell = W$, $W \rightarrow \ell\nu$) and 2-lepton ($V_\ell = Z$, $Z \rightarrow \ell\ell$) channels. Other lepton multiplicities are excluded from the analysis. Although specific selections differ, the three channels follow the same analysis flow as illustrated in Fig. 2. For each channel, events are further classified into two exclusive VBF and ggF/DY cate-

gories as described in Sect. 5.1, targeting their corresponding production processes for heavy resonances.

The selection proceeds to identify the hadronically decaying boson V_h . Depending on the V_h -boson momentum, the energy deposits of the two jets from the hadronically decaying V bosons can be well separated or can largely overlap in the detector. Thus the $V \rightarrow qq$ decay, including $Z \rightarrow bb$, can be either reconstructed from two resolved small- R jets ($V \rightarrow jj$) for low-energy bosons or identified as one merged large- R jet ($V \rightarrow J$) for energetic bosons. The V_h candidates are identified first through the merged $V \rightarrow J$ identification and then, if it fails, through the resolved $V \rightarrow jj$ reconstruction.

Selections specific to each channel are presented in Sect. 5.3. Multiple signal regions (SRs) are defined in order to enhance search sensitivities, as described in Sect. 5.4. Section 5.5 discusses the mass variables used as the final discriminants. The analysis flow is run twice, once for $V_h = W$ and once for $V_h = Z$, which involves selecting different ranges of m_{jj} or m_J .

5.1 Categorisation of production processes

For the three production processes shown in Fig. 1, the ggF and DY processes have the same final states while the VBF process possesses two additional jets, called VBF-tag jets. The kinematics of these jets differ from those from the V -boson hadronic decays. They are typically well separated in pseudorapidity and usually have large dijet invariant mass. These characteristics were used in previous searches [22, 23] to separate VBF production from ggF/DY production. In this search, a recurrent neural network (RNN) [74, 75] is used to classify the VBF and ggF/DY event topologies. It is built with the Keras [76] library using the Theano python library [77] as a back end for mathematical computations. The RNN has 2 hidden layers with 25 recurrent cells to exploit the hidden correlation of the input sequence.

The RNN uses the four-momenta of small- R jets as input. It is well suited for a variable-length input sequence such as the jet information. The RNN allows to recover events with only one VBF-tag jet reconstructed ($\sim 30\%$ of signal events), and those events were not selected in previous searches where two VBF-tag jets were required [22, 23]. Although the RNN permits to deal with a large number of input jets, a maximum of two input jets is chosen to minimise the impact of systematic uncertainties associated with additional jets. Only a small increase (2–3%) in the tagging efficiency of VBF events is observed if more than two jets are used as inputs.

For events with large- R jets, small- R jets with angular separations of $\Delta R < 1$ from the leading large- R jets are removed. If there is no large- R jet in an event, the pair of small- R jets with dijet invariant mass closest to the V -boson mass is removed. Up to two remaining small- R jets with the

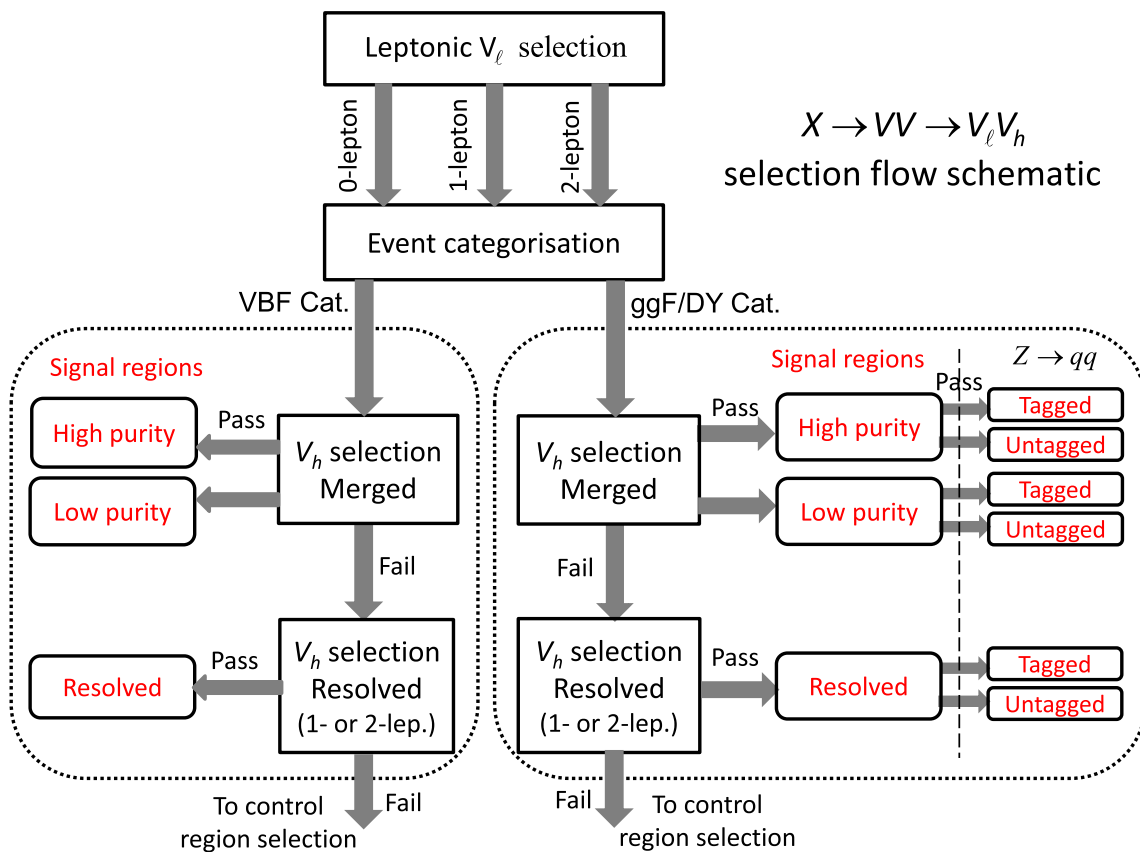


Fig. 2 Illustration of the selection flow and signal regions of the $X \rightarrow VV \rightarrow V_\ell V_h$ search. The VBF category targets VBF production whereas the ggF/DY category is for the rest. Three signal regions (high purity, low purity and resolved) are selected for each category, based on the $V \rightarrow qq$ reconstruction. For the 0-lepton channel, no resolved

selection is considered. For final states with hadronically decaying Z bosons, the three signal regions in the ggF/DY category are each further split into tagged and untagged according to the b -tagging information about jets from $Z \rightarrow qq$ decays

highest p_T are chosen as the input to the RNN. Events with no small- R jets left are automatically classified as ggF/DY events.

The RNN score distributions depend on the assumed model of a heavy resonance, its mass and decay mode. The RNN trained with the 1 TeV scalar resonance in the $X \rightarrow ZZ \rightarrow \ell\ell qq$ decay is applied for the three leptonic channels, the three resonance models, and all resonance masses.

Figure 3a compares the RNN score of simulated events from VBF and ggF/DY production of a 1 TeV resonance in the signal models considered in this search. The RNN discrimination power increases with the resonance mass. An event is classified as a VBF event if its RNN score is above 0.8 and otherwise as a ggF/DY event. The threshold is chosen to maximise the sensitivity to VBF signals. Figure 3b shows the fractions of simulated signal events passing the RNN requirement as functions of the resonance mass for different signal models. The RNN correctly classifies VBF events more than 40% of the time for a diboson resonance

heavier than 1 TeV with a ggF/DY contamination of about 2–5%. It yields a relative increase in the VBF event selection efficiency from 10% (5%) at 0.5 TeV to 60% (50%) at 3 TeV for a scalar resonance (spin-1 or spin-2 resonance) compared to the previous cut-based selection [22, 23], with similar background rejections.

5.2 Reconstruction and identification of the $V \rightarrow qq$ decay

The $V \rightarrow J$ candidates are identified from the highest- p_T large- R jet in an event by requiring its mass m_J to be in a p_T -dependent window centred around the expected value of the V -boson mass from simulations [78, 79], as shown in Fig. 4a. The mass window depends on the jet mass resolution [69] and is approximately 30 GeV wide at $p_T = 500$ GeV and increases to about 60 GeV at $p_T = 2.5$ TeV. A jet substructure variable $D_2^{(\beta=1)}$ is used to assess the quality of the $V \rightarrow J$ candidates. The variable $D_2^{(\beta=1)}$ is defined as the ratio of three-point to two-point energy correlation functions [80, 81] based on the energies and pairwise angular dis-

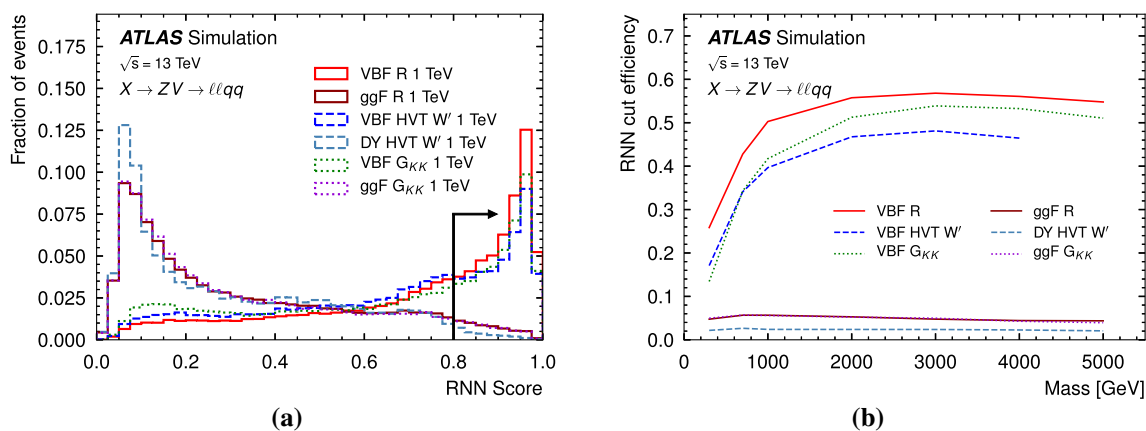


Fig. 3 **a** RNN score distributions for the production of a 1 TeV resonance in the signal models considered for this search; **b** the fractions of signal events passing the VBF requirement on the RNN score as functions of the resonance mass for both VBF and ggF production

tances of particles within a large- R jet. The variable is optimised to distinguish between jets originating from a single parton and those originating from $V \rightarrow qq$ decays. A p_T -dependent upper (lower) requirement on $D_2^{(\beta=1)}$, shown in Fig. 4b, is employed to select high (low)-purity signal regions as described in Sect. 5.4. Efficiencies for the m_J requirement alone and for the combined m_J and $D_2^{(\beta=1)}$ requirements as functions of the large- R jet p_T are shown in Fig. 5. The efficiency for tagging $V \rightarrow qq$ decay varies from approximately 40% at low p_T to 70% at high p_T . The background rejection factor of the W (Z) tagger is estimated using the simulated $W \rightarrow \ell\nu$ ($Z \rightarrow \ell\ell$)+jets events, and is approximately 5 (6) at $p_T = 200$ GeV and 35 (30) at $p_T > 700$ GeV.

The $V \rightarrow jj$ candidates are reconstructed from two small- R jets within $|\eta| < 2.5$. The leading jet is required to have $p_T > 60$ GeV and the subleading jet is required to have $p_T > 30$ (45) GeV in the 2-lepton (1-lepton) channel. No resolved $V \rightarrow jj$ reconstruction is considered for the 0-lepton channel due to the large multijet background. The two highest- p_T small- R jets in $|\eta| < 2.5$ are chosen to form the $V \rightarrow jj$ candidate except for the $Z \rightarrow bb$ reconstruction, for which events are required to have exactly two b -tagged jets, and in which case they are used. The invariant mass of the two jets, m_{jj} , must be consistent with that of the V boson by satisfying $62 < m_{jj} < 97$ GeV for $W \rightarrow jj$ and $70 < m_{jj} < 105$ GeV for $Z \rightarrow jj$. Fixed mass windows are applied because the dijet mass resolution is largely independent of the dijet p_T for the resonance masses to which the resolved analysis is sensitive.

5.3 Event selections for individual leptonic channels

Event selections for all three leptonic channels consist of the selections for the leptonically and hadronically decaying V bosons and an event-level selection designed to reduce backgrounds specific to each channel. The selection of hadroni-

cally decaying V bosons is common to all three channels. It requires a $V \rightarrow qq$ candidate identified by either the merged or resolved technique as discussed above. The other selections are specific to individual leptonic channels and are described below. An overview of the selections is shown in Table 2.

For the merged selection, since the leading large- R jet is considered as the $V \rightarrow J$ candidate, any small- R jet within an angular radius $R = 1$ around it is removed. For the resolved selection, large- R jets are ignored and no small- R jets are removed.

An event veto based on b -tagging information is also applied. For signal events, b -jets can arise from the $Z \rightarrow bb$ decays. For $V_h = Z$, classification based on number of b -tagged jets in $Z \rightarrow qq$ candidates is applied, as described in Sect. 5.4. For $V_h = W$, events are required to have at most one b -tagged jets in $W \rightarrow qq$ candidates, considering misidentification rate for charm hadrons from $W \rightarrow sc$ decay. In the merged selection, events are vetoed if there are more than two b -tagged variable-radius jets associated with the leading large- R jets.

Unless specifically noted, the same selections are applied for the VBF and ggF/DY categories. The merged selection is applied first and the resolved selection is applied only to events failing the merged selection.

5.3.1 0-lepton: $ZV \rightarrow \nu\nu qq$

The 0-lepton channel targets the $ZV \rightarrow \nu\nu qq$ final state from $R \rightarrow ZZ$, $W' \rightarrow ZW$ and $G_{KK} \rightarrow ZZ$ decays. Events in this final state have a large E_T^{miss} and a $V \rightarrow qq$ candidate. Due to high E_T^{miss} trigger thresholds and the expected large multijet background from mismeasurement at low E_T^{miss} , events are required to have $E_T^{\text{miss}} > 250$ GeV and no *Loose* leptons, to suppress background from multijet events and single W bosons respectively.

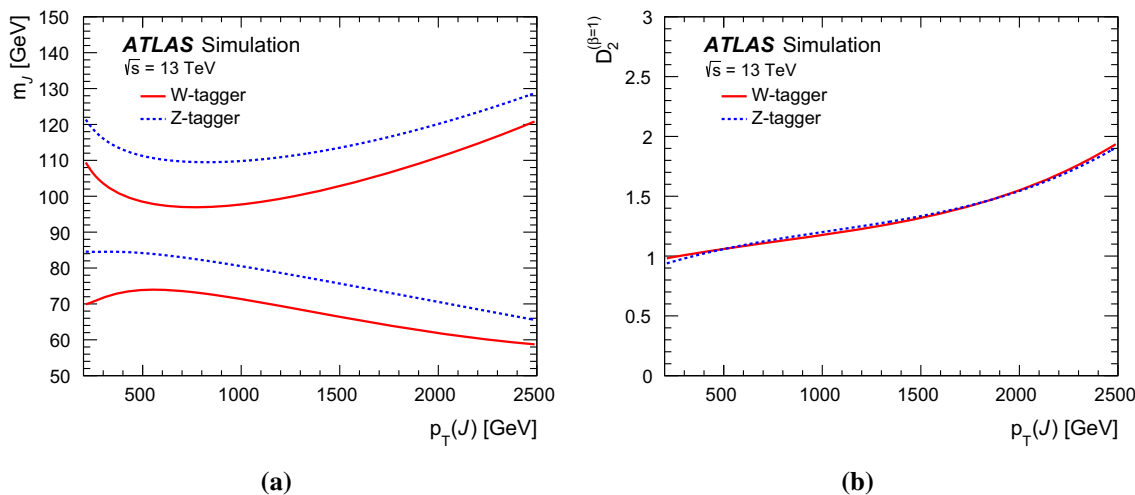


Fig. 4 **a** The upper and lower bounds of m_J and **b** the upper (lower) requirements on $D_2^{(\beta=1)}$ selecting the high (low)-purity signal regions as functions of the large- R jet p_T for the $V \rightarrow J$ tagging for the W boson and the Z boson

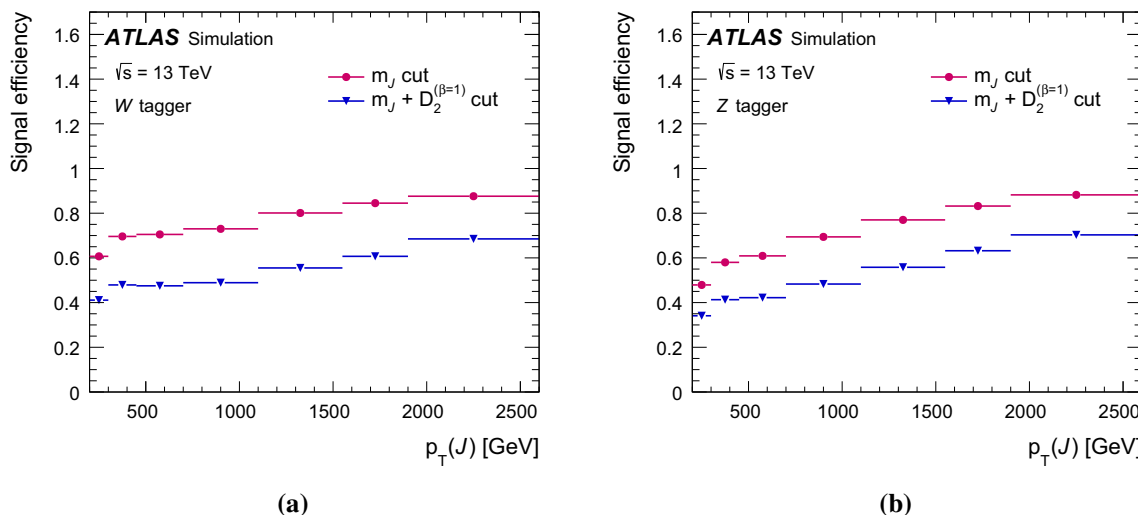


Fig. 5 Efficiencies of the m_J and $D_2^{(\beta=1)}$ requirements as functions of the large- R jet p_T for the $V \rightarrow J$ tagging for **a** the W boson and **b** the Z boson

Additional requirements are applied to further reduce the multijet background. These include $p_T^{\text{miss}} > 50$ GeV, and an azimuthal opening angle between \vec{E}_T^{miss} and \vec{p}_T^{miss} satisfying $\Delta\phi(\vec{E}_T^{\text{miss}}, \vec{p}_T^{\text{miss}}) < 1$. Furthermore, the azimuthal angle between \vec{E}_T^{miss} and the nearest small- R jet must satisfy $\min \Delta\phi(\vec{E}_T^{\text{miss}}, j) > 0.4$. With these angular requirements along with the E_T^{miss} and p_T^{miss} requirements, the multijet background becomes negligible.

The high E_T^{miss} requirement is efficient only for signal events with very heavy resonances. Therefore, only the merged selection is considered for this channel.

5.3.2 1-lepton: $WV \rightarrow \ell\nu qq$

The 1-lepton channel is designed for the $WV \rightarrow \ell\nu qq$ final state from $R \rightarrow WW, W' \rightarrow WZ, Z' \rightarrow WW$, and $G_{KK} \rightarrow WW$. Events in this channel must have exactly one *Tight* electron or *Medium* muon, with $p_T > 30$ GeV, and no other leptons satisfying the *Loose* quality; E_T^{miss} greater than 60 GeV; and a transverse momentum of the lepton- \vec{E}_T^{miss} system (i.e. the reconstructed V_ℓ), $p_T^{V_\ell}$, greater than 75 GeV.

For the merged selection, the E_T^{miss} and $p_T^{V_\ell}$ thresholds are raised to 100 GeV and 200 GeV, respectively. Considering that boson p_T is expected to be approximately $0.5m_{VV}$, events are further required to have $\mathcal{R}_{p_T/m}$, defined as $\min(p_T^{V_\ell}, p_T^{V_h})/m_{VV}$, greater than 0.35 (0.25) for the

Table 2 Overview of the main $X \rightarrow VV \rightarrow V_\ell V_h$ selection criteria; the text gives more details. $\mathcal{R}_{p_T/m}$ stands for $\min(p_T^{V_\ell}, p_T^{V_h})/m_{VV}$

Event selection	0-lepton ($ZV \rightarrow \nu\nu V_h$)	1-lepton ($WV \rightarrow \ell\nu V_h$)	2-lepton ($ZV \rightarrow \ell\ell V_h$)
V_ℓ selection	No <i>Loose</i> lepton $E_T^{\text{miss}} > 250$ GeV $p_T^{\text{miss}} > 50$ GeV	1 <i>Tight</i> electron or 1 <i>Medium</i> muon with $p_T^\ell > 30$ GeV $E_T^{\text{miss}} > 60$ GeV $p_T^{V_\ell} > 75$ GeV	2 <i>Loose</i> leptons with $p_T^\ell > 30$ GeV from the $Z \rightarrow \ell\ell$ candidate
Event veto	No additional <i>Loose</i> leptons		
		Veto events with <i>b</i> -jets not associated with the $V \rightarrow qq$ candidate	
Event categorisation	≥ 1 large- <i>R</i> jets or ≥ 2 small- <i>R</i> jets VBF and ggF/DY classification according to RNN score		
V_h selection (Merged)		$E_T^{\text{miss}} > 100$ GeV $p_T^{V_\ell} > 200$ GeV	
	≥ 1 large- <i>R</i> jets The leading jet passing p_T -dependent m_J requirement		
		$\mathcal{R}_{p_T/m} > 0.35$ (ggF/DY) $\mathcal{R}_{p_T/m} > 0.25$ (VBF)	$\mathcal{R}_{p_T/m} > 0.35$ (ggF/DY) $\mathcal{R}_{p_T/m} > 0.25$ (VBF)
V_h selection (Resolved)	Not Performed	Failed merged selection ≥ 2 small- <i>R</i> jets with $ \eta < 2.5$ $62 < m_{jj} < 97$ GeV for $W \rightarrow jj$ $70 < m_{jj} < 105$ GeV for $Z \rightarrow jj$	
		$\mathcal{R}_{p_T/m} > 0.35$ (ggF/DY) $\mathcal{R}_{p_T/m} > 0.25$ (VBF)	$\mathcal{R}_{p_T/m} > 0.35$ (ggF/DY) $\mathcal{R}_{p_T/m} > 0.35$ (VBF)

ggF/DY (VBF) category. Here $p_T^{V_h}$ is the p_T of the V_h candidate, i.e. the leading large-*R* jet, and m_{VV} is the invariant mass of the VV system reconstructed from the $\ell\nu$ and the leading large-*R* jet.² This requirement suppresses background significantly at large m_{VV} while maintaining high efficiencies for signal events.

For the resolved selection, a set of azimuthal angular requirements are designed and applied to reduce large multijet backgrounds expected at low E_T^{miss} and $p_T^{V_\ell}$. They are $\Delta\phi(\ell, \vec{E}_T^{\text{miss}}) < 1.5$, $\Delta\phi(j_1, j_2) < 1.5$, $\Delta\phi(\ell, j_{1/2}) > 1.0$ and $\Delta\phi(\vec{E}_T^{\text{miss}}, j_{1/2}) > 1.0$. Here $j_{1/2}$ refers to both j_1 and j_2 , which form the $V \rightarrow jj$ candidate. Similarly to the merged selection, a kinematic criterion of $\mathcal{R}_{p_T/m} > 0.35$ (0.25) is imposed for the ggF/DY (VBF) category, where $p_T^{V_h}$ is the

p_T of the $V \rightarrow jj$ candidate and m_{VV} is reconstructed from the $\ell\nu$ and dijet system.

Additional *b*-jets can originate from background $t\bar{t}$ and single-top-quark events. To reduce this background, events are vetoed if there are one or more small-*R* *b*-jets beyond those selected as the $V \rightarrow qq$ candidate.

5.3.3 2-lepton: $ZV \rightarrow \ell\ell qq$

The 2-lepton channel is intended for the $ZV \rightarrow \ell\ell qq$ final state from $R \rightarrow ZZ$, $W' \rightarrow ZW$ and $G_{KK} \rightarrow ZZ$. The event selection begins with the identification of the $Z \rightarrow \ell\ell$ decay. The $Z \rightarrow \ell\ell$ candidates are formed from two same-flavour leptons with $p_T > 30$ GeV and satisfying the *Loose* criteria defined in Sect. 4. Muon pairs are required to have opposite charges. Because electrons are more susceptible to charge misidentification, no charge requirement is applied. The dilepton invariant mass, $m_{\ell\ell}$, must be consistent with the Z boson mass. A fixed $m_{\ell\ell}$ window of [83, 99] GeV is applied to electron pairs, while the

² The unknown neutrino longitudinal momentum, p_z , is determined by fixing the invariant mass of the $\ell\nu$ system to the W -boson mass, resulting in a quadratic equation. The p_z is chosen to be either the real component of the two complex solutions or the smaller of the two real solutions.

dilepton p_T is used to define a $p_T^{\ell\ell}$ -dependent window of $[85.6 \text{ GeV} - 0.0117 \times p_T^{\ell\ell}, 94.0 \text{ GeV} + 0.0185 \times p_T^{\ell\ell}]$ that is required for the muon pairs because of the deteriorating muon momentum resolution at high p_T . The mass windows are chosen to maintain approximately 95% selection efficiency for $Z \rightarrow \ell\ell$. Events with additional *Loose* leptons are removed.

The selected $Z \rightarrow \ell\ell$ events are required to have $\mathcal{R}_{p_T/m} > 0.35$ (0.25) for the ggF/DY (VBF) category for the merged selection and $\mathcal{R}_{p_T/m} > 0.35$ for both the ggF/DY and VBF categories for the resolved selection. Again, $p_T^{V_\ell}$ is the p_T of the leptonic V candidate ($p_T^{V_\ell} = p_T^{\ell\ell}$ in this case), $p_T^{V_h}$ is the p_T of the V_h candidate, and m_{VV} is the invariant mass of the V_ℓ and V_h system. This requirement exploits the kinematic feature of highly boosted boson decays expected from heavy resonances to reduce backgrounds.

5.4 Signal region definitions

Multiple signal regions are defined using the properties of the hadronically decaying V boson as illustrated in Fig. 2. Events passing the merged selection are assigned to either high-purity (HP) or low-purity (LP) signal regions according to the quality of their $V \rightarrow J$ candidates. Those with $V \rightarrow J$ candidates passing the $D_2^{(\beta=1)}$ requirement of the boson tagger [78] are selected for the HP SR, otherwise for the LP SR. The combined m_J and $D_2^{(\beta=1)}$ efficiencies for the HR SR are shown in Fig. 5 as functions of $V p_T$. Events passing the resolved selection form the resolved SR.

For $V_h = Z$, about 21% of $Z \rightarrow qq$ decays are $Z \rightarrow bb$, whereas jets from the dominant background source, V +jets, have a smaller heavy-quark content. To exploit this difference, the HP, LP, and resolved SRs are each further split into tagged and untagged SRs in the ggF/DY category if the hadronically decaying boson is a Z boson, i.e. $V = Z$. The b -tagging is not applied in the VBF category due to the limited number of events. Classification based on the b -tagging is not applied for $V_h = W$. For the merged selection, the splitting is made by applying b -tagging to variable-radius jets associated to the leading large- R jet. Events are tagged only if the two leading variable-radius jets are both b -tagged. For the resolved selection, events are tagged if the $Z \rightarrow jj$ is formed from two b -jets and untagged otherwise.

Classifications in terms of ggF/DY and VBF categories include: merged and resolved reconstruction of the $V_h \rightarrow qq$ decay, high and low purity for the merged reconstruction, tagged and untagged identification of the $Z \rightarrow qq$ decay, and different mass windows for the $W \rightarrow qq$ and $Z \rightarrow qq$ decays. This results in 10 SRs for the 0-lepton channel and 15 SRs each for the 1-lepton and 2-lepton channels, for a total of 40 SRs. Because of overlapping mass windows used to select the hadronic decays of the W and Z bosons, these

SRs are not orthogonal. In terms of the diboson final states of resonance decays, there are 6 SRs for $X \rightarrow WW$, 15 for $X \rightarrow ZZ$, and 19 for $X \rightarrow WZ$. SRs in each diboson final state are orthogonal. The $X \rightarrow WW$ and $X \rightarrow ZZ$ SRs are orthogonal by design, while the $X \rightarrow WZ$ SRs can overlap with either $X \rightarrow WW$ or $X \rightarrow ZZ$ SRs.

5.5 Reconstruction of invariant and transverse resonance mass

Either the invariant mass m_{VV} or the transverse mass m_T of the selected VV final states is used as the final discriminant to extract the signal. Heavy resonances would manifest themselves as resonant structures above the SM background in the invariant mass distributions or as broad enhancements in the transverse mass distributions.

For the 0-lepton channel of $X \rightarrow ZV \rightarrow \nu\nu qq$, no resonance mass reconstruction is possible because of the two undetected neutrinos. Instead a transverse mass defined as:

$$m_T = \sqrt{(p_T^J + E_T^{\text{miss}})^2 - (\vec{p}_T^J + \vec{E}_T^{\text{miss}})^2}$$

is used as the discriminant for the merged selection. For the 1-lepton and 2-lepton channels, the VV mass is calculated for both the merged and the resolved reconstruction of the $V \rightarrow qq$ decay.

Muon momentum resolution deteriorates at high p_T , significantly impacting the $Z \rightarrow \mu\mu$ mass resolution and consequently the resonance mass resolution in the 2-lepton channel. This deterioration is particularly severe for very heavy resonances, especially in the merged selection. To mitigate the impact, a scale of $m_Z/m_{\mu\mu}$ is applied to the four-momentum of the dimuon system, effectively fixing the dimuon mass to the Z boson mass [82]. This scaling improves the $m_{\mu\mu}$ resolution by about 7% in the merged analysis for a scalar resonance. The scaling is not applied for $W \rightarrow \mu\nu$ because of the undetected neutrino.

For the resolved selection, the m_{VV} resolution is improved by 2% through the scaling of the dijet four-momentum by a factor of m_V/m_{jj} , with m_V being either the Z or W boson mass [82]. No m_V/m_J scaling is applied to the merged selection as the improvement in the m_{VV} resolution is found to be negligible.

5.6 Signal efficiencies and mass resolutions

Signal selection efficiencies depend on the signal model, the production process, and the mass of heavy resonances. Figures 6, 7 and 8 show the acceptance times efficiency ($A \times \epsilon$) of the signal events from MC simulations as a function of the resonance mass for (a) ggF/DY and (b) VBF production, combining all SRs of both the ggF/DY and VBF categories of both the resolved and merged analyses. The $A \times \epsilon$ curves

are largely determined by the merged analyses. The resolved analyses contribute only in the low mass region, up to approximately 1 TeV.

Large differences in $A \times \epsilon$ shown in the figures for different resonances are due to the different spins of these resonances. The spin-0 RS radions are produced with isotropic angular distributions for both ggF and VBF production. On the other hand, the spin-1 HVT resonances and spin-2 RS gravitons are produced more centrally (more forward) for ggF/DY (VBF) production. These different angular distributions lead to very different efficiencies of the $\mathcal{R}_{p_T/m}$ requirement. Moreover, the angular requirements between jets and E_T^{miss} in the 0-lepton channel are more efficient for DY production of HVT resonances than for ggF production of RS radions and RS gravitons due to the different colour factors for initial-state quarks and gluons.

Signal contributions from $W \rightarrow \tau\nu \rightarrow \ell\nu\nu\nu$ decays are included in the 1-lepton channel, but not in the 2-lepton channels. Approximately 10–12% of the signal events in SRs are from $W \rightarrow \tau\nu \rightarrow \ell\nu\nu\nu$ decays in the 1-lepton channel. These events have mass distributions similar to those from $W \rightarrow \ell\nu$ decays. In the 2-lepton channel, signal contributions from $Z \rightarrow \tau\tau \rightarrow 2\ell + 4\nu$ decays are suppressed by the small $\tau\tau \rightarrow 2\ell + 4\nu$ branching ratio and the Z boson mass requirement. They are found to be negligible. The 0-lepton channel targeting the $X \rightarrow ZV \rightarrow \nu\nu qq$ signal should also be sensitive to the $X \rightarrow WV \rightarrow \ell\nu qq, \tau\nu qq$ signal due to either the inefficiency of the lepton veto or the lack of a τ -veto. This additional ‘cross-channel’ signal contribution is neglected in this search.

The resonance decays are fully reconstructed in the 1-lepton and 2-lepton channels. In the 1-lepton channel, the $m_{\ell\nu jj}$ distributions from the resolved $V \rightarrow jj$ reconstruction have widths of approximately 8% of the resonance mass for narrow resonances, whose intrinsic widths are smaller than the detector mass resolution, with masses of 0.5–1 TeV.³ The width of the $m_{\ell\nu J}$ distribution from the merged $V \rightarrow J$ reconstruction varies from 7% at 1 TeV to 4% at 5 TeV. Similarly, in the 2-lepton channel the $m_{\ell\ell jj}$ resolution is $\sim 6\%$ for resonance masses of 0.5–1 TeV and the $m_{\ell\ell J}$ resolution varies from approximately 4% at 1 TeV to 2% at 5 TeV.

6 Background estimations

Relevant background sources for the search are V +jets, $t\bar{t}$ and single top, non-resonant diboson, and multijet production. Their relative importance depends on the final state. The largest contributions are from Z +jets and W +jets in the 0-lepton channel and W +jets and $t\bar{t}$ in the 1-lepton channel.

³ The width of the reconstructed mass distribution is defined as the standard deviation of a Gaussian function fit to the peak region.

In the 2-lepton channel, the Z +jets background dominates. The multijet background is negligible except in the resolved SRs of the 1-lepton channel. In the tagged SRs, the $t\bar{t}$ and single-top-quark contributions are enhanced and are in fact dominant in the 1-lepton channel.

MC simulations are used to simulate kinematics of background events except for multijet events. Contributions from diboson and single-top-quark processes are normalised to their theoretical cross-sections, whereas the V +jets and $t\bar{t}$ contributions are normalised using data through control regions. The multijet background is estimated from data. The definitions of control regions and the method of multijet estimation are described below.

6.1 Control regions for W +jets, Z +jets, and $t\bar{t}$

Control regions (CR) are designed to constrain the normalisations of the W +jets, Z +jets and $t\bar{t}$ background contributions using data, eliminating the reliance on the theoretical cross-sections, which are often less reliable in the phase-space regions covered by this search. Events in CRs are selected from those failing the selections of the SRs, but are otherwise expected to have event topologies similar to those in SRs and small contaminations from potential signals.

CRs for the W +jets background are defined using events in the 1-lepton channel by reversing the m_J or m_{jj} requirements of the SR selections, but events are otherwise selected in the same way as those in the corresponding SRs. For the merged selection, m_J must fall outside of the mass windows of both W and Z boson tagging. For the resolved selection, m_{jj} is required to be in the range from 50 to 150 GeV, excluding the combined W and Z mass window of 62–105 GeV. The W +jets events are expected to be the dominant contribution in these CRs, except in the b -tagged CRs, where the $t\bar{t}$ contribution dominates. CRs for the Z +jets background are defined the same way, but using 2-lepton events. The Z +jets events dominate in all Z +jets CRs, even in the tagged CRs.

CRs for the $t\bar{t}$ background are defined using 1-lepton events, selected in the same way as the 1-lepton SRs except for the requirement of an additional small- R b -jet unassociated with the $V \rightarrow jj/J$ candidate instead of the b -jet veto. Moreover, m_{jj} is required to be between 50 and 150 GeV in the case of the resolved selection.

6.2 Multijet background

In the resolved SRs of the 1-lepton channel, multijet production is a non-negligible background source. Multijet events can mimic signal events if there is a lepton from either jet misidentification or heavy-quark decay, along with a large E_T^{miss} from energy mismeasurements. The multijet contributions are difficult to model through MC simulations and are therefore estimated from data. A template method is used

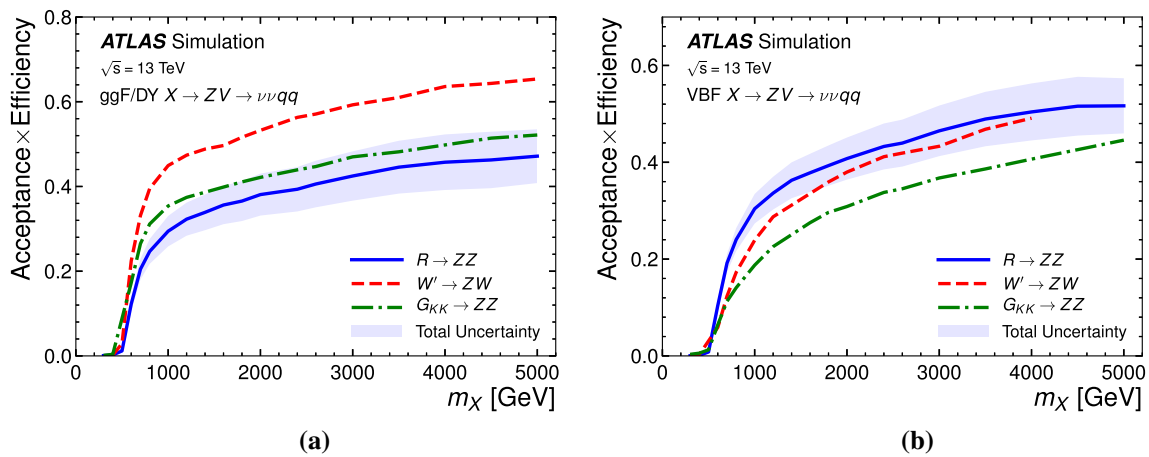


Fig. 6 Selection acceptance times efficiency for the $X \rightarrow ZV \rightarrow \nu\nu qq$ signal events from MC simulations as a function of the resonance mass for **a** ggF/DY and **b** VBF production, combining HP and LP signal

regions. The light shaded band represents the total statistical and systematic uncertainties for the RS radion model, and the total uncertainties are similar for the other signal models

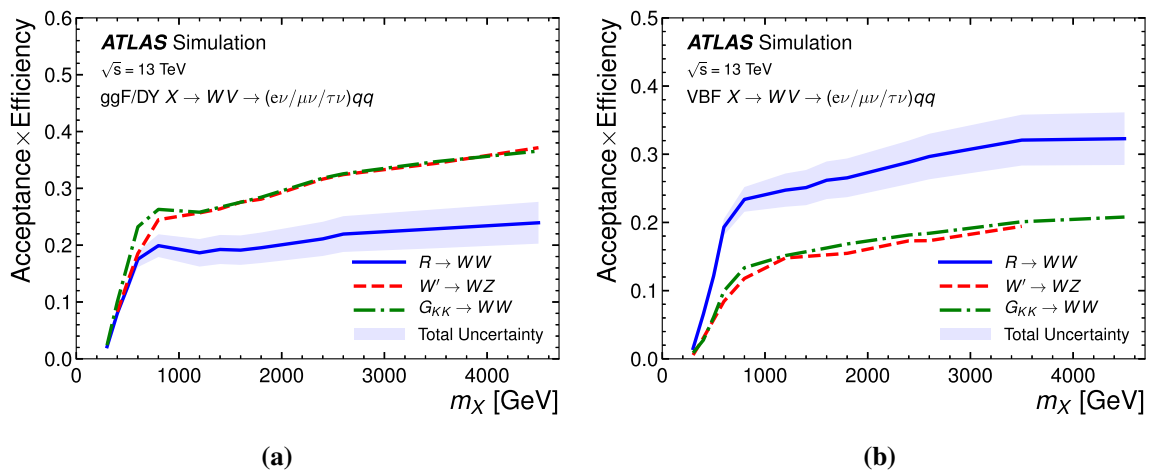


Fig. 7 Selection acceptance times efficiency for the $X \rightarrow WV \rightarrow (e\nu/\mu\nu/\tau\nu) qq$ signal events from MC simulations as a function of the resonance mass for **a** ggF/DY and **b** VBF production, combining all SRs of both the resolved and merged analyses. Signal contributions from $W \rightarrow \tau\nu$ decays are included in the acceptance calculation. The

light shaded band represents the total statistical and systematic uncertainties for the RS radion model, and the total uncertainties are similar for the other signal models. The ‘bump’ structure around 800 GeV is due to the decreasing contribution from the resolved analysis at higher masses

to estimate the multijet contributions. The method derives the shapes of the E_T^{miss} distributions of the multijet contributions from multijet-enriched control regions (MJCR), one for each signal and control region. MJCRs are designed to be orthogonal to both the SRs and CRs as defined above. For the muon channel, MJCRs are defined only for the single-muon trigger, i.e. events with $p_T(\mu\nu) < 150$ GeV, since the multijet contributions to the E_T^{miss} -triggered events with $p_T(\mu\nu) > 150$ GeV are found to be negligible.

Events in MJCRs are selected by modifying the lepton requirements used for the SR and CR selections. Electron candidates are required to satisfy the *Medium* quality criteria and not the *Tight* quality criteria. Muon candidates must pass

a relaxed, but fail the tight, isolation requirement. All other selections remain unchanged. More than 80% of the selected events in MJCRs are estimated to originate from multijet production. These MJCR samples are used to model the kinematics of multijet contributions in their corresponding CRs and SRs, after subtracting contributions from other sources. The multijet scale factors, the ratios of the multijet contributions in the CRs to those in their MJCRs, are extracted through fits to the E_T^{miss} distributions in CRs using the multijet E_T^{miss} distribution shapes in MJCRs as templates. In the fits, contributions from other sources are constrained to their expectations from MC simulations within their uncertainties.

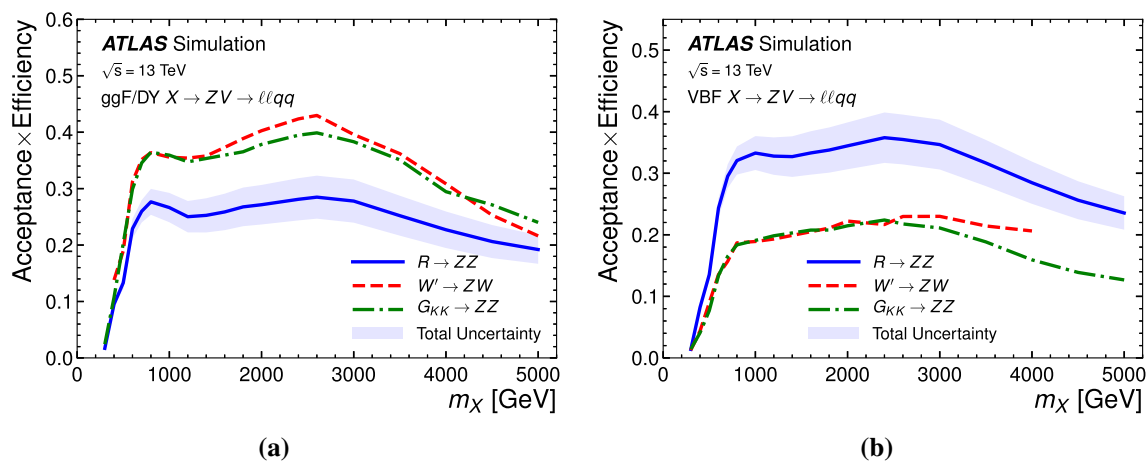


Fig. 8 Selection acceptance times efficiency for the $X \rightarrow ZV \rightarrow \ell\ell qq$ signal events from MC simulations as a function of the resonance mass for **a** ggF/DY and **b** VBF production, combining all SRs of both the resolved and merged analyses. The light shaded band represents the total statistical and systematic uncertainties for the RS radion model,

and the total uncertainties are similar for the other signal models. The decreases in efficiencies for resonance masses above approximately 2.5 TeV are due to the merging of electrons from the highly boosted $Z \rightarrow ee$ decays. The ‘bump’ structure around 800 GeV is due to the decreasing contribution from the resolved analysis at higher masses

These scale factors are then applied to their corresponding SRs to estimate multijet contributions.

7 Systematic uncertainties

Systematic uncertainties impact the search sensitivity through their effects on background estimations, signal selection efficiencies, and the distributions of the mass discriminants. The sources of these uncertainties can be classified broadly into two groups: (a) those experimental in nature related to the detector and reconstruction performance and (b) those of theoretical origins associated with the MC modelling of both the background and signal processes. The uncertainties and the methods used to evaluate them are discussed below. Unless explicitly stated, the uncertainties quoted are the uncertainties in the quantities themselves, not the impact on the search sensitivity.

7.1 Experimental uncertainties

Experimental uncertainties arise from the luminosity, triggers, and reconstruction and identification of leptons and jets, as well as the calculation of the E_T^{miss} . They also include uncertainties in the energy and momentum scales and resolutions of leptons and jets.

The uncertainty of the combined 2015–2018 integrated luminosity is 1.7%. It is derived from the calibration of the luminosity scale using x - y beam-separation scans, following a methodology similar to that detailed in Ref. [27], and using the LUCID-2 detector for the baseline luminosity measurement [83]. A variation in the pile-up reweighting of MC

events is included to cover the uncertainty in the ratio of the predicted and measured inelastic cross-sections [84].

Uncertainties in the efficiencies of lepton triggers are found to be negligible. The modelling of the electron and muon reconstruction, identification and isolation efficiencies is studied with a tag-and-probe method using $Z \rightarrow \ell\ell$ events in data and simulation [62,63]. Small corrections are applied to the simulation to better model the performance seen in data. These corrections have associated uncertainties of the order of 1%. Uncertainties in the lepton energy (or momentum) scale and resolution, especially for muon momentum resolution (3%), are also taken into account.

Uncertainties for the energy scale and resolution of the small- R jets are determined using MC simulation and in situ techniques [66]. For central jets, the total relative uncertainty in the jet energy scale varies in the range 1–4% for $p_T > 20$ GeV. For forward jets, additional 2–4% uncertainty depending on p_T is applied based on η -intercalibration study. The uncertainty in the jet energy resolution ranges from 20% for jets with a p_T of 20 GeV to less than 5% for jets with $p_T > 200$ GeV.

Uncertainties in the scale of the large- R jet p_T are estimated by comparing the calorimeter- and track-based energy and mass measurements in data and simulation [85]. The precision of the relative jet energy scale is 1–2% for $200 \text{ GeV} < p_T < 2 \text{ TeV}$, while that of the mass scale is 2–10%. The jet energy resolution uncertainty is estimated to be approximately 2%. The efficiency of the W/Z boson tagging based on the m_J and $D_2^{(\beta=1)}$ requirements is estimated using data control samples, following the technique described in Ref. [86]. The efficiency for large- R jets from W/Z boson decays is estimated using $t\bar{t}$ control samples for $p_T < 600$ GeV.

The measurement is extrapolated to the higher p_T region with additional uncertainties estimated from simulations [87]. The efficiency for background large- R jets from gluons or light quarks is estimated using dijet and γ +jets samples.

Uncertainties in the efficiencies for tagging b -jets and for mis-tagging light-flavour jets are determined from $t\bar{t}$ control samples [68, 88, 89]. The total uncertainties are 1–10%, 15–50%, and 50–100% for b -jets, c -jets, and light-flavour jets respectively.

Uncertainties in the E_T^{miss} trigger efficiencies have negligible impact on the search as the efficiencies for the selected signal events are high. The uncertainty in E_T^{miss} is calculated from those in the energy scales and resolutions of leptons and jets as well as those in the energy deposits unassociated with any identified physics objects [73].

Multijet backgrounds are only important for the resolved analysis in the 1-lepton channel and are estimated using data control regions. The dominant uncertainties are from the multijet E_T^{miss} and mass templates, obtained from MJCRs after subtracting W +jets and $t\bar{t}$ contributions. They are estimated by varying the W +jets and $t\bar{t}$ subtractions and are found to range from a few percent to up to 15%.

7.2 Theoretical uncertainties

Theoretical uncertainties affect the normalisations of diboson and single-top-quark backgrounds, the shapes of mass distributions of background processes, and the signal acceptances. They arise from sources such as the choices of event generators, parton distribution functions (PDFs), parton shower models, and underlying-event tunes. Modelling uncertainties in the shapes of the mass distributions are estimated by varying the renormalisation/factorisation scales, PDF set and α_s values used in the nominal MC samples. Alternative generators are used to estimate the uncertainties due to the choices of generators, parton shower models and event tunes.

Background contributions from diboson and single-top-quark processes are estimated from MC simulations and are normalised to their theoretical cross-sections. For the diboson process, the cross-section uncertainty is estimated to be 10% [61, 90]. An additional contribution from electroweak production, simulated with MADGRAPH5_AMC@NLO+PYTHIA8, leads to an increase in the normalisation of the diboson background for the VBF process by a factor of 1.60 (1.85) in the resolved (merged) analyses. A uncertainty of 50% is applied to the normalisation of the electroweak diboson contribution. The impact on the ggF/DY analysis is negligible. For the cross-section of single-top-quark processes, an uncertainty of 20% is assumed [91].

Background contributions from V +jets and $t\bar{t}$ are normalised using data control regions in the 1-lepton and 2-lepton channels. Their overall normalisations are free parameters in the likelihood fit (Sect. 8) and thus only uncertain-

ties in the shapes of discriminant variables are considered. For V +jets, the nominal SHERPA samples are compared with samples produced using MADGRAPH5_AMC@NLO. Moreover, the resummation scale and the CKKW [48, 49] matching scale in the nominal samples are also varied. The shape systematic uncertainty varies the background expectation in each bin and it is typically smaller than 10%, with the SHERPA-MADGRAPH comparison reaching 25% at the highest mass bin in the merged ggF/DY WZ untagged signal regions for the 1-lepton channel. For $t\bar{t}$, the default POWHEG-BOX sample is compared with the alternative MADGRAPH5_AMC@NLO sample interfaced with PYTHIA 8.230. The difference is found to be approximately 4% in the merged signal regions, twice the value in the resolved signal regions. The difference between the PYTHIA 8.230 sample using the A14 tune and the alternative HERWIG 7.04 [92, 93] sample using the H7UE set of tuned parameters [93] and the MMHT2014LO PDF set [94] is found to be between 2 and 5% in the various mass bins. The changes resulting from varying the parameter values for the nominal generator are less than 5%. In the 0-lepton channel, there is no pure control region to evaluate the V +jets and $t\bar{t}$ background, so the normalisation factors for the 0-lepton channel are assumed to be the same as for the 1-lepton channel (W +jets and $t\bar{t}$) and 2-lepton channel (Z +jets). Systematic uncertainties in this normalisation are obtained by the data/prediction double ratio between the default and the alternative MC generator and is estimated to be between 10 and 20% for V +jets and up to 30% for $t\bar{t}$. The $t\bar{t}$ background is negligible in the 2-lepton channel and therefore its uncertainty is not considered for this channel.

Uncertainties in the signal acceptances are estimated for the choice of PDF set and the modelling of initial- and final-state radiation. The PDF uncertainties are estimated by taking the acceptance difference due to applying internal PDF error sets and the difference due to choosing different PDF sets. The uncertainty due to ISR/FSR modelling is studied by varying parameter values in the tunes used and applied to the HVT, the RS graviton, and the RS radion models. These uncertainties, calculated for several resonant mass points, are retrieved for each model, production process and decay. The PDF uncertainties are evaluated to be under 5% for all models. ISR/FSR uncertainties range from 2% for the merged analysis of ggF HVT production to about 11% for the resolved analysis of VBF HVT production.

7.3 Impact of systematic uncertainties

The effects of systematic uncertainties on the search are studied for hypothesised signals using the signal-strength parameter μ , the ratio of the extracted cross-section (Sect. 8) to the injected hypothesised signal cross-section. The expected relative uncertainties in the best-fit μ value from the lead-

Table 3 Dominant relative uncertainties in the best-fit signal-strength parameter μ of hypothesised signal production of ggF RS graviton with $m(G_{KK}) = 600$ GeV and $m(G_{KK}) = 2$ TeV. For this study, the RS graviton production cross-section is assumed to be 100 fb at 600 GeV and 2 fb at 2 TeV, corresponding to approximately the expected median upper limits at these two mass values. Uncertainties with smaller contributions are not included

$m(G_{KK}) = 600$ GeV		$m(G_{KK}) = 2$ TeV	
Uncertainty source	$\Delta\mu/\mu$ (%)	Uncertainty source	$\Delta\mu/\mu$ (%)
Total	50	Total	59
Statistical	29	Statistical	48
Systematic	41	Systematic	34
Large- R jet	18	Large- R jet	24
MC statistics	16	MC statistics	17
Background normalisations	15	W/Z +jets modelling	15
Diboson modelling	12	Flavour tagging	5.5
W/Z +jets modelling	11	$t\bar{t}$ modelling	4.2
Small- R jet	9.7	Diboson modelling	3.9
$t\bar{t}$ modelling	8.1	Single- t modelling	3.3

ing sources of systematic uncertainties are shown in Table 3 for the ggF production of an RS graviton with $m(G_{KK}) = 600$ GeV and 2 TeV. Apart from the statistical uncertainties in the data, the uncertainties with the largest impact on the sensitivity of the searches are from the sizes of the MC samples, measurements of small- R and large- R jets, background normalisations and modellings. Uncertainties related to the jet measurements, such as jet energy scale and resolution, affect the search primarily through their impacts on the shapes of the discriminant mass distributions of both signal and background processes. Uncertainties on the normalisations of background contributions estimated using CRs arise from CR statistics as well as MC event generators used to extrapolate from CRs to SRs. Background modelling uncertainties include uncertainties on their normalisations, if estimated from MC simulations, as well as on the shapes of the mass distributions. The normalisations are affected by the uncertainties on the theoretical cross sections and on the luminosity. The shapes are affected by, in addition to experimental sources, theoretical sources such as PDF, ISR/FSR, and MC generator etc. For signals with higher mass, the data statistical uncertainty becomes dominant. The effects of systematic uncertainties for the other searches are similar.

8 Results and interpretations

8.1 Statistical procedure

The statistical analysis is based on the framework described in Refs. [95–97]. A profile-likelihood-ratio test statistic is used to test the compatibility of the background-only hypothesis and the observed data, and to test the signal-plus-background hypothesis for the production of a heavy resonance X , with its production cross-section in the VV decay mode, $\sigma(pp \rightarrow X \rightarrow VV)$, as the parameter of interest. Maximum-likelihood fits are made to the observed binned

distributions of the final discriminants in SRs, m_T in 0-lepton, $m_{\ell\nu J}$ or $m_{\ell\nu jj}$ in 1-lepton and $m_{\ell\ell J}$ or $m_{\ell\ell jj}$ in 2-lepton, and to the numbers of observed events in CRs simultaneously. The mass ranges fitted are 300–3000 GeV for the resolved analysis and 500–6000 GeV for the merged analysis. The normalisations of the V +jets and $t\bar{t}$ contributions are free parameters in these fits and are constrained by the data in both the CRs and SRs. Systematic uncertainties, described in Sect. 7, and their correlations are incorporated as constraints into the likelihood calculations through nuisance parameters, where each is given a prior distribution based on individual studies or is allowed to float freely, constrained simultaneously by the SRs and CRs.

Two types of fits, referred to as the $WW + ZZ$ and WZ fits below, are performed. The $WW + ZZ$ fits include all 21 SRs of the $X \rightarrow WW$ and $X \rightarrow ZZ$ searches and the WZ fit includes the 19 SRs of the $X \rightarrow WZ$ search, along with their respective CRs. Separate fits are performed for the ggF/DY and VBF production modes and for different resonance mass hypotheses, but including SRs and CRs in both the ggF/DY and VBF categories. The $WW + ZZ$ fits are used to search for the RS radion and RS graviton signals as both the WW and ZZ decay modes are expected from these resonances. The fits are also used to search for HVT $Z' \rightarrow WW$ production. In this case, the $X \rightarrow ZZ$ SRs effectively become additional CRs for the search. The WZ fits are used to search for HVT $W' \rightarrow WZ$ production.

8.2 Data and background comparisons

To test the compatibility of the data and the background expectations, the data are first fit to the background-only hypothesis for both the $WW + ZZ$ and WZ fits. Good agreement is found between the observed mass distributions and the estimated post-fit background contributions in all SRs. As examples, the data are compared with the expected backgrounds from the $WW + ZZ$ fit in Fig. 9 for the m_T distribu-

Fig. 9 Comparisons of the observed data and the expected background distributions of m_T in the 6 ZZ SRs of the 0-lepton channel. The background predictions are obtained through a background-only simultaneous fit to the 6 WW and 15 ZZ SRs and their respective V +jets and $t\bar{t}$ CRs (see text). The bottom panes show the ratios of the observed data to the background predictions. The blue triangles indicate bins where the ratio is non-zero and outside the vertical range of the plot. The hatched bands represent the uncertainties in the total background predictions, combining statistical and systematic contributions

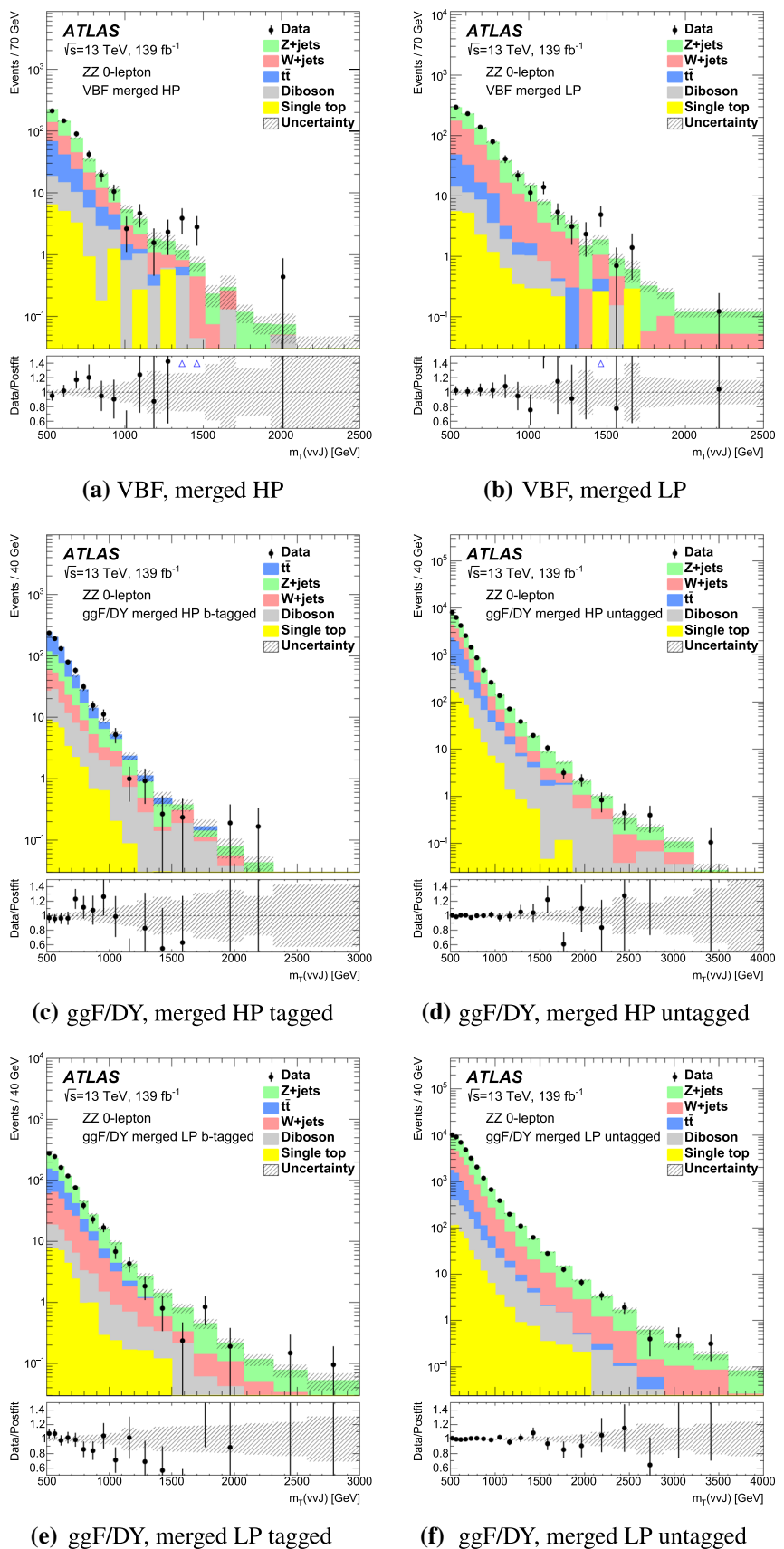
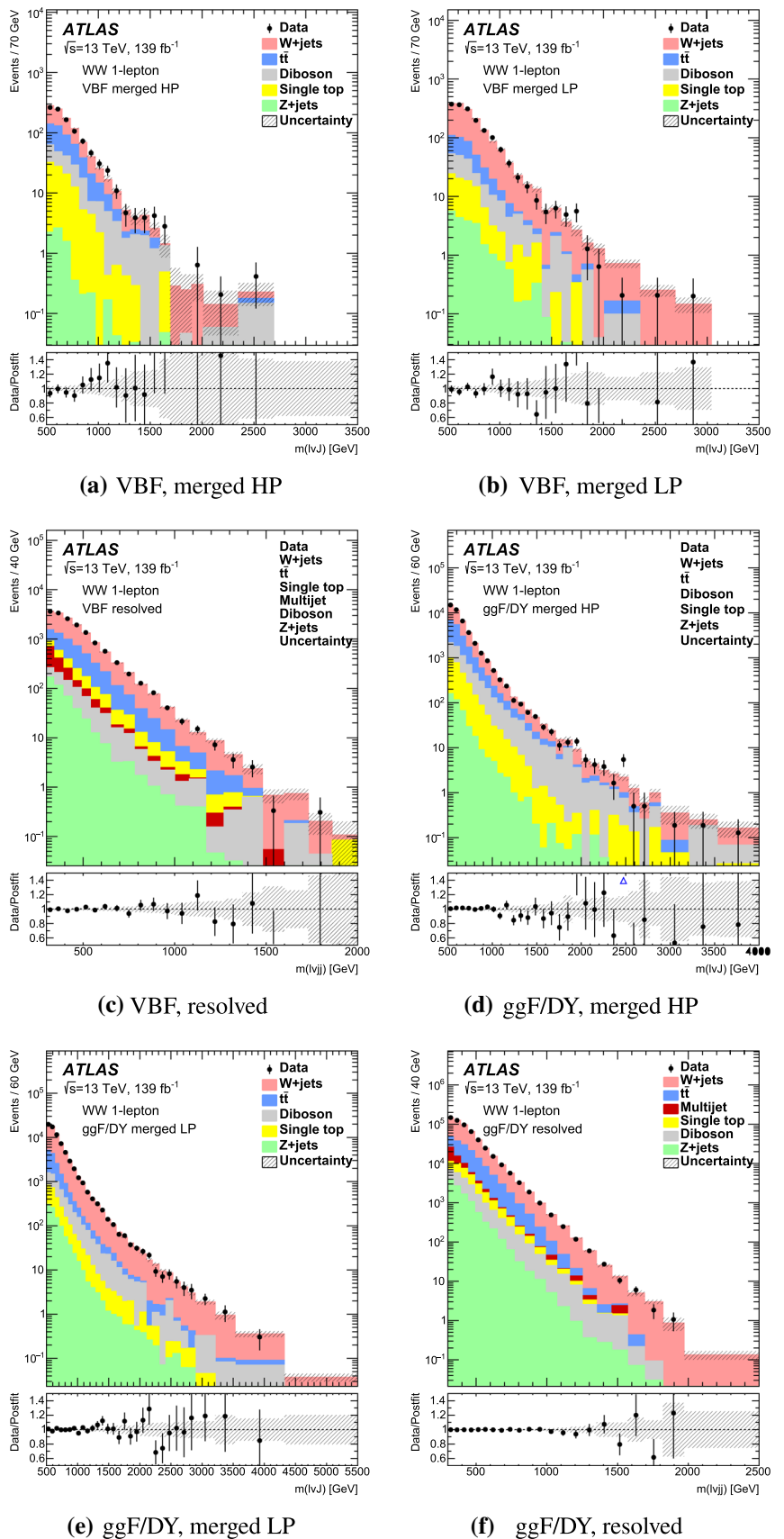


Fig. 10 Comparisons of the observed data and the expected background distributions of $m_{\ell\nu jj}$ or $m_{\ell\nu J}$ in the 6 WW SRs of the 1-lepton channel. The background predictions are obtained through a background-only simultaneous fit to the 6 WW and 15 ZZ SRs and their respective V +jets and $t\bar{t}$ CRs (see text). The bottom panes show the ratios of the observed data to the background predictions. The blue triangles indicate bins where the ratio is non-zero and outside the vertical range of the plot. The hatched bands represent the uncertainties in the total background predictions, combining statistical and systematic contributions



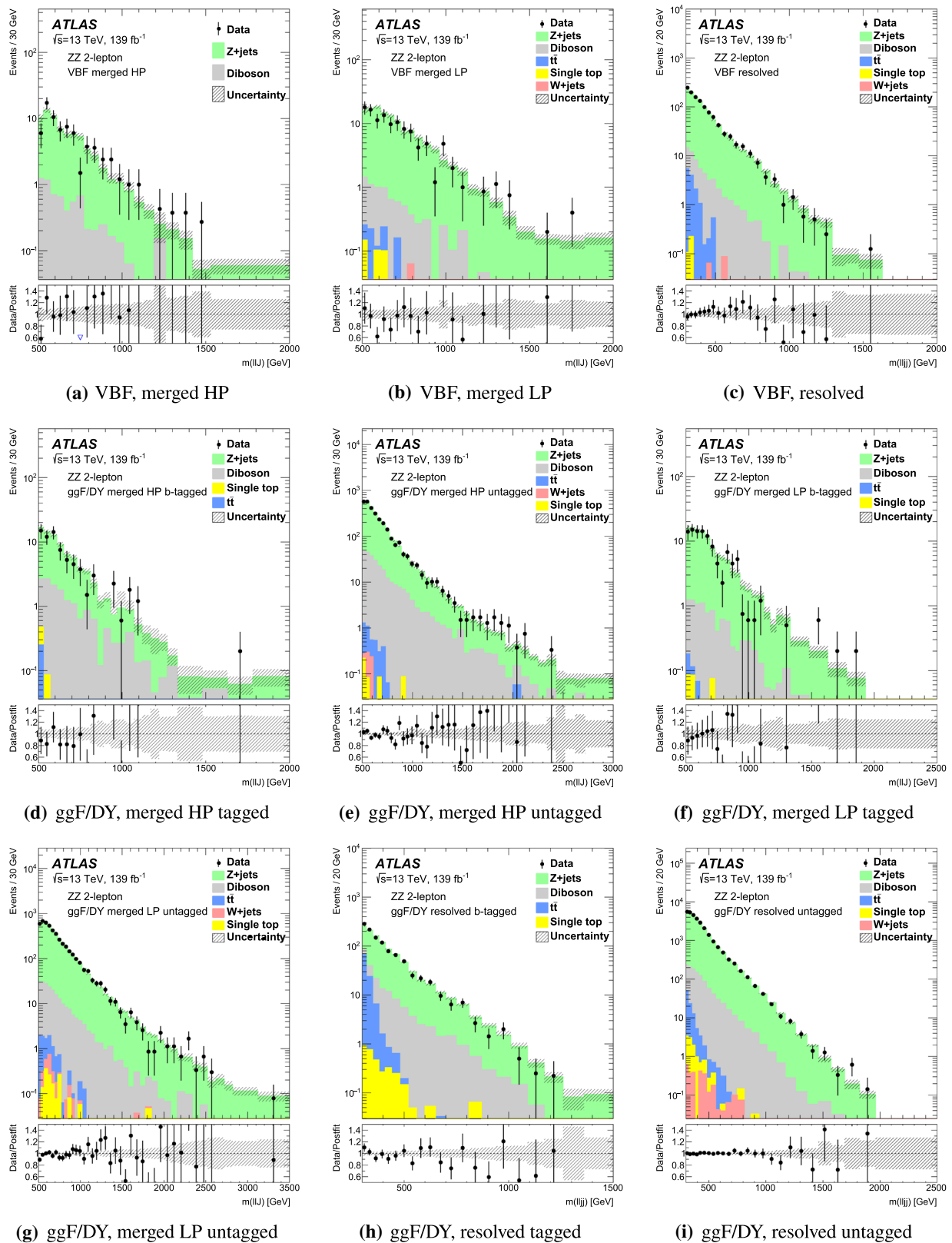


Fig. 11 Comparisons of the observed data and the expected background distributions of $m_{\ell\ell jj}$ or $m_{\ell\ell j}$ in the 9 ZZ SRs of the 2-lepton channel. The background predictions are obtained through a background-only simultaneous fit to the 6 WW and 15 ZZ SRs and their respective $V + \text{jets}$ and $t\bar{t}$ CRs (see text). The bottom panes show

the ratios of the observed data to the background predictions. The blue triangles indicate bins where the ratio is non-zero and outside the vertical range of the plot. The hatched bands represent the uncertainties in the total background predictions, combining statistical and systematic contributions

Table 4 The expected background events with contributions from individual sources in 6 WW and 15 ZZ SRs compared with the data. The backgrounds are estimated from a background-only simultaneous fit to all WW and ZZ SRs and their corresponding CRs

Channel	$V \rightarrow qq$ recon.	Signal regions	Background estimates							Data	
			W+jets	Z+jets	$t\bar{t}$	Diboson	Single-t	Multijet	Total		
0-lepton (ZZ)											
VBF category											
Merged	HP		169 ± 12	228 ± 16	102 ± 10	51 ± 10	24 ± 4	-	574 ± 25	589	
	LP		370 ± 23	411 ± 20	75 ± 8	30 ± 4	21 ± 4	-	906 ± 33	936	
ggF/DY category											
Merged	HP	Tag	133 ± 14	270 ± 40	437 ± 31	100 ± 10	45 ± 7	-	982 ± 60	978	
		Untag	7600 ± 400	14 300 ± 600	6030 ± 270	2300 ± 180	840 ± 110	-	31 100 ± 800	31 074	
	LP	Tag	259 ± 28	560 ± 50	342 ± 24	67 ± 7	43 ± 7	-	1270 ± 70	1277	
		Untag	16 300 ± 900	28 600 ± 1100	5040 ± 220	1760 ± 150	600 ± 80	-	52 400 ± 1500	52 396	
VBF category											
Merged	HP		530 ± 28	8.3 ± 0.5	321 ± 22	141 ± 27	113 ± 21	-	1110 ± 50	1096	
	LP		1380 ± 40	24.5 ± 1.1	228 ± 17	150 ± 33	83 ± 16	-	1870 ± 60	1846	
Resolved			11 360 ± 190	530 ± 10	4060 ± 130	590 ± 80	1070 ± 210	960 ± 110	18 570 ± 340	18 530	
ggF/DY category											
Merged	HP		24 820 ± 170	463 ± 5	13 890 ± 220	4910 ± 250	2800 ± 400	-	46 900 ± 500	47330	
	LP		60 270 ± 240	1095 ± 8	11 050 ± 160	3950 ± 210	1970 ± 250	-	78 300 ± 400	78380	
Resolved			443 500 ± 1800	12 480 ± 40	126 000 ± 1500	16 800 ± 1200	21 200 ± 2800	27 200 ± 1400	647 000 ± 4000	645610	
VBF category											
Merged	HP		0	87 ± 6	0.081 ± 0.009	9.6 ± 1.2	0	-	97 ± 6	101	
	LP		0.133 ± 0.011	170 ± 8	0.85 ± 0.07	9.9 ± 1.2	0.43 ± 0.07	-	181 ± 8	162	
Resolved			0.272 ± 0.012	1566 ± 29	17.0 ± 0.7	72 ± 10	0.48 ± 0.32	-	1656 ± 31	1685	
ggF/DY category											
2-lepton (ZZ)	Merged	HP	Tag	0.0135 ± 0.0043	85 ± 6	0.283 ± 0.035	21.1 ± 2.3	0.34 ± 0.05	-	107 ± 7	94
			Untag	0.772 ± 0.010	3300 ± 40	4.27 ± 0.08	361 ± 32	0.58 ± 0.11	-	3670 ± 50	3671
	LP	Tag	0.0135 ± 0.0043	138 ± 8	0.313 ± 0.034	12.8 ± 1.4	0.30 ± 0.04	-	152 ± 8	141	
		Untag	2.341 ± 0.017	5920 ± 50	10.16 ± 0.16	278 ± 26	2.03 ± 0.29	-	6220 ± 60	6095	
	Resolved	Tag	-	1323 ± 26	110 ± 10	159 ± 12	4.7 ± 0.8	-	1600 ± 30	1583	
		Untag	4.681 ± 0.026	42 750 ± 160	110.6 ± 1.5	1800 ± 100	13.4 ± 2.0	-	44 650 ± 190	44 604	

tions of the 0-lepton channel, in Fig. 10 for the $m_{\ell\nu jj}/m_{\ell\nu J}$ distributions of the 1-lepton channel, and in Fig. 11 for the $m_{\ell\ell jj}/m_{\ell\ell J}$ distributions of the 2-lepton channel. The largest excess is seen at $m_T \sim 1.5$ TeV in Fig. 9a. This excess is estimated to have a local significance of 2.8 standard deviations when modelled using RS radion production. The differences between the pre- and post-fit background estimates are less than 10% for a majority of the bins of the mass distributions. Larger differences, but comparable with the sizes of the statistical uncertainties, are observed for some bins with small numbers of events. Moreover the fits do not significantly alter the shapes of the background distributions for most of the signal regions. The largest change in the shape, up to 15%, is seen in the mass distribution of the VBF merged HP signal region in the 1-lepton channel. The difference is traced primarily to the difference in the simulated $V + jets$ samples produced with the SHERPA and MADGRAPH5 programs. Table 4 shows the post-fit estimated background event yields from different sources in all WW and ZZ SRs compared with the numbers of observed events in data. A similar level of agreement is obtained for the WZ fit.

8.3 Limits on the production of heavy resonances

Constraints on the production of heavy resonances are derived by repeating the fit to the signal-plus-background hypothesis for different signal models. Upper limits on cross-sections are calculated with a modified frequentist method [98], also known as CL_s , using the \tilde{q}_μ test statistic in the asymptotic approximation [99] for resonance masses below 3 (1) TeV for ggF/DY (VBF) production. For heavier resonances, the low number of events makes the approximation unreliable and the limits are obtained through pseudo-experiments instead. The observed (expected) limits from pseudo-experiments are approximately 20–30% (10–20%) higher than those from the asymptotic calculations at the highest resonance masses in the search.

8.3.1 Limits on the production of RS radions

Upper limits on the production cross-section of an RS radion in its VV decay modes, $\sigma(pp \rightarrow R \rightarrow VV)$, are obtained by combining the $R \rightarrow WW$ and $R \rightarrow ZZ$ searches in the three leptonic final states. The 1-lepton channel is sensitive to the $R \rightarrow WW$ decay while the 0-lepton and 2-lepton channels are sensitive to the $R \rightarrow ZZ$ decay. The limits are

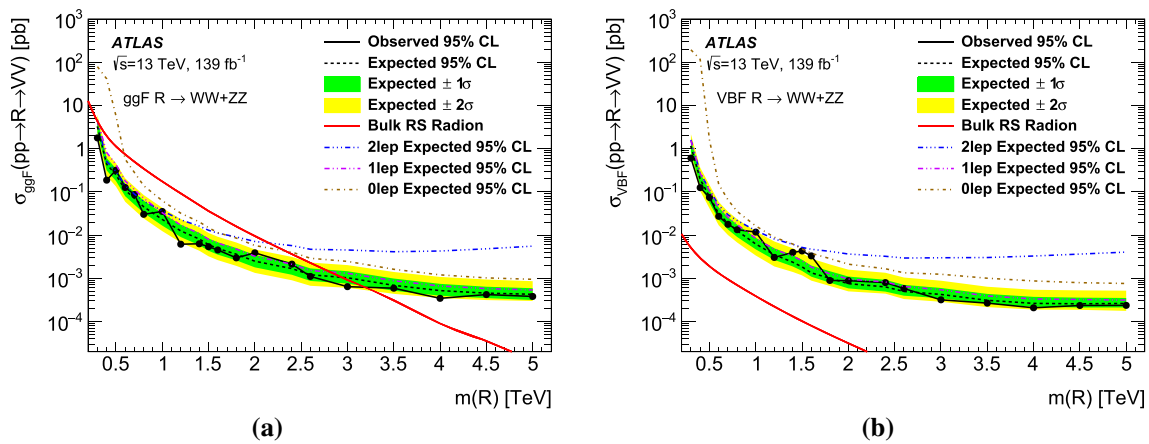


Fig. 12 Observed (black solid curve) and expected (black dashed curve) 95% CL upper limits on the **a** ggF and **b** VBF production cross-section of an RS radion at $\sqrt{s} = 13$ TeV in its diboson (WW and ZZ) decay mode as functions of the RS radion mass, combining the $R \rightarrow WW$ and $R \rightarrow ZZ$ searches in the three leptonic channels. The theoretical prediction for $\mathcal{B}(R \rightarrow WW)/\mathcal{B}(R \rightarrow ZZ)$ is assumed for the combination of the WW and ZZ decay modes. The green (inner)

and yellow (outer) bands represent $\pm 1\sigma$ and $\pm 2\sigma$ uncertainty in the expected limits. Limits expected from individual leptonic channels (dot-dashed curves in blue, magenta, and brown) are also shown for comparison. Limits are calculated in the asymptotic approximation below 3 (1) TeV and are obtained from pseudo-experiments above that for ggF (VBF) production. Theoretical predictions (red solid curve) as functions of the RS radion mass are overlaid

derived separately for the ggF and VBF processes through the $WW + ZZ$ fits for different RS radion mass hypotheses. Figure 12 shows the observed and expected upper limits at 95% confidence level (CL) as functions of its mass for both the ggF and VBF processes. The observed limits for the VBF process are noticeably higher than the expected limits around an RS radion mass of 1.5 TeV, reflecting the excess seen in the m_T distribution from the merged HP signal region of the 0-lepton channel. The observed (expected) combined limit on $\sigma(pp \rightarrow R \rightarrow VV)$ varies from 1.8 (3.3) pb at 300 GeV to 0.38 (0.43) fb at 5 TeV for the ggF production process and from 0.60 (1.15) pb at 300 GeV to 0.23 (0.26) fb at 5 TeV for the VBF production process. These observed (expected) upper limits exclude the ggF production of an RS radion with a mass below 3.2 (2.9) TeV while no mass exclusion can be derived for the VBF production.

Except for masses below approximately 1 TeV, the 1-lepton channel dominates the combined search sensitivities for both the ggF and VBF processes. This is not surprising as $\mathcal{B}(R \rightarrow WW)$ is $\approx 2 \times \mathcal{B}(R \rightarrow ZZ)$ in the RS radion model. The 2-lepton channel is the most sensitive at low masses, benefiting from its good mass resolution and small background contributions, and is the least sensitive at high masses because of its small expected signal yields. The 0-lepton channel has the worst sensitivity at low masses and contributes non-negligibly at high masses.

For the RS radion search here as well as the HVT and RS graviton searches presented below, the resolved analysis is important for masses below 600 GeV while the merged analysis dominates the search for higher masses. The LP signal regions improve the cross-section sensitivities of the

merged analysis by approximately 5% for the entire mass range of the search. The missing $X \rightarrow WV \rightarrow \ell\nu qq, \tau\nu qq$ signal contribution in the 0-lepton channel as discussed in Sect. 5.6, if included, would lower the expected cross-section upper limits by up to 4% at 2 TeV and up to 10% at 5 TeV.

8.3.2 Limits on the production of HVT resonances

Upper limits on the production cross-sections of HVT W' and Z' bosons in their WZ and WW decays are obtained through the WZ and $WW + ZZ$ fits, respectively. All leptonic channels contribute to the $W' \rightarrow WZ$ search while only the 1-lepton channel contributes to the $Z' \rightarrow WW$ search. Limits as functions of resonance masses are shown in Figs. 13 and 14 for $W' \rightarrow WZ$ and $Z' \rightarrow WW$, respectively, for both DY and VBF processes. The theoretical predictions of the HVT Model A, Model B, and Model C are also shown for comparison. The observed (expected) $\sigma(pp \rightarrow W' \rightarrow WZ)$ limit ranges from 1.9 (2.5) pb at 300 GeV to 0.16 (0.17) fb at 5 TeV for DY production and from 1.3 (1.8) pb at 300 GeV to 0.35 (0.51) fb at 4 TeV for VBF production. These observed (expected) limits exclude an HVT W' boson produced in the DY process lighter than 3.9 (3.8) TeV for Model A and 4.3 (4.0) TeV for Model B, but fail to exclude any mass region in the VBF process for the benchmark Model C. For both production processes, the 2-lepton channel is the most sensitive for masses up to ~ 1.5 TeV. At high masses, the sensitivity is dominated by the 0-lepton and 1-lepton channels.

Only the 1-lepton channel contributes to the $Z' \rightarrow WW$ search. The observed (expected) $\sigma(pp \rightarrow Z' \rightarrow WW)$ limit ranges from 0.9 (2.7) pb at 300 GeV to 0.18 (0.18) fb at 5 TeV

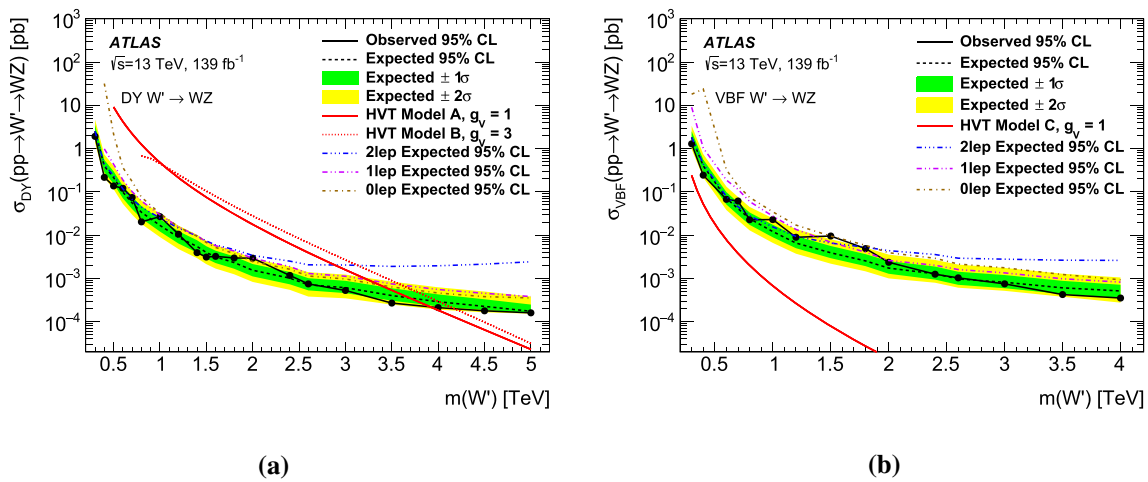


Fig. 13 Observed (black solid curve) and expected (black dashed curve) 95% CL upper limits on the **a** DY and **b** VBF production cross-section of an HVT W' boson at $\sqrt{s} = 13$ TeV in the WZ decay mode as functions of its mass, combining searches in the three leptonic channels. The green (inner) and yellow (outer) bands represent $\pm 1\sigma$ and $\pm 2\sigma$ uncertainty in the expected limits. Limits expected from individual leptonic channels (dot-dashed curves in blue, magenta, and brown) are also

shown for comparison. Limits are calculated in the asymptotic approximation below 3 (1) TeV and are obtained from pseudo-experiments above that for DY (VBF) production. Theoretical predictions as functions of the W' boson mass are overlaid in **a** for Model A (red solid curve) and Model B (red dotted curve) and in **b** for Model C (red solid curve)

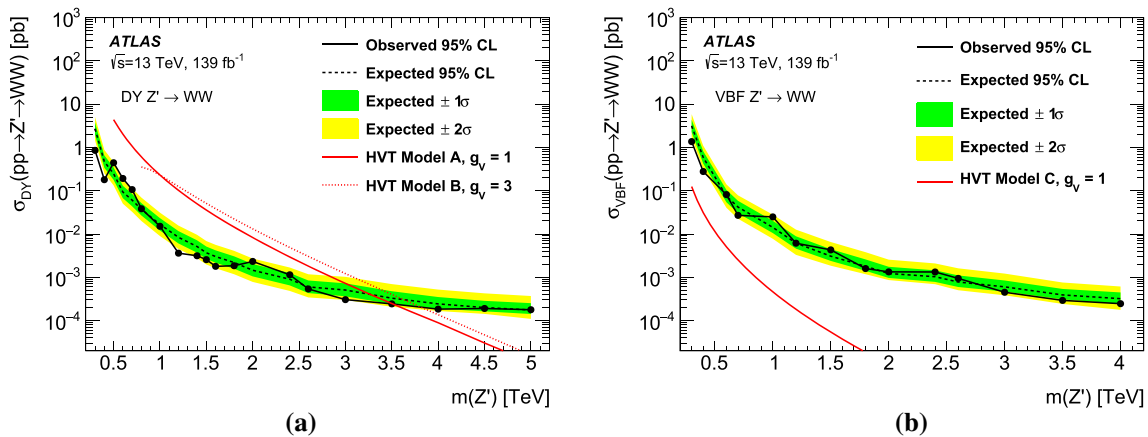


Fig. 14 Observed (black solid curve) and expected (black dashed curve) 95% CL upper limits on the **a** DY and **b** VBF production cross-section of an HVT Z' boson at $\sqrt{s} = 13$ TeV in the WW decay mode from the search in the 1-lepton channel. The green (inner) and yellow (outer) bands represent $\pm 1\sigma$ and $\pm 2\sigma$ uncertainty in

the expected limits. Limits are calculated in the asymptotic approximation below 3 (1) TeV and are obtained from pseudo-experiments above that for DY (VBF) production. Theoretical predictions of the Z' boson mass are overlaid in **a** for Model A (red solid curve) and Model B (red dotted curve) and in **b** for Model C (red solid curve)

for the DY process and from 1.36 (3.15) pb at 300 GeV to 0.25 (0.32) fb at 4 TeV for the VBF process. These limits exclude an HVT Z' boson lighter than 3.5 (3.4) TeV for Model A and 3.9 (3.7) TeV for Model B in the DY process.

8.3.3 Limits on the production of RS gravitons

Upper limits on the production cross-section of an RS graviton in its VV decays, $\sigma(pp \rightarrow G_{KK} \rightarrow VV)$, are obtained following the same procedure used to derive the RS radion

limits. The observed and expected upper limits as functions of its mass for both the ggF and VBF processes are shown in Fig. 15. The observed (expected) limit varies from 1.4 (3.6) pb at 300 GeV to 0.26 (0.28) fb at 5 TeV for the ggF production process and from 0.40 (0.61) pb at 300 GeV to 0.30 (0.33) fb at 5 TeV for the VBF production process. Compared with theory cross-sections, with the benchmark parameters, the observed (expected) upper limits at 95% CL exclude the production of an RS graviton

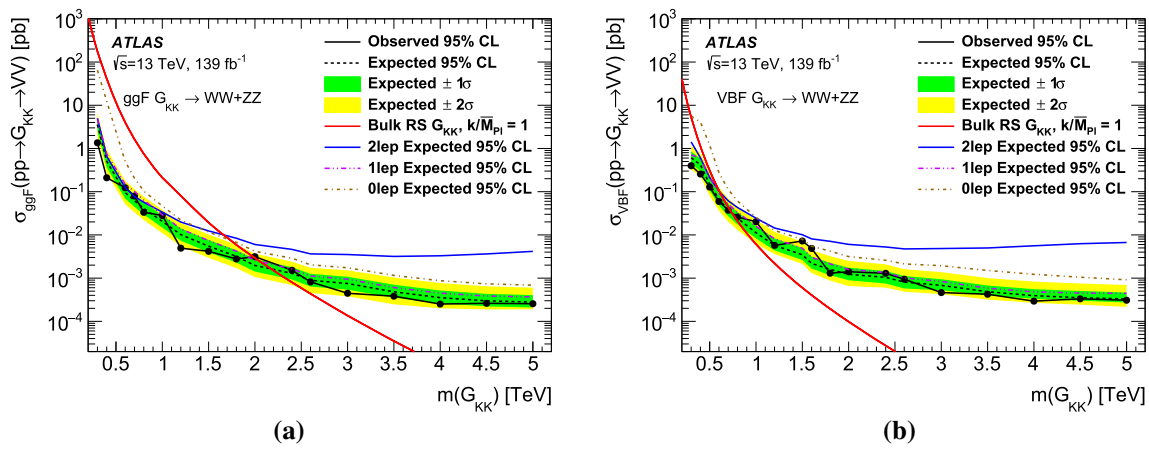


Fig. 15 Observed (black solid curve) and expected (black dashed curve) 95% CL upper limits on the **a** ggF and **b** VBF production cross-section of an RS graviton at $\sqrt{s} = 13$ TeV in its diboson (WW and ZZ) decay mode as functions of its mass, combining the searches for the $G_{KK} \rightarrow WW$ and $G_{KK} \rightarrow ZZ$ decays in the three leptonic channels. The theoretical prediction for $\mathcal{B}(G_{KK} \rightarrow WW)/\mathcal{B}(G_{KK} \rightarrow ZZ)$ is assumed for the combination of the WW and ZZ decay modes. The

green (inner) and yellow (outer) bands represent $\pm 1\sigma$ and $\pm 2\sigma$ uncertainty in the expected limits. Limits expected from individual leptonic channels (dashed curves in blue, magenta, and brown) are also shown for comparison. Limits are calculated in the asymptotic approximation below 3 (1) TeV and are obtained from pseudo-experiments above that for ggF (VBF) production. Theoretical predictions (red solid curves) for the chosen model as functions of the RS graviton mass are overlaid

Table 5 Observed (expected) 95% CL lower limits on the mass, in TeV, of different resonances in the benchmark models studied. The symbol “–” means no limit is set

Production process	RS radion	HVT		RS graviton
		W'	Z'	
ggF/DY	3.2 (2.9)	Model A	3.9 (3.8) 3.5 (3.4)	2.0 (2.2)
		Model B	4.3 (4.0) 3.9 (3.7)	
VBF	–	Model C	– –	0.76 (0.77)

lighter than 2.0 (2.2) TeV in the ggF process and lighter than 0.76 (0.77) TeV in the VBF process.

Similar to the RS radion case, the 1-lepton channel contributes dominantly to the combined search sensitivities at high masses while the 2-lepton channel is slightly more sensitive than the 1-lepton channel for masses below ~ 1 TeV. The 0-lepton channel is the least sensitive at low masses, but provides significant contributions at high masses.

8.4 Comparisons of the limits

Table 5 summarises the observed and expected 95% CL lower limits on the masses of the resonances in the benchmark models studied in this paper. These mass limits and the cross-section upper limits presented above are significantly more stringent than those published previously from similar searches. The cross-section upper limits are a factor of

three or more lower than those of the search using the same data set, but in the hadronic $VV \rightarrow JJ$ final state [16]. Compared to the searches with the 36.1 fb¹ data set in the same leptonic final states [22,23], an improvement of a factor of three or more in the cross-section upper limits is also obtained for most of the searches at the highest masses. The observed lower mass limits of this search for the HVT W' and Z' as well as for the RS graviton are also similar to those from the combinations of searches in the fully-leptonic, semi-leptonic, and fully-hadronic final states from smaller datasets of ~ 36 fb¹ [12,15].

9 Summary

Searches for the production of heavy diboson resonances are performed using the proton–proton collision data with an

integrated luminosity of 139 fb^{-1} at $\sqrt{s} = 13 \text{ TeV}$. The data were recorded by the ATLAS experiment between 2015 and 2018 at the LHC. The WW , ZZ and WZ decay modes of the heavy resonances in the 0-lepton, 1-lepton and 2-lepton final states are considered. The data are found to be in good agreement with background expectations. Upper limits on the production of heavy resonances in the mass range 300–5000 GeV through gluon–gluon fusion, Drell–Yan or vector-boson fusion processes are derived for Standard Model extensions with an additional neutral scalar, a heavy vector triplet, or warped extra dimensions.

Combining the WW and ZZ decay modes, the observed 95% confidence-level upper limit on $\sigma(pp \rightarrow X \rightarrow VV)$ for the ggF (VBF) process ranges from 1.8 (0.60) pb at 300 GeV to 0.38 (0.23) fb at 5 TeV for an RS radion and from 1.4 (0.40) pb at 300 GeV to 0.26 (0.30) fb at 5 TeV for an RS graviton. These observed limits set lower mass limits of 3.2 TeV for the ggF production of an RS radion, and 2.0 (0.76) TeV for the ggF (VBF) production of an RS graviton.

For the production of W' and Z' bosons in the HVT framework, the observed upper limit on $\sigma(pp \rightarrow W' \rightarrow WZ)$ varies from 1.9 pb at 300 GeV to 0.16 fb at 5 TeV for DY production and from 1.3 pb at 300 GeV to 0.35 fb at 4 TeV for VBF production. Similarly, the limits on $\sigma(pp \rightarrow Z' \rightarrow WW)$ are observed to vary from 0.9 pb at 300 GeV to 0.18 fb at 5 TeV for DY production and from 1.36 pb at 300 GeV to 0.25 fb at 4 TeV for VBF production. In the benchmark Model A (Model B), these cross-section upper limits exclude the ggF production of a W' boson with $m(W') < 3.9$ (4.3) TeV and a Z' boson with $m(Z') < 3.5$ (3.9) TeV.

Acknowledgements We thank CERN for the very successful operation of the LHC, as well as the support staff from our institutions without whom ATLAS could not be operated efficiently. We acknowledge the support of ANPCyT, Argentina; YerPhI, Armenia; ARC, Australia; BMWFW and FWF, Austria; ANAS, Azerbaijan; SSTC, Belarus; CNPq and FAPESP, Brazil; NSERC, NRC and CFI, Canada; CERN; ANID, Chile; CAS, MOST and NSFC, China; COLCIENCIAS, Colombia; MSMT CR, MPO CR and VSC CR, Czech Republic; D NRF and DNSRC, Denmark; IN2P3-CNRS and CEA-DRF/IRFU, France; SRNSFG, Georgia; BMBF, HGF and MPG, Germany; GSRT, Greece; RGC and Hong Kong SAR, China; ISF and Benozziyo Center, Israel; INFN, Italy; MEXT and JSPS, Japan; CNRST, Morocco; NWO, Netherlands; RCN, Norway; MNiSW and NCN, Poland; FCT, Portugal; MNE/IFA, Romania; MES of Russia and NRC KI, Russia Federation; JINR; MESTD, Serbia; MSSR, Slovakia; ARRS and MIZŠ, Slovenia; DST/NRF, South Africa; MICINN, Spain; SRC and Wallenberg Foundation, Sweden; SERI, SNSF and Cantons of Bern and Geneva, Switzerland; MOST, Taiwan; TAEK, Turkey; STFC, UK; DOE and NSF, United States of America. In addition, individual groups and members have received support from BCKDF, CANARIE, Compute Canada and CRC, Canada; ERC, ERDF, Horizon 2020, Marie Skłodowska-Curie Actions and COST, European Union; Investissements d'Avenir Labex, Investissements d'Avenir Idex and ANR, France; DFG and AvH Foundation, Germany; Herakleitos, Thales and Aristeia programmes co-financed by EU-ESF and the Greek NSRF, Greece; BSF-NSF and GIF, Israel; La Caixa Banking Foundation, CERCA Programme Gener-

alitat de Catalunya and PROMETEO and GenT Programmes Generalitat Valenciana, Spain; Göran Gustafssons Stiftelse, Sweden; The Royal Society and Leverhulme Trust, UK.

The crucial computing support from all WLCG partners is acknowledged gratefully, in particular from CERN, the ATLAS Tier-1 facilities at TRIUMF (Canada), NDGF (Denmark, Norway, Sweden), CC-IN2P3 (France), KIT/GridKA (Germany), INFN-CNAF (Italy), NL-T1 (Netherlands), PIC (Spain), ASGC (Taiwan), RAL (UK) and BNL (USA), the Tier-2 facilities worldwide and large non-WLCG resource providers. Major contributors of computing resources are listed in Ref. [100].

Data Availability Statement This manuscript has no associated data or the data will not be deposited. [Authors' comment: All ATLAS scientific output is published in journals, and preliminary results are made available in Conference Notes. All are openly available, without restriction on use by external parties beyond copyright law and the standard conditions agreed by CERN. Data associated with journal publications are also made available: tables and data from plots (e.g. cross section values, likelihood profiles, selection efficiencies, cross section limits, ...) are stored in appropriate repositories such as HEPDATA (<http://hepdata.cedar.ac.uk/>). ATLAS also strives to make additional material related to the paper available that allows a reinterpretation of the data in the context of new theoretical models. For example, an extended encapsulation of the analysis is often provided for measurements in the framework of RIVET (<http://rivet.hepforge.org/>). This information is taken from the ATLAS Data Access Policy, which is a public document that can be downloaded from <http://opendata.cern.ch/record/413> [opendata.cern.ch].].

Open Access This article is licensed under a Creative Commons Attribution 4.0 International License, which permits use, sharing, adaptation, distribution and reproduction in any medium or format, as long as you give appropriate credit to the original author(s) and the source, provide a link to the Creative Commons licence, and indicate if changes were made. The images or other third party material in this article are included in the article's Creative Commons licence, unless indicated otherwise in a credit line to the material. If material is not included in the article's Creative Commons licence and your intended use is not permitted by statutory regulation or exceeds the permitted use, you will need to obtain permission directly from the copyright holder. To view a copy of this licence, visit <http://creativecommons.org/licenses/by/4.0/>.

Funded by SCOAP³.

References

1. G.C. Branco et al., Theory and phenomenology of two-Higgs-doublet models. *Phys. Rep.* **516**, 1 (2012). [arXiv:1106.0034](https://arxiv.org/abs/1106.0034) [hep-ph]
2. M.J. Dugan, H. Georgi, D.B. Kaplan, Anatomy of a composite Higgs model. *Nucl. Phys. B* **254**, 299 (1985)
3. K. Agashe, R. Contino, A. Pomarol, The minimal composite Higgs model. *Nucl. Phys. B* **719**, 165 (2005). [arXiv:hep-ph/0412089](https://arxiv.org/abs/hep-ph/0412089)
4. E. Eichten, K. Lane, Low-scale technicolor at the Tevatron and LHC. *Phys. Lett. B* **669**, 235 (2008). [arXiv:0706.2339](https://arxiv.org/abs/0706.2339) [hep-ph]
5. S. Catterall, L. Del Debbio, J. Giedt, L. Keegan, MCRG minimal walking technicolor. *Phys. Rev. D* **85**, 094501 (2012). [arXiv:1108.3794](https://arxiv.org/abs/1108.3794) [hep-ph]
6. J.R. Andersen et al., Discovering technicolor. *Eur. Phys. J. Plus* **126**, 81 (2011). [arXiv:1104.1255](https://arxiv.org/abs/1104.1255) [hep-ph]

7. L. Randall, R. Sundrum, A large mass hierarchy from a small extra dimension. *Phys. Rev. Lett.* **83**, 3370 (1999). [arXiv:hep-ph/9905221](#)
8. H. Davoudiasl, J.L. Hewett, T.G. Rizzo, Bulk gauge fields in the Randall–Sundrum model. *Phys. Lett. B* **473**, 43 (2000). [arXiv:hep-ph/9911262](#)
9. ATLAS Collaboration, Search for an additional, heavy Higgs boson in the $H \rightarrow ZZ$ decay channel at $\sqrt{s} = 8$ TeV in pp collision data with the ATLAS detector. *Eur. Phys. J. C* **76**, 45 (2016). [arXiv:1507.05930](#) [hep-ex]
10. ATLAS Collaboration, Combination of searches for WW, WZ, and ZZ resonances in pp collisions at $\sqrt{s} = 8$ TeV with the ATLAS detector. *Phys. Lett. B* **755**, 285 (2016). [arXiv:1512.05099](#) [hep-ex]
11. C.M.S. Collaboration, Combination of searches for heavy resonances decaying to WW, WZ, ZZ, WH, and ZH boson pairs in proton-proton collisions at $\sqrt{s} = 8$ TeV and 13 TeV. *Phys. Lett. B* **774**, 533 (2017). [arXiv:1705.09171](#) [hep-ex]
12. C.M.S. Collaboration, Combination of CMS searches for heavy resonances decaying to pairs of bosons or leptons. *Phys. Lett. B* **798**, 134952 (2019). [arXiv:1906.00057](#) [hep-ex]
13. ATLAS Collaboration, Searches for heavy diboson resonances in pp collisions at $\sqrt{s} = 13$ TeV with the ATLAS detector. *JHEP* **09**, 173 (2016). [arXiv:1606.04833](#) [hep-ex]
14. ATLAS Collaboration, Search for diboson resonances with boson-tagged jets in pp collisions at $\sqrt{s} = 13$ TeV with the ATLAS detector. *Phys. Lett. B* **777**, 91 (2018). [arXiv:1708.04445](#) [hep-ex]
15. ATLAS Collaboration, Combination of searches for heavy resonances decaying into bosonic and leptonic final states using 36 fb^{-1} of proton–proton collision data at $\sqrt{s} = 13$ TeV with the ATLAS detector. *Phys. Rev. D* **98**, 052008 (2018). [arXiv:1808.02380](#) [hep-ex]
16. ATLAS Collaboration, Search for diboson resonances in hadronic final states in 139 fb^{-1} of pp collisions at $\sqrt{s} = 13$ TeV with the ATLAS detector. *JHEP* **09**, 091 (2019). [arXiv:1906.08589](#) [hep-ex]
17. W.D. Goldberger, M.B. Wise, Modulus stabilization with bulk fields. *Phys. Rev. Lett.* **83**, 4922 (1999). [arXiv:hep-ph/9907447](#)
18. W.D. Goldberger, M.B. Wise, Phenomenology of a stabilized modulus. *Phys. Lett. B* **475**, 275 (2000). [arXiv:hep-ph/9911457](#)
19. D. Pappadopulo, A. Thamm, R. Torre, A. Wulzer, Heavy vector triplets: bridging theory and data. *JHEP* **09**, 060 (2014). [arXiv:1402.4431](#) [hep-ph]
20. T. Han, J.D. Lykken, R.-J. Zhang, On Kaluza–Klein states from large extra dimensions. *Phys. Rev. D* **59**, 105006 (1999). [arXiv:hep-ph/9811350](#)
21. K. Agashe, H. Davoudiasl, G. Perez, A. Soni, Warped gravitons at the LHC and beyond. *Phys. Rev. D* **76**, 036006 (2007). [arXiv:hep-ph/0701186](#)
22. ATLAS Collaboration, Search for WW/WZ resonance production in $lvqq$ final states in pp collisions at $\sqrt{s} = 13$ TeV with the ATLAS detector. *JHEP* **03**, 042 (2018). [arXiv:1710.07235](#) [hep-ex]
23. ATLAS Collaboration, Searches for heavy ZZ and ZW resonances in the $llqq$ and $vvqq$ final states in pp collisions at $\sqrt{s} = 13$ TeV with the ATLAS detector. *JHEP* **03**, 009 (2018). [arXiv:1708.09638](#) [hep-ex]
24. ATLAS Collaboration, The ATLAS Experiment at the CERN Large Hadron Collider. *JINST* **3**, S08003 (2008)
25. B. Abbott et al., Production and integration of the ATLAS insertable B-Layer. *JINST* **13**, T05008 (2018). [arXiv:1803.00844](#) [physics.ins-det]
26. ATLAS Collaboration, Performance of the ATLAS trigger system in 2015. *Eur. Phys. J. C* **77**, 317 (2017). [arXiv:1611.09661](#) [hep-ex]
27. ATLAS Collaboration, Luminosity determination in pp collisions at $\sqrt{s} = 13$ TeV using the ATLAS detector at the LHC. *ATLAS-CONF-2019-021* (2019). <https://cds.cern.ch/record/2677054>
28. ATLAS Collaboration, Performance of electron and photon triggers in ATLAS during LHC Run 2. *Eur. Phys. J. C* **80**, 47 (2020). [arXiv:1909.00761](#) [hep-ex]
29. ATLAS Collaboration, Selection of jets produced in 13 TeV proton-proton collisions with the ATLAS detector. *ATLAS-CONF-2015-029* (2015). <https://cds.cern.ch/record/2037702>
30. ATLAS Collaboration, The ATLAS simulation infrastructure. *Eur. Phys. J. C* **70**, 823 (2010). [arXiv:1005.4568](#) [physics.ins-det]
31. S. Agostinelli et al., GEANT4: a simulation toolkit. *Nucl. Instrum. Methods A* **506**, 250 (2003)
32. T. Sjöstrand, S. Mrenna, P.Z. Skands, A brief introduction to PYTHIA 8.1. *Comput. Phys. Commun.* **178**, 852 (2008). [arXiv:0710.3820](#) [hep-ph]
33. ATLAS Collaboration, The Pythia 8 A3 tune description of ATLAS minimum bias and inelastic measurements incorporating the Donnachie–Landshoff diffractive model. *ATL-PHYS-PUB-2016-017* (2016) <https://cds.cern.ch/record/2206965>
34. R.D. Ball et al., Parton distributions with LHC data. *Nucl. Phys. B* **867**, 244 (2013). [arXiv:1207.1303](#) [hep-ph]
35. A. Oliveira, Gravity particles from Warped Extra Dimensions, predictions for LHC (2014). [arXiv:1404.0102](#) [hep-ph]
36. V. Barger, M. Ishida, Randall–Sundrum reality at the LHC. *Phys. Lett. B* **709**, 185 (2012). [arXiv:1110.6452](#) [hep-ph]
37. C. Csaki, J. Hubisz, S.J. Lee, Radion phenomenology in realistic warped space models. *Phys. Rev. D* **76**, 125015 (2007). [arXiv:0705.3844](#) [hep-ph]
38. J. Alwall et al., The automated computation of tree-level and next-to-leading order differential cross sections, and their matching to parton shower simulations. *JHEP* **07**, 079 (2014). [arXiv:1405.0301](#) [hep-ph]
39. T. Sjöstrand et al., An introduction to PYTHIA 8.2. *Comput. Phys. Commun.* **191**, 159 (2015). [arXiv:1410.3012](#) [hep-ph]
40. ATLAS Collaboration, ATLAS Pythia 8 tunes to 7 TeV data. *ATL-PHYS-PUB-2014-021* (2014) <https://cds.cern.ch/record/1966419>
41. E. Bothmann et al., Event generation with Sherpa 2.2. *Sci. Post Phys.* **7**, 34 (2019). [arXiv:1905.09127](#) [hep-ph]
42. T. Gleisberg, S. Höche, Comix, a new matrix element generator. *JHEP* **12**, 039 (2008). [arXiv:0808.3674](#) [hep-ph]
43. F. Cascioli, P. Maierhofer, S. Pozzorini, Scattering amplitudes with open loops. *Phys. Rev. Lett.* **108**, 111601 (2012). [arXiv:1111.5206](#) [hep-ph]
44. A. Denner, S. Dittmaier, L. Hofer, Collier: a fortran-based complex one-loop library in extended regularizations. *Comput. Phys. Commun.* **212**, 220 (2017). [arXiv:1604.06792](#) [hep-ph]
45. S. Schumann, F. Krauss, A Parton shower algorithm based on Catani–Seymour dipole factorisation. *JHEP* **03**, 038 (2008). [arXiv:0709.1027](#) [hep-ph]
46. S. Höche, F. Krauss, M. Schönherr, F. Siegert, A critical appraisal of NLO+PS matching methods. *JHEP* **09**, 049 (2012). [arXiv:1111.1220](#) [hep-ph]
47. S. Höche, F. Krauss, M. Schönherr, F. Siegert, QCD matrix elements + parton showers: the NLO case. *JHEP* **04**, 027 (2013). [arXiv:1207.5030](#) [hep-ph]
48. S. Catani, F. Krauss, R. Kuhn, B.R. Webber, QCD matrix elements + parton showers. *JHEP* **11**, 063 (2001). [arXiv:hep-ph/0109231](#)
49. S. Höche, F. Krauss, S. Schumann, F. Siegert, QCD matrix elements and truncated showers. *JHEP* **05**, 053 (2009). [arXiv:0903.1219](#) [hep-ph]
50. R.D. Ball et al., Parton distributions for the LHC Run II. *JHEP* **04**, 040 (2015). [arXiv:1410.8849](#) [hep-ph]
51. C. Anastasiou, L.J. Dixon, K. Melnikov, F. Petriello, High precision QCD at hadron colliders: electroweak gauge boson rapid-

- ity distributions at NNLO. *Phys. Rev. D* **69**, 094008 (2004). [arXiv:hep-ph/0312266](#)
52. S. Frixione, P. Nason, G. Ridolfi, A positive-weight next-to-leading-order Monte Carlo for heavy flavour hadroproduction. *JHEP* **09**, 126 (2007). [arXiv:0707.3088](#) [hep-ph]
 53. P. Nason, A new method for combining NLO QCD with shower Monte Carlo algorithms. *JHEP* **11**, 040 (2004). [arXiv:hep-ph/0409146](#)
 54. S. Frixione, P. Nason, C. Oleari, Matching NLO QCD computations with Parton Shower simulations: the POWHEG method. *JHEP* **11**, 070 (2007). [arXiv:0709.2092](#) [hep-ph]
 55. S. Alioli, P. Nason, C. Oleari, E. Re, A general framework for implementing NLO calculations in shower Monte Carlo programs: the POWHEG BOX. *JHEP* **06**, 043 (2010). [arXiv:1002.2581](#) [hep-ph]
 56. ATLAS Collaboration, Studies on top-quark Monte Carlo modelling for Top2016, ATL-PHYS-PUB-2016-020 (2016) <https://cds.cern.ch/record/2216168>
 57. P. Kant et al., HatHor for single top-quark production: updated predictions and uncertainty estimates for single top-quark production in hadronic collisions. *Comput. Phys. Commun.* **191**, 74 (2015). [arXiv:1406.4403](#) [hep-ph]
 58. M. Aliev et al., HATHOR-HAdronic Top and Heavy quarks crOss section calculator. *Comput. Phys. Commun.* **182**, 1034 (2011). [arXiv:1007.1327](#) [hep-ph]
 59. N. Kidonakis, Next-to-next-to-leading-order collinear and soft gluon corrections for t-channel single top quark production. *Phys. Rev. D* **83**, 091503 (2011). [arXiv:1103.2792](#) [hep-ph]
 60. N. Kidonakis, Two-loop soft anomalous dimensions for single top quark associated production with a W- or H-. *Phys. Rev. D* **82**, 054018 (2010). [arXiv:1005.4451](#) [hep-ph]
 61. J.M. Campbell, R.K. Ellis, C. Williams, Vector boson pair production at the LHC. *JHEP* **07**, 018 (2011). [arXiv:1105.0020](#) [hep-ph]
 62. ATLAS Collaboration, Electron and photon performance measurements with the ATLAS detector using the 2015–2017 LHC proton–proton collision data. *JINST* **14**, P12006 (2019). [arXiv:1908.00005](#) [hep-ex]
 63. ATLAS Collaboration, Muon reconstruction performance of the ATLAS detector in proton–proton collision data at $\sqrt{s} = 13 \text{ TeV}$. *Eur. Phys. J. C* **76**, 292 (2016). [arXiv:1603.05598](#) [hep-ex]
 64. M. Cacciari, G.P. Salam, G. Soyez, The anti- k_T jet clustering algorithm. *JHEP* **04**, 063 (2008). [arXiv:0802.1189](#) [hep-ph]
 65. M. Cacciari, G.P. Salam, G. Soyez, FastJet user manual. *Eur. Phys. J. C* **72**, 1896 (2012). [arXiv:1111.6097](#) [hep-ph]
 66. ATLAS Collaboration, Jet energy scale measurements and their systematic uncertainties in proton–proton collisions at $\sqrt{s} = 13 \text{ TeV}$ with the ATLAS detector. *Phys. Rev. D* **96**, 072002 (2017). [arXiv:1703.09665](#) [hep-ex]
 67. ATLAS Collaboration, Tagging and suppression of pileup jets with the ATLAS detector, ATLAS-CONF-2014-018 (2014) <https://cds.cern.ch/record/1700870>
 68. ATLAS Collaboration, ATLAS b-jet identification performance and efficiency measurement with $t\bar{t}$ events in pp collisions at $\sqrt{s} = 13 \text{ TeV}$. *Eur. Phys. J. C* **79**, 970 (2019). [arXiv:1907.05120](#) [hep-ex]
 69. ATLAS Collaboration, Improving jet substructure performance in ATLAS using Track-CaloClusters, ATL-PHYS-PUB-2017-015 (2017) <https://cds.cern.ch/record/2275636>
 70. D. Krohn, J. Thaler, L.-T. Wang, Jet trimming. *JHEP* **02**, 084 (2010). [arXiv:0912.1342](#) [hep-ph]
 71. S.D. Ellis, D.E. Soper, Successive combination jet algorithm for hadron collisions. *Phys. Rev. D* **48**, 3160 (1993)
 72. ATLAS Collaboration, Variable radius, exclusive- k_T , and Center-of-Mass Subjet Reconstruction for Higgs($\rightarrow b\bar{b}$) Tagging in ATLAS, ATL-PHYS-PUB-2017-010 (2017) <https://cds.cern.ch/record/2268678>
 73. ATLAS Collaboration, Performance of missing transverse momentum reconstruction with the ATLAS detector using proton–proton collisions at $\sqrt{s} = 13 \text{ TeV}$. *Eur. Phys. J. C* **78**, 903 (2018). [arXiv:1802.08168](#) [hep-ex]
 74. A. Sherstinsky, Fundamentals of recurrent neural network (RNN) and long short-term memory (LSTM) network. *Phys. D* **404**, 132306 (2018). [arXiv:1808.03314](#)
 75. ATLAS Collaboration, Identification of jets containing b-hadrons with recurrent neural networks at the ATLAS Experiment, ATL-PHYS-PUB-2017-003 (2017) <https://cds.cern.ch/record/2255226>
 76. F. Chollet et al., Keras, GitHub repository (2015) <https://github.com/fchollet/keras>
 77. R. Al-Rfou et al. (Theano Development Team), Theano: a Python framework for fast computation of mathematical expressions (2016). [arXiv:1605.02688](#) [cs.SC]
 78. ATLAS Collaboration, Identification of boosted, hadronically decaying W bosons and comparisons with ATLAS data taken at $\sqrt{s} = 8 \text{ TeV}$. *Eur. Phys. J. C* **76**, 154 (2016). [arXiv:1510.05821](#) [hep-ex]
 79. ATLAS Collaboration, Identification of boosted, hadronically-decaying W and Z Bosons in $\sqrt{s} = 13 \text{ TeV}$ Monte Carlo Simulations for ATLAS, ATL-PHYS-PUB-2015-033 (2015) <https://cds.cern.ch/record/2041461>
 80. A.J. Larkoski, I. Moult, D. Neill, Power counting to better jet observables. *JHEP* **12**, 009 (2014). [arXiv:1409.6298](#) [hep-ph]
 81. A.J. Larkoski, I. Moult, D. Neill, Analytic boosted boson discrimination. *JHEP* **05**, 117 (2016). [arXiv:1507.03018](#) [hep-ph]
 82. K.A. Olive et al., Review of particle physics. *Chin. Phys. C* **38**, 090001 (2014)
 83. G. Avoni et al., The new LUCID-2 detector for luminosity measurement and monitoring in ATLAS. *JINST* **13**, P07017 (2018)
 84. ATLAS Collaboration, Measurement of the inelastic proton–proton cross section at $\sqrt{s} = 13 \text{ TeV}$ with the ATLAS Detector at the LHC. *Phys. Rev. Lett.* **117**, 182002 (2016). [arXiv:1606.02625](#) [hep-ex]
 85. ATLAS Collaboration, In situ calibration of large-radius jet energy and mass in 13 TeV proton–proton collisions with the ATLAS detector. *Eur. Phys. J. C* **79**, 135 (2019). [arXiv:1807.09477](#) [hep-ex]
 86. ATLAS Collaboration, A W/Z-boson tagger using Track-CaloCluster jets with ATLAS, ATLAS-PHYS-PUB-2020-008 (2020) <https://cds.cern.ch/record/2718218>
 87. ATLAS Collaboration, Boosted hadronic vector boson and top quark tagging with ATLAS using Run 2 data, ATL-PHYS-PUB-2020-017 (2020) <https://cds.cern.ch/record/2724149>
 88. ATLAS Collaboration, Calibration of light-flavour b-jet mistagging rates using ATLAS proton–proton collision data at $\sqrt{s} = 13 \text{ TeV}$, ATLAS-CONF-2018-006 (2018) <https://cds.cern.ch/record/2314418>
 89. ATLAS Collaboration, Calibration of the ATLAS b-tagging algorithm in $t\bar{t}$ semileptonic events, ATLAS-CONF-2018-045 (2018) <https://cds.cern.ch/record/2638455>
 90. T. Gleisberg et al., Event generation with SHERPA 1.1. *JHEP* **02**, 007 (2009). [arXiv:0811.4622](#) [hep-ph]
 91. ATLAS Collaboration, Measurement of the cross-section for producing a W boson in association with a single top quark in pp collisions at $\sqrt{s} = 13 \text{ TeV}$ with ATLAS. *JHEP* **01**, 063 (2018). [arXiv:1612.07231](#) [hep-ex]
 92. M. Bahr et al., Herwig++ physics and manual. *Eur. Phys. J. C* **58**, 639 (2008). [arXiv:0803.0883](#) [hep-ph]
 93. J. Bellm et al., Herwig 7.0/Herwig++ 3.0 release note. *Eur. Phys. J. C* **76**, 196 (2016). [arXiv:1512.01178](#) [hep-ph]
 94. L. Harland-Lang, A. Martin, P. Motylinski, R. Thorne, Parton distributions in the LHC era: MMHT 2014 PDFs. *Eur. Phys. J. C* **75**, 204 (2015). [arXiv:1412.3989](#) [hep-ph]

95. ATLAS Collaboration, Combined search for the Standard Model Higgs boson in pp collisions at $\sqrt{s} = 7$ TeV with the ATLAS detector. *Phys. Rev. D* **86**, 032003 (2012). [arXiv:1207.0319](https://arxiv.org/abs/1207.0319) [hep-ex]
96. L. Moneta et al., The RooStats Project. *PoS ACAT* **2010**, 057 (2010). [arXiv:1009.1003](https://arxiv.org/abs/1009.1003) [physics.data-an]
97. W. Verkerke, D.P. Kirkby, The RooFit toolkit for data modeling, eConf C0303241 (2003) MOLT007. [arXiv:physics/0306116](https://arxiv.org/abs/physics/0306116) [physics]
98. A.L. Read, Presentation of search results: the CL_S technique. *J. Phys. G* **28**, 2693 (2002)
99. G. Cowan, K. Cranmer, E. Gross, O. Vitells, Asymptotic formulae for likelihood-based tests of new physics. *Eur. Phys. J. C* **71**, 1554 (2011). [Erratum: *Eur. Phys. J. C* **73**, 2501 (2013)]. [arXiv:1007.1727](https://arxiv.org/abs/1007.1727) [physics.data-an]
100. ATLAS Collaboration, ATLAS Computing Acknowledgements, ATL-SOFT-PUB-2020-001. <https://cds.cern.ch/record/2717821>

ATLAS Collaboration

G. Aad¹⁰², B. Abbott¹²⁸, D. C. Abbott¹⁰³, A. Abed Abud³⁶, K. Abeling⁵³, D. K. Abhayasinghe⁹⁴, S. H. Abidi¹⁶⁶, O. S. AbouZeid⁴⁰, N. L. Abraham¹⁵⁵, H. Abramowicz¹⁶⁰, H. Abreu¹⁵⁹, Y. Abulaiti⁶, B. S. Acharya^{67a,67b,n}, B. Achkar⁵³, L. Adam¹⁰⁰, C. Adam Bourdarios⁵, L. Adamczyk^{84a}, L. Adamek¹⁶⁶, J. Adelman¹²¹, M. Adersberger¹¹⁴, A. Adiguzel^{12c}, S. Adorni⁵⁴, T. Adye¹⁴³, A. A. Affolder¹⁴⁵, Y. Afik¹⁵⁹, C. Agapopoulou⁶⁵, M. N. Agaras³⁸, A. Aggarwal¹¹⁹, C. Agheorghiesei^{27c}, J. A. Aguilar-Saavedra^{139a,139f,ad}, A. Ahmad³⁶, F. Ahmadov⁸⁰, W. S. Ahmed¹⁰⁴, X. Ai¹⁸, G. Aielli^{74a,74b}, S. Akatsuka⁸⁶, T. P. A. Åkesson⁹⁷, E. Akilli⁵⁴, A. V. Akimov¹¹¹, K. Al Khoury⁶⁵, G. L. Alberghi^{23a,23b}, J. Albert¹⁷⁵, M. J. Alconada Verzini¹⁶⁰, S. Alderweireldt³⁶, M. Aleksa³⁶, I. N. Aleksandrov⁸⁰, C. Alexa^{27b}, T. Alexopoulos¹⁰, A. Alfonsi¹²⁰, F. Alfonsi^{23a,23b}, M. Alhroob¹²⁸, B. Ali¹⁴¹, S. Ali¹⁵⁷, M. Aliev¹⁶⁵, G. Alimonti^{69a}, C. Allaire³⁶, B. M. M. Allbrooke¹⁵⁵, B. W. Allen¹³¹, P. P. Allport²¹, A. Aloisio^{70a,70b}, F. Alonso⁸⁹, C. Alpigiani¹⁴⁷, E. Alunno Camelia^{74a,74b}, M. Alvarez Estevez⁹⁹, M. G. Alvigi^{70a,70b}, Y. Amaral Coutinho^{81b}, A. Ambler¹⁰⁴, L. Ambroz¹³⁴, C. Amelung²⁶, D. Amidei¹⁰⁶, S. P. Amor Dos Santos^{139a}, S. Amoroso⁴⁶, C. S. Amrouche⁵⁴, F. An⁷⁹, C. Anastopoulos¹⁴⁸, N. Andari¹⁴⁴, T. Andeen¹¹, J. K. Anders²⁰, S. Y. Andreev^{45a,45b}, A. Andreazza^{69a,69b}, V. Andrei^{61a}, C. R. Anelli¹⁷⁵, S. Angelidakis⁹, A. Angerami³⁹, A. V. Anisenkov^{122a,122b}, A. Annovi^{72a}, C. Antel⁵⁴, M. T. Anthony¹⁴⁸, E. Antipov¹²⁹, M. Antonelli⁵¹, D. J. A. Antrim¹⁷⁰, F. Anulli^{73a}, M. Aoki⁸², J. A. Aparisi Pozo¹⁷³, M. A. Aparo¹⁵⁵, L. Aperio Bella⁴⁶, N. Aranzabal³⁶, V. Araujo Ferraz^{81a}, R. Araujo Pereira^{81b}, C. Arcangeletti⁵¹, A. T. H. Arce⁴⁹, F. A. Arduh⁸⁹, J.-F. Arguin¹¹⁰, S. Argyropoulos⁵², J.-H. Arling⁴⁶, A. J. Armbruster³⁶, A. Armstrong¹⁷⁰, O. Arnaez¹⁶⁶, H. Arnold¹²⁰, Z. P. Arrubarrena Tame¹¹⁴, G. Artoni¹³⁴, K. Asai¹²⁶, S. Asai¹⁶², T. Asawatavonvanich¹⁶⁴, N. Asbah⁵⁹, E. M. Asimakopoulou¹⁷¹, L. Asquith¹⁵⁵, J. Assahsah^{35d}, K. Assamagan²⁹, R. Astalos^{28a}, R. J. Atkin^{33a}, M. Atkinson¹⁷², N. B. Atlay¹⁹, H. Atmani⁶⁵, K. Augsten¹⁴¹, S. Auricchio^{70b}, V. A. Austrup¹⁸¹, G. Avolio³⁶, M. K. Ayoub^{15a}, G. Azuelos^{110,al}, H. Bachacou¹⁴⁴, K. Bachas¹⁶¹, M. Backes¹³⁴, F. Backman^{45a,45b}, P. Bagnaia^{73a,73b}, M. Bahmani⁸⁵, H. Bahramsemani¹⁵¹, A. J. Bailey¹⁷³, V. R. Bailey¹⁷², J. T. Baines¹⁴³, C. Bakalis¹⁰, O. K. Baker¹⁸², P. J. Bakker¹²⁰, E. Bakos¹⁶, D. Bakshi Gupta⁸, S. Balaji¹⁵⁶, E. M. Baldin^{122a,122b}, P. Balek¹⁷⁹, F. Balli¹⁴⁴, W. K. Balunas¹³⁴, J. Balz¹⁰⁰, E. Banas⁸⁵, M. Bandieramonte¹³⁸, A. Bandyopadhyay²⁴, Sw. Banerjee^{180,i}, L. Barak¹⁶⁰, W. M. Barbe³⁸, E. L. Barberio¹⁰⁵, D. Barberis^{55a,55b}, M. Barbero¹⁰², G. Barbour⁹⁵, T. Barillari¹¹⁵, M.-S. Barisits³⁶, J. Barkeloo¹³¹, T. Barklow¹⁵², R. Barnea¹⁵⁹, B. M. Barnett¹⁴³, R. M. Barnett¹⁸, Z. Barnovska-Blenessy^{60a}, A. Baroncelli^{60a}, G. Barone²⁹, A. J. Barr¹³⁴, L. Barranco Navarro^{45a,45b}, F. Barreiro⁹⁹, J. Barreiro Guimarães da Costa^{15a}, U. Barron¹⁶⁰, S. Barsov¹³⁷, F. Bartels^{61a}, R. Bartoldus¹⁵², G. Bartolini¹⁰², A. E. Barton⁹⁰, P. Bartos^{28a}, A. Basalae⁴⁶, A. Basan¹⁰⁰, A. Bassalat^{65,ai}, M. J. Basso¹⁶⁶, R. L. Bates⁵⁷, S. Batlamous^{35e}, J. R. Batley³², B. Batool¹⁵⁰, M. Battaglia¹⁴⁵, M. Bauce^{73a,73b}, F. Bauer¹⁴⁴, K. T. Bauer¹⁷⁰, H. S. Bawa³¹, A. Bayirli^{12c}, J. B. Beacham⁴⁹, T. Beau¹³⁵, P. H. Beauchemin¹⁶⁹, F. Becherer⁵², P. Bechtel²⁴, H. C. Beck⁵³, H. P. Beck^{20,p}, K. Becker¹⁷⁷, C. Becot⁴⁶, A. Beddall^{12d}, A. J. Beddall^{12a}, V. A. Bednyakov⁸⁰, M. Bedognetti¹²⁰, C. P. Bee¹⁵⁴, T. A. Beermann¹⁸¹, M. Begalli^{81b}, M. Beger²⁹, A. Behera¹⁵⁴, J. K. Behr⁴⁶, F. Beisiegel²⁴, M. Belfkir⁵, A. S. Bell⁹⁵, G. Bella¹⁶⁰, L. Bellagamba^{23b}, A. Bellerive³⁴, P. Bellos⁹, K. Beloborodov^{122a,122b}, K. Belotskiy¹¹², N. L. Belyaev¹¹², D. Benchechroun^{35a}, N. Benekos¹⁰, Y. Benhammou¹⁶⁰, D. P. Benjamin⁶, M. Benoit⁵⁴, J. R. Bensinger²⁶, S. Bentvelsen¹²⁰, L. Beresford¹³⁴, M. Beretta⁵¹, D. Berge¹⁹, E. Bergeas Kuutmann¹⁷¹, N. Berger⁵, B. Bergmann¹⁴¹, L. J. Bergsten²⁶, J. Beringer¹⁸, S. Berlendis⁷, G. Bernardi¹³⁵, C. Bernius¹⁵², F. U. Bernlochner²⁴, T. Berry⁹⁴, P. Berta¹⁰⁰, C. Bertella^{15a}, A. Berthold⁴⁸, I. A. Bertram⁹⁰, O. Bessidskaia Bylund¹⁸¹, N. Besson¹⁴⁴, A. Bethani¹⁰¹, S. Bethke¹¹⁵, A. Betti⁴², A. J. Bevan⁹³, J. Beyer¹¹⁵, D. S. Bhattacharya¹⁷⁶, P. Bhattacharai²⁶,

V. S. Bhopatkar⁶, R. Bi¹³⁸, R. M. Bianchi¹³⁸, O. Biebel¹¹⁴, D. Biedermann¹⁹, R. Bielski³⁶, K. Bierwagen¹⁰⁰, N. V. Biesuz^{72a,72b}, M. Biglietti^{75a}, T. R. V. Billoud¹¹⁰, M. Bindi⁵³, A. Bingul^{12d}, C. Bini^{73a,73b}, S. Biondi^{23a,23b}, C. J. Birch-sykes¹⁰¹, M. Birman¹⁷⁹, T. Bisanz³⁶, J. P. Biswal³, D. Biswas^{180,i}, A. Bitadze¹⁰¹, C. Bittrich⁴⁸, K. Bjørke¹³³, T. Blazek^{28a}, I. Bloch⁴⁶, C. Blocker²⁶, A. Blue⁵⁷, U. Blumenschein⁹³, G. J. Bobbink¹²⁰, V. S. Bobrovnikov^{122a,122b}, S. S. Bocchetta⁹⁷, D. Bogavac¹⁴, A. G. Bogdanchikov^{122a,122b}, C. Bohm^{45a}, V. Boisvert⁹⁴, P. Bokan^{53,171}, T. Bold^{84a}, A. E. Bolz^{61b}, M. Bomben¹³⁵, M. Bona⁹³, J. S. Bonilla¹³¹, M. Boonekamp¹⁴⁴, C. D. Booth⁹⁴, H. M. Borecka-Bielska⁹¹, L. S. Borgna⁹⁵, A. Borisov¹²³, G. Borissov⁹⁰, J. Bortfeldt³⁶, D. Bortoletto¹³⁴, D. Boscherini^{23b}, M. Bosman¹⁴, J. D. Bossio Sola¹⁰⁴, K. Bouaouda^{35a}, J. Boudreau¹³⁸, E. V. Bouhova-Thacker⁹⁰, D. Boumediene³⁸, S. K. Boutle⁵⁷, A. Boveia¹²⁷, J. Boyd³⁶, D. Boye^{33c}, I. R. Boyko⁸⁰, A. J. Bozson⁹⁴, J. Bracinik²¹, N. Brahimi^{60d}, G. Brandt¹⁸¹, O. Brandt³², F. Braren⁴⁶, B. Brau¹⁰³, J. E. Brau¹³¹, W. D. Breaden Madden⁵⁷, K. Brendlinger⁴⁶, L. Brenner³⁶, R. Brenner¹⁷¹, S. Bressler¹⁷⁹, B. Brickwedde¹⁰⁰, D. L. Briglin²¹, D. Britton⁵⁷, D. Britzger¹¹⁵, I. Brock²⁴, R. Brock¹⁰⁷, G. Brooijmans³⁹, W. K. Brooks^{146d}, E. Brost²⁹, P. A. Bruckman de Renstrom⁸⁵, B. Brüers⁴⁶, D. Bruncko^{28b}, A. Bruni^{23b}, G. Bruni^{23b}, L. S. Bruni¹²⁰, S. Bruno^{74a,74b}, M. Bruschi^{23b}, N. Bruscinò^{73a,73b}, L. Bryngemark¹⁵², T. Buanes¹⁷, Q. Buat³⁶, P. Buchholz¹⁵⁰, A. G. Buckley⁵⁷, I. A. Budagov⁸⁰, M. K. Bugge¹³³, F. Bühner⁵², O. Bulekov¹¹², B. A. Bullard⁵⁹, T. J. Burch¹²¹, S. Burdin⁹¹, C. D. Burgard¹²⁰, A. M. Burger¹²⁹, B. Burghgrave⁸, J. T. P. Burr⁴⁶, C. D. Burton¹¹, J. C. Burzynski¹⁰³, V. Büscher¹⁰⁰, E. Buschmann⁵³, P. J. Bussey⁵⁷, J. M. Butler²⁵, C. M. Buttar⁵⁷, J. M. Butterworth⁹⁵, P. Butti³⁶, W. Buttinger³⁶, C. J. Buxo Vazquez¹⁰⁷, A. Buzatu¹⁵⁷, A. R. Buzykaev^{122a,122b}, G. Cabras^{23a,23b}, S. Cabrera Urbán¹⁷³, D. Caforio⁵⁶, H. Cai¹³⁸, V. M. M. Cairo¹⁵², O. Cakir^{4a}, N. Calace³⁶, P. Calafiura¹⁸, G. Calderini¹³⁵, P. Calfayan⁶⁶, G. Callea⁵⁷, L. P. Caloba^{81b}, A. Caltabiano^{74a,74b}, S. Calvente Lopez⁹⁹, D. Calvet³⁸, S. Calvet³⁸, T. P. Calvet¹⁰², M. Calvetti^{72a,72b}, R. Camacho Toro¹³⁵, S. Camarda³⁶, D. Camarero Munoz⁹⁹, P. Camarri^{74a,74b}, M. T. Camerlingo^{75a,75b}, D. Cameron¹³³, C. Camincher³⁶, S. Campana³⁶, M. Campanelli⁹⁵, A. Camplani⁴⁰, V. Canale^{70a,70b}, A. Canesse¹⁰⁴, M. Cano Bret⁷⁸, J. Cantero¹²⁹, T. Cao¹⁶⁰, Y. Cao¹⁷², M. D. M. Capeans Garrido³⁶, M. Capua^{41a,41b}, R. Cardarelli^{74a}, F. Cardillo¹⁴⁸, G. Carducci^{41a,41b}, I. Carli¹⁴², T. Carli³⁶, G. Carlino^{70a}, B. T. Carlson¹³⁸, E. M. Carlson^{167a,175}, L. Carminati^{69a,69b}, R. M. D. Carney¹⁵², S. Caron¹¹⁹, E. Carquin^{146d}, S. Carrà⁴⁶, G. Carratta^{23a,23b}, J. W. S. Carter¹⁶⁶, T. M. Carter⁵⁰, M. P. Casado^{14,f}, A. F. Casha¹⁶⁶, F. L. Castillo¹⁷³, L. Castillo Garcia¹⁴, V. Castillo Gimenez¹⁷³, N. F. Castro^{139a,139e}, A. Catinaccio³⁶, J. R. Catmore¹³³, A. Cattai³⁶, V. Cavaliere²⁹, V. Cavasinni^{72a,72b}, E. Celebi^{12b}, F. Celli¹³⁴, K. Cerny¹³⁰, A. S. Cerqueira^{81a}, A. Cerri¹⁵⁵, L. Cerrito^{74a,74b}, F. Cerutti¹⁸, A. Cervelli^{23a,23b}, S. A. Cetin^{12b}, Z. Chadi^{35a}, D. Chakraborty¹²¹, J. Chan¹⁸⁰, W. S. Chan¹²⁰, W. Y. Chan⁹¹, J. D. Chapman³², B. Chargeishvili^{158b}, D. G. Charlton²¹, T. P. Charman⁹³, C. C. Chau³⁴, S. Che¹²⁷, S. Chekanov⁶, S. V. Chekulaev^{167a}, G. A. Chelkov^{80,ag}, B. Chen⁷⁹, C. Chen^{60a}, C. H. Chen⁷⁹, H. Chen²⁹, J. Chen^{60a}, J. Chen³⁹, J. Chen²⁶, S. Chen¹³⁶, S. J. Chen^{15c}, X. Chen^{15b}, Y. Chen^{60a}, Y.-H. Chen⁴⁶, H. C. Cheng^{63a}, H. J. Cheng^{15a}, A. Cheplakov⁸⁰, E. Cheremushkina¹²³, R. Cherkaoui El Moursli^{35e}, E. Cheu⁷, K. Cheung⁶⁴, T. J. A. Chevalérias¹⁴⁴, L. Chevalier¹⁴⁴, V. Chiarella⁵¹, G. Chiarelli^{72a}, G. Chiodini^{68a}, A. S. Chisholm²¹, A. Chitan^{27b}, I. Chiu¹⁶², Y. H. Chiu¹⁷⁵, M. V. Chizhov⁸⁰, K. Choi¹¹, A. R. Chomont^{73a,73b}, Y. S. Chow¹²⁰, L. D. Christopher^{33e}, M. C. Chu^{63a}, X. Chu^{15a,15d}, J. Chudoba¹⁴⁰, J. J. Chwastowski⁸⁵, L. Chytka¹³⁰, D. Cieri¹¹⁵, K. M. Ciesla⁸⁵, D. Cinca⁴⁷, V. Cindro⁹², I. A. Cioară^{27b}, A. Ciochio¹⁸, F. Ciroto^{70a,70b}, Z. H. Citron^{179,j}, M. Citterio^{69a}, D. A. Ciubotaru^{27b}, B. M. Ciungu¹⁶⁶, A. Clark⁵⁴, M. R. Clark³⁹, P. J. Clark⁵⁰, S. E. Clawson¹⁰¹, C. Clement^{45a,45b}, Y. Coadou¹⁰², M. Cobl^{67a,67c}, A. Coccaro^{55b}, J. Cochran⁷⁹, R. Coelho Lopes De Sa¹⁰³, H. Cohen¹⁶⁰, A. E. C. Coimbra³⁶, B. Cole³⁹, A. P. Colijn¹²⁰, J. Collot⁵⁸, P. Conde Muiño^{139a,139h}, S. H. Connell^{33c}, I. A. Connelly⁵⁷, S. Constantinescu^{27b}, F. Conventi^{70a,am}, A. M. Cooper-Sarkar¹³⁴, F. Cormier¹⁷⁴, K. J. R. Cormier¹⁶⁶, L. D. Corpe⁹⁵, M. Corradi^{73a,73b}, E. E. Corrigan⁹⁷, F. Corrivéau^{104,ab}, M. J. Costa¹⁷³, F. Costanza⁵, D. Costanzo¹⁴⁸, G. Cowan⁹⁴, J. W. Cowley³², J. Crane¹⁰¹, K. Cranmer¹²⁵, R. A. Creager¹³⁶, S. Crépé-Renaudin⁵⁸, F. Crescioli¹³⁵, M. Cristinziani²⁴, V. Croft¹⁶⁹, G. Crosetti^{41a,41b}, A. Cueto⁵, T. Cuhadar Donszelmann¹⁷⁰, H. Cui^{15a,15d}, A. R. Cukierman¹⁵², W. R. Cunningham⁵⁷, S. Czekerda⁸⁵, P. Czodrowski³⁶, M. M. Czurylo^{61b}, M. J. Da Cunha Sargedas De Sousa^{60b}, J. V. Da Fonseca Pinto^{81b}, C. Da Via¹⁰¹, W. Dabrowski^{84a}, F. Dachs³⁶, T. Dado⁴⁷, S. Dahbi^{33e}, T. Dai¹⁰⁶, C. Dallapiccola¹⁰³, M. Dam⁴⁰, G. D’amen²⁹, V. D’Amico^{75a,75b}, J. Damp¹⁰⁰, J. R. Dandoy¹³⁶, M. F. Daneri³⁰, M. Danninger¹⁵¹, V. Dao³⁶, G. Darbo^{55b}, O. Dartsis⁵, A. Dattagupta¹³¹, T. Daubney⁴⁶, S. D’Auria^{69a,69b}, C. David^{167b}, T. Davidek¹⁴², D. R. Davis⁴⁹, I. Dawson¹⁴⁸, K. De⁸, R. De Asmundis^{70a}, M. De Beurs¹²⁰, S. De Castro^{23a,23b}, N. De Groot¹¹⁹, P. de Jong¹²⁰

H. De la Torre¹⁰⁷, A. De Maria^{15c}, D. De Pedis^{73a}, A. De Salvo^{73a}, U. De Sanctis^{74a,74b}, M. De Santis^{74a,74b}, A. De Santo¹⁵⁵, J. B. De Vivie De Regie⁶⁵, C. Debenedetti¹⁴⁵, D. V. Dedovich⁸⁰, A. M. Deiana⁴², J. Del Peso⁹⁹, Y. Delabat Diaz⁴⁶, D. Delgove⁶⁵, F. Deliot¹⁴⁴, C. M. Delitzsch⁷, M. Della Pietra^{70a,70b}, D. Della Volpe⁵⁴, A. Dell'Acqua³⁶, L. Dell'Asta^{74a,74b}, M. Delmastro⁵, C. Delporte⁶⁵, P. A. Delsart⁵⁸, D. A. DeMarco¹⁶⁶, S. Demers¹⁸², M. Demichev⁸⁰, G. Demontigny¹¹⁰, S. P. Denisov¹²³, L. D'Eramo¹²¹, D. Derendarz⁸⁵, J. E. Derkaoui^{35d}, F. Derue¹³⁵, P. Dervan⁹¹, K. Desch²⁴, K. Dette¹⁶⁶, C. Deutsch²⁴, M. R. Devesa³⁰, P. O. Deviveiros³⁶, F. A. Di Bello^{73a,73b}, A. Di Ciaccio^{74a,74b}, L. Di Ciaccio⁵, W. K. Di Clemente¹³⁶, C. Di Donato^{70a,70b}, A. Di Girolamo³⁶, G. Di Gregorio^{72a,72b}, B. Di Micco^{75a,75b}, R. Di Nardo^{75a,75b}, K. F. Di Petrillo⁵⁹, R. Di Sipio¹⁶⁶, C. Diaconu¹⁰², F. A. Dias⁴⁰, T. Dias Do Vale^{139a}, M. A. Diaz^{146a}, F. G. Diaz Capriles²⁴, J. Dickinson¹⁸, M. Didenko¹⁶⁵, E. B. Diehl¹⁰⁶, J. Dietrich¹⁹, S. Díez Cornell⁴⁶, A. Dimitrievska¹⁸, W. Ding^{15b}, J. Dingfelder²⁴, S. J. Dittmeier^{61b}, F. Dittus³⁶, F. Djama¹⁰², T. Djobava^{158b}, J. I. Djuvslund¹⁷, M. A. B. Do Vale^{81c}, M. Dobre^{27b}, D. Dodsworth²⁶, C. Doglioni⁹⁷, J. Dolejsi¹⁴², Z. Dolezal¹⁴², M. Donadelli^{81d}, B. Dong^{60c}, J. Donini³⁸, A. D'onofrio^{15c}, M. D'Onofrio⁹¹, J. Dopke¹⁴³, A. Doria^{70a}, M. T. Dova⁸⁹, A. T. Doyle⁵⁷, E. Drechsler¹⁵¹, E. Dreyer¹⁵¹, T. Dreyer⁵³, A. S. Drobac¹⁶⁹, D. Du^{60b}, T. A. du Pree¹²⁰, Y. Duan^{60d}, F. Dubinin¹¹¹, M. Dubovsky^{28a}, A. Dubreuil⁵⁴, E. Duchovni¹⁷⁹, G. Ducek¹¹⁴, O. A. Ducu³⁶, D. Duda¹¹⁵, A. Dudarev³⁶, A. C. Dudder¹⁰⁰, E. M. Duffield¹⁸, M. D'uffizi¹⁰¹, L. Dufflot⁶⁵, M. Dührssen³⁶, C. Dülsen¹⁸¹, M. Dumancic¹⁷⁹, A. E. Dumitriu^{27b}, M. Dunford^{61a}, A. Duperrin¹⁰², H. Duran Yildiz^{4a}, M. Düren⁵⁶, A. Durglishvili^{158b}, D. Dusching⁴⁸, B. Dutta⁴⁶, D. Duvnjak¹, G. I. Dyckes¹³⁶, M. Dyndal³⁶, S. Dysch¹⁰¹, B. S. Dziedzic⁸⁵, M. G. EGGLESTON⁴⁹, T. Eifert⁸, G. Eigen¹⁷, K. Einsweiler¹⁸, T. Ekelof¹⁷¹, H. El Jarrari¹⁷¹, V. Ellajosyula¹⁷¹, M. Ellert¹⁷¹, F. Ellinghaus¹⁸¹, A. A. Elliot⁹³, N. Ellis³⁶, J. Elmsheuser²⁹, M.elsing³⁶, D. Emel'yanov¹⁴³, A. Emerman³⁹, Y. Enari¹⁶², M. B. Epland⁴⁹, J. Erdmann⁴⁷, A. Ereditato²⁰, P. A. Erland⁸⁵, M. Errenst³⁶, M. Escalier⁶⁵, C. Escobar¹⁷³, O. Estrada Pastor¹⁷³, E. Etzion¹⁶⁰, H. Evans⁶⁶, M. O. Evans¹⁵⁵, A. Ezhilov¹³⁷, F. Fabbri⁵⁷, L. Fabbri^{23a,23b}, V. Fabiani¹¹⁹, G. Facini¹⁷⁷, R. M. Faisca Rodrigues Pereira^{139a}, R. M. Fakhruddinov¹²³, S. Falciano^{73a}, P. J. Falke²⁴, S. Falke³⁶, J. Faltova¹⁴², Y. Fang^{15a}, Y. Fang^{15a}, G. Fanourakis⁴⁴, M. Fanti^{69a,69b}, M. Faraj^{67a,67c,q}, A. Farbin⁸, A. Farilla^{75a}, E. M. Farina^{71a,71b}, T. Farooque¹⁰⁷, S. M. Farrington⁵⁰, P. Farthouat³⁶, F. Fassi^{35e}, P. Fasnacht³⁶, D. Fassoulitis⁹, M. Fauci Giannelli⁵⁰, W. J. Fawcett³², L. Fayard⁶⁵, O. L. Fedin^{137,o}, W. Fedorko¹⁷⁴, A. Fehr²⁰, M. Feickert¹⁷², L. Felgioni¹⁰², A. Fell¹⁴⁸, C. Feng^{60b}, M. Feng⁴⁹, M. J. Fenton¹⁷⁰, A. B. Fenyuk¹²³, S. W. Ferguson⁴³, J. Ferrando⁴⁶, A. Ferrante¹⁷², A. Ferrari¹⁷¹, P. Ferrari¹²⁰, R. Ferrari^{71a}, D. E. Ferreira de Lima^{61b}, A. Ferrer¹⁷³, D. Ferrere⁵⁴, C. Ferretti¹⁰⁶, F. Fiedler¹⁰⁰, A. Filipčić⁹², F. Filthaut¹¹⁹, K. D. Finelli²⁵, M. C. N. Fiolhais^{139a,139c,a}, L. Fiorini¹⁷³, F. Fischer¹¹⁴, J. Fischer¹⁰⁰, W. C. Fisher¹⁰⁷, T. Fitschen²¹, I. Fleck¹⁵⁰, P. Fleischmann¹⁰⁶, T. Flick¹⁸¹, B. M. Flieler¹¹⁴, L. Flores¹³⁶, L. R. Flores Castillo^{63a}, F. M. Follega^{76a,76b}, N. Fomin¹⁷, J. H. Foo¹⁶⁶, G. T. Forcolin^{76a,76b}, B. C. Forland⁶⁶, A. Formica¹⁴⁴, F. A. Förster¹⁴, A. C. Forti¹⁰¹, E. Fortin¹⁰², M. G. Foti¹³⁴, D. Fournier⁶⁵, H. Fox⁹⁰, P. Francavilla^{72a,72b}, S. Francescato^{73a,73b}, M. Franchini^{23a,23b}, S. Franchino^{61a}, D. Francis³⁶, L. Franco⁵, L. Franconi²⁰, M. Franklin⁵⁹, G. Frattari^{73a,73b}, A. N. Fray⁹³, P. M. Freeman²¹, B. Freund¹¹⁰, W. S. Freund^{81b}, E. M. Freundlich⁴⁷, D. C. Frizzell¹²⁸, D. Froidevaux³⁶, J. A. Frost¹³⁴, M. Fujimoto¹²⁶, C. Fukunaga¹⁶³, E. Fullana Torregrosa¹⁷³, T. Fusayasu¹¹⁶, J. Fuster¹⁷³, A. Gabrielli^{23a,23b}, A. Gabrielli³⁶, S. Gadatsch⁵⁴, P. Gadow¹¹⁵, G. Gagliardi^{55a,55b}, L. G. Gagnon¹¹⁰, G. E. Gallardo¹³⁴, E. J. Gallas¹³⁴, B. J. Gallop¹⁴³, G. Galster⁴⁰, R. Gamboa Goni⁹³, K. K. Gan¹²⁷, S. Ganguly¹⁷⁹, J. Gao^{60a}, Y. Gao⁵⁰, Y. S. Gao^{31,l}, F. M. Garay Walls^{146a}, C. García¹⁷³, J. E. García Navarro¹⁷³, J. A. García Pascual^{15a}, C. Garcia-Argos⁵², M. Garcia-Sciveres¹⁸, R. W. Gardner³⁷, N. Garelli¹⁵², S. Gargiulo⁵², C. A. Garner¹⁶⁶, V. Garonne¹³³, S. J. Gasirowski¹⁴⁷, P. Gaspar^{81b}, A. Gaudiello^{55a,55b}, G. Gaudio^{71a}, I. L. Gavrilenko¹¹¹, A. Gavrilyuk¹²⁴, C. Gay¹⁷⁴, G. Gaycken⁴⁶, E. N. Gazis¹⁰, A. A. Geanta^{27b}, C. M. Gee¹⁴⁵, C. N. P. Gee¹⁴³, J. Geisen⁹⁷, M. Geisen¹⁰⁰, C. Gemme^{55b}, M. H. Genest⁵⁸, C. Geng¹⁰⁶, S. Gentile^{73a,73b}, S. George⁹⁴, T. Gerialis⁴⁴, L. O. Gerlach⁵³, P. Gessinger-Befurt¹⁰⁰, G. Gessner⁴⁷, S. Ghasemi¹⁵⁰, M. Ghasemi Bostanabad¹⁷⁵, M. Ghneimat¹⁵⁰, A. Ghosh⁶⁵, A. Ghosh⁷⁸, B. Giacobbe^{23b}, S. Giagu^{73a,73b}, N. Giangiacomi^{23a,23b}, P. Giannetti^{72a}, A. Giannini^{70a,70b}, G. Giannini¹⁴, S. M. Gibson⁹⁴, M. Gignac¹⁴⁵, D. T. Gil^{84b}, D. Gillberg³⁴, G. Gilles¹⁸¹, D. M. Gingrich^{3,al}, M. P. Giordani^{67a,67c}, P. F. Giraud¹⁴⁴, G. Giugliarelli^{67a,67c}, D. Giugni^{69a}, F. Giuli^{74a,74b}, S. Gkaitatzis¹⁶¹, I. Gkialas^{9,g}, E. L. Gkoukousis¹⁴, P. Gkoutoumis¹⁰, L. K. Gladilin¹¹³, C. Glasman⁹⁹, J. Glatzer¹⁴, P. C. F. Glaysher⁴⁶, A. Glazov⁴⁶, G. R. Gledhill¹³¹, I. Gnani^{41b,b}, M. Goblirsch-Kolb²⁶, D. Godin¹¹⁰, S. Goldfarb¹⁰⁵, T. Golling⁵⁴, D. Golubkov¹²³, A. Gomes^{139a,139b}, R. Goncalves Gama⁵³, R. Gonçalves^{139a,139c}, G. Gonella¹³¹, L. Gonella²¹, A. Gongadze⁸⁰

R. Keeler¹⁷⁵, R. Kehoe⁴², J. S. Keller³⁴, E. Kellermann⁹⁷, D. Kelsey¹⁵⁵, J. J. Kempster²¹, J. Kendrick²¹, K. E. Kennedy³⁹, O. Kepka¹⁴⁰, S. Kersten¹⁸¹, B. P. Kerševan⁹², S. Ketabchi Haghighat¹⁶⁶, M. Khader¹⁷², F. Khalil-Zada¹³, M. Khandoga¹⁴⁴, A. Khanov¹²⁹, A. G. Kharlamov^{122a,122b}, T. Kharlamova^{122a,122b}, E. E. Khoda¹⁷⁴, A. Khodinov¹⁶⁵, T. J. Khoo⁵⁴, G. Khorauli¹⁷⁶, E. Khramov⁸⁰, J. Khubua^{158b}, S. Kido⁸³, M. Kiehn⁵⁴, C. R. Kilby⁹⁴, E. Kim¹⁶⁴, Y. K. Kim³⁷, N. Kimura⁹⁵, B. T. King^{91,*}, A. Kirchoff⁵³, D. Kirchmeier⁴⁸, J. Kirk¹⁴³, A. E. Kiryunin¹¹⁵, T. Kishimoto¹⁶², D. P. Kisliuk¹⁶⁶, V. Kitali⁴⁶, C. Kitsaki¹⁰, O. Kivernyk²⁴, T. Klapdor-Kleingrothaus⁵², M. Klassen^{61a}, C. Klein³⁴, M. H. Klein¹⁰⁶, M. Klein⁹¹, U. Klein⁹¹, K. Kleinknecht¹⁰⁰, P. Klimek¹²¹, A. Klimentov²⁹, T. Klingl²⁴, T. Klioutchnikova³⁶, F. F. Klitzner¹¹⁴, P. Kluit¹²⁰, S. Kluth¹¹⁵, E. Kneringer⁷⁷, E. B. F. G. Knoops¹⁰², A. Knue⁵², D. Kobayashi⁸⁸, T. Kobayashi¹⁶², M. Kobel⁴⁸, M. Kocian¹⁵², T. Kodama¹⁶², P. Kodys¹⁴², D. M. Koeck¹⁵⁵, P. T. Koenig²⁴, T. Koffas³⁴, N. M. Köhler³⁶, M. Kolb¹⁴⁴, I. Koletsou⁵, T. Komarek¹³⁰, T. Kondo⁸², K. Köneke⁵², A. X. Y. Kong¹, A. C. König¹¹⁹, T. Kono¹²⁶, V. Konstantinides⁹⁵, N. Konstantinidis⁹⁵, B. Konya⁹⁷, R. Kopeliansky⁶⁶, S. Koperny^{84a}, K. Korcyl⁸⁵, K. Kordas¹⁶¹, G. Koren¹⁶⁰, A. Korn⁹⁵, I. Korolkov¹⁴, E. V. Korolkova¹⁴⁸, N. Korotkova¹¹³, O. Kortner¹¹⁵, S. Kortner¹¹⁵, V. V. Kostyukhin^{148,165}, A. Kotsokechagia⁶⁵, A. Kotwal⁴⁹, A. Koulouris¹⁰, A. Kourkoumeli-Charalampidi^{71a,71b}, C. Kourkoumelis⁹, E. Kourlitis⁶, V. Kouskoura²⁹, R. Kowalewski¹⁷⁵, W. Kozanecki¹⁰¹, A. S. Kozhin¹²³, V. A. Kramarenko¹¹³, G. Kramberger⁹², D. Krasnopevtsev^{60a}, M. W. Krasny¹³⁵, A. Krasznahorkay³⁶, D. Krauss¹¹⁵, J. A. Kremer¹⁰⁰, J. Kretzschmar⁹¹, P. Krieger¹⁶⁶, F. Krieter¹¹⁴, A. Krishnan^{61b}, K. Krizka¹⁸, K. Kroeninger⁴⁷, H. Kroha¹¹⁵, J. Kroll¹⁴⁰, J. Kroll¹³⁶, K. S. Krowpman¹⁰⁷, U. Kruchonak⁸⁰, H. Krüger²⁴, N. Krumnack⁷⁹, M. C. Kruse⁴⁹, J. A. Krzysiak⁸⁵, O. Kuchinskaia¹⁶⁵, S. Kudach^{4b}, D. Kuechler⁴⁶, J. T. Kuechler⁴⁶, S. Kuehn³⁶, A. Kugel^{61a}, T. Kuhl⁴⁶, V. Kukhtin⁸⁰, Y. Kulchitsky^{108,ac}, S. Kuleshov^{146b}, Y. P. Kulinich¹⁷², M. Kuna⁵⁸, T. Kunigo⁸⁶, A. Kupco¹⁴⁰, T. Kupfer⁴⁷, O. Kuprash⁵², H. Kurashige⁸³, L. L. Kurchaninov^{167a}, Y. A. Kurochkin¹⁰⁸, A. Kurova¹¹², M. G. Kurth^{15a,15d}, E. S. Kuwertz³⁶, M. Kuze¹⁶⁴, A. K. Kvam¹⁴⁷, J. Kvita¹³⁰, T. Kwan¹⁰⁴, F. La Ruffa^{41a,41b}, C. Lacasta¹⁷³, F. Lacava^{73a,73b}, D. P. J. Lack¹⁰¹, H. Lacker¹⁹, D. Lacour¹³⁵, E. Ladygin⁸⁰, R. Lafaye⁵, B. Laforge¹³⁵, T. Lagouri^{146b}, S. Lai⁵³, I. K. Lakomic^{84a}, J. E. Lambert¹²⁸, S. Lammers⁶⁶, W. Lampl⁷, C. Lampoudis¹⁶¹, E. Lançon²⁹, U. Landgraf⁵², M. P. J. Landon⁹³, M. C. Lanfermann⁵⁴, V. S. Lang⁵², J. C. Lange⁵³, R. J. Langenberg¹⁰³, A. J. Lankford¹⁷⁰, F. Lanni²⁹, K. Lantzsch²⁴, A. Lanza^{71a}, A. Lapertosa^{55a,55b}, S. Laplace¹³⁵, J. F. Laporte¹⁴⁴, T. Lari^{69a}, F. Lasagni Manghi^{23a,23b}, M. Lassnig³⁶, T. S. Lau^{63a}, A. Laudrain⁶⁵, A. Laurier³⁴, M. Lavorgna^{70a,70b}, S. D. Lawlor⁹⁴, M. Lazzaroni^{69a,69b}, B. Le¹⁰¹, E. Le Guirriec¹⁰², A. Lebedev⁷⁹, M. LeBlanc⁷, T. LeCompte⁶, F. Ledroit-Guillon⁵⁸, A. C. A. Lee⁹⁵, C. A. Lee²⁹, G. R. Lee¹⁷, L. Lee⁵⁹, S. C. Lee¹⁵⁷, S. Lee⁷⁹, B. Lefebvre^{167a}, H. P. Lefebvre⁹⁴, M. Lefebvre¹⁷⁵, C. Leggett¹⁸, K. Lehmann¹⁵¹, N. Lehmann²⁰, G. Lehmann Miotto³⁶, W. A. Leight⁴⁶, A. Leisos^{161,u}, M. A. L. Leite^{81d}, C. E. Leitgeb¹¹⁴, R. Leitner¹⁴², D. Lellouch^{179,*}, K. J. C. Leney⁴², T. Lenz²⁴, S. Leone^{72a}, C. Leonidopoulos⁵⁰, A. Leopold¹³⁵, C. Leroy¹¹⁰, R. Les¹⁰⁷, C. G. Lester³², M. Levchenko¹³⁷, J. Levêque⁵, D. Levin¹⁰⁶, L. J. Levinson¹⁷⁹, D. J. Lewis²¹, B. Li^{15b}, B. Li¹⁰⁶, C.-Q. Li^{60a}, F. Li^{60c}, H. Li^{60a}, H. Li^{60b}, J. Li^{60c}, K. Li¹⁴⁷, L. Li^{60c}, M. Li^{15a,15d}, Q. Li^{15a,15d}, Q. Y. Li^{60a}, S. Li^{60c,60d}, X. Li⁴⁶, Y. Li⁴⁶, Z. Li^{60b}, Z. Li¹³⁴, Z. Li¹⁰⁴, Z. Liang^{15a}, M. Liberatore⁴⁶, B. Liberti^{74a}, A. Liblong¹⁶⁶, K. Lie^{63c}, S. Lim²⁹, C. Y. Lin³², K. Lin¹⁰⁷, R. A. Linck⁶⁶, R. E. Lindley⁷, J. H. Lindon²¹, A. Linss⁴⁶, A. L. Lioni⁵⁴, E. Lipeles¹³⁶, A. Lipniacka¹⁷, T. M. Liss^{172,ak}, A. Lister¹⁷⁴, J. D. Little⁸, B. Liu⁷⁹, B. L. Liu⁶, H. B. Liu²⁹, J. B. Liu^{60a}, J. K. K. Liu³⁷, K. Liu^{60d}, M. Liu^{60a}, P. Liu^{15a}, Y. Liu⁴⁶, Y. Liu^{15a,15d}, Y. L. Liu¹⁰⁶, Y. W. Liu^{60a}, M. Livan^{71a,71b}, A. Lleres⁵⁸, J. Llorente Merino¹⁵¹, S. L. Lloyd⁹³, C. Y. Lo^{63b}, E. M. Lobodzinska⁴⁶, P. Loch⁷, S. Loffredo^{74a,74b}, T. Lohse¹⁹, K. Lohwasser¹⁴⁸, M. Lokajicek¹⁴⁰, J. D. Long¹⁷², R. E. Long⁹⁰, I. Longarini^{73a,73b}, L. Longo³⁶, K. A. Looper¹²⁷, I. Lopez Paz¹⁰¹, A. Lopez Solis¹⁴⁸, J. Lorenz¹¹⁴, N. Lorenzo Martinez⁵, A. M. Lory¹¹⁴, P. J. Lösel¹¹⁴, A. Lösle⁵², X. Lou⁴⁶, X. Lou^{15a}, A. Lounis⁶⁵, J. Love⁶, P. A. Love⁹⁰, J. J. Lozano Bahilo¹⁷³, M. Lu^{60a}, Y. J. Lu⁶⁴, H. J. Lubatti¹⁴⁷, C. Luci^{73a,73b}, F. L. Lucio Alves^{15c}, A. Lucotte⁵⁸, F. Luehring⁶⁶, I. Luise¹³⁵, L. Luminari^{73a}, B. Lund-Jensen¹⁵³, M. S. Lutz¹⁶⁰, D. Lynn²⁹, H. Lyons⁹¹, R. Lysak¹⁴⁰, E. Lytken⁹⁷, F. Lyu^{15a}, V. Lyubushkin⁸⁰, T. Lyubushkina⁸⁰, H. Ma²⁹, L. L. Ma^{60b}, Y. Ma⁹⁵, D. M. Mac Donell¹⁷⁵, G. Maccarrone⁵¹, A. Macchiolo¹¹⁵, C. M. Macdonald¹⁴⁸, J. C. MacDonald¹⁴⁸, J. Machado Miguens¹³⁶, D. Madaffari¹⁷³, R. Madar³⁸, W. F. Mader⁴⁸, M. Madugoda Ralalage Don¹²⁹, N. Madysa⁴⁸, J. Maeda⁸³, T. Maeno²⁹, M. Maerker⁴⁸, V. Magerl⁵², N. Magini⁷⁹, J. Magro^{67a,67c,q}, D. J. Mahon³⁹, C. Maidantchik^{81b}, T. Maier¹¹⁴, A. Maio^{139a,139b,139d}, K. Maj^{84a}, O. Majersky^{28a}, S. Majewski¹³¹, Y. Makida⁸², N. Makovec⁶⁵, B. Malaescu¹³⁵, Pa. Malecki⁸⁵, V. P. Maleev¹³⁷, F. Malek⁵⁸

D. Malito^{41a,41b}, U. Mallik⁷⁸, D. Malon⁶, C. Malone³², S. Maltezos¹⁰, S. Malyukov⁸⁰, J. Mamuzic¹⁷³, G. Mancini^{70a,70b}, I. Mandić⁹², L. Manhaes de Andrade Filho^{81a}, I. M. Maniatis¹⁶¹, J. Manjarres Ramos⁴⁸, K. H. Mankinen⁹⁷, A. Mann¹¹⁴, A. Manousos⁷⁷, B. Mansoulie¹⁴⁴, I. Manthos¹⁶¹, S. Manzoni¹²⁰, A. Marantis¹⁶¹, G. Marceca³⁰, L. Marchese¹³⁴, G. Marchiori¹³⁵, M. Marcisovsky¹⁴⁰, L. Marcoccia^{74a,74b}, C. Marcon⁹⁷, C. A. Marin Tobon³⁶, M. Marjanovic¹²⁸, Z. Marshall¹⁸, M. U. F. Martensson¹⁷¹, S. Marti-Garcia¹⁷³, C. B. Martin¹²⁷, T. A. Martin¹⁷⁷, V. J. Martin⁵⁰, B. Martin dit Latour¹⁷, L. Martinelli^{75a,75b}, M. Martinez^{14,w}, P. Martinez Agullo¹⁷³, V. I. Martinez Outschoorn¹⁰³, S. Martin-Haugh¹⁴³, V. S. Martoiu^{27b}, A. C. Martyniuk⁹⁵, A. Marzin³⁶, S. R. Maschek¹¹⁵, L. Masetti¹⁰⁰, T. Mashimo¹⁶², R. Mashinistov¹¹¹, J. Masik¹⁰¹, A. L. Maslennikov^{122a,122b}, L. Massa^{23a,23b}, P. Massarotti^{70a,70b}, P. Mastrandrea^{72a,72b}, A. Mastroberardino^{41a,41b}, T. Masubuchi¹⁶², D. Matakias²⁹, A. Matic¹¹⁴, N. Matsuzawa¹⁶², P. Mättig²⁴, J. Maurer^{27b}, B. Maček⁹², D. A. Maximov^{122a,122b}, R. Mazini¹⁵⁷, I. Maznas¹⁶¹, S. M. Mazza¹⁴⁵, J. P. Mc Gowan¹⁰⁴, S. P. Mc Kee¹⁰⁶, T. G. McCarthy¹¹⁵, W. P. McCormack¹⁸, E. F. McDonald¹⁰⁵, J. A. Mcfayden³⁶, G. Mchedlidze^{158b}, M. A. McKay⁴², K. D. McLean¹⁷⁵, S. J. McMahan¹⁴³, P. C. McNamara¹⁰⁵, C. J. McNicol¹⁷⁷, R. A. McPherson^{175.ab}, J. E. Mdhuli^{33e}, Z. A. Meadows¹⁰³, S. Meehan³⁶, T. Megy³⁸, S. Mehlhase¹¹⁴, A. Mehta⁹¹, B. Meirose⁴³, D. Melini¹⁵⁹, B. R. Mellado Garcia^{33e}, J. D. Mellenthin⁵³, M. Melo^{28a}, F. Meloni⁴⁶, A. Melzer²⁴, E. D. Mendes Gouveia^{139a,139e}, L. Meng³⁶, X. T. Meng¹⁰⁶, S. Menke¹¹⁵, E. Meoni^{41a,41b}, S. Mergelmeyer¹⁹, S. A. M. Merkt¹³⁸, C. Merlassino¹³⁴, P. Mermod⁵⁴, L. Merola^{70a,70b}, C. Meroni^{69a}, G. Merz¹⁰⁶, O. Meshkov^{113,111}, J. K. R. Meshreki¹⁵⁰, J. Metcalfe⁶, A. S. Mete⁶, C. Meyer⁶⁶, J.-P. Meyer¹⁴⁴, M. Michetti¹⁹, R. P. Middleton¹⁴³, L. Mijovic⁵⁰, G. Mikenberg¹⁷⁹, M. Mikestikova¹⁴⁰, M. Mikuž⁹², H. Mildner¹⁴⁸, A. Milic¹⁶⁶, C. D. Milke⁴², D. W. Miller³⁷, A. Milov¹⁷⁹, D. A. Milstead^{45a,45b}, R. A. Mina¹⁵², A. A. Minaenko¹²³, I. A. Minashvili^{158b}, A. I. Mincer¹²⁵, B. Mindur^{84a}, M. Mineev⁸⁰, Y. Minegishi¹⁶², L. M. Mir¹⁴, M. Mironova¹³⁴, A. Mirto^{68a,68b}, K. P. Mistry¹³⁶, T. Mitani¹⁷⁸, J. Mitrevski¹¹⁴, V. A. Mitsou¹⁷³, M. Mittal^{60c}, O. Miu¹⁶⁶, A. Miucci²⁰, P. S. Miyagawa⁹³, A. Mizukami⁸², J. U. Mjörnmark⁹⁷, T. Mkrtchyan^{61a}, M. Mlynarikova¹⁴², T. Moa^{45a,45b}, S. Mobius⁵³, K. Mochizuki¹¹⁰, P. Mogg¹¹⁴, S. Mohapatra³⁹, R. Moles-Valls²⁴, K. Mönig⁴⁶, E. Monnier¹⁰², A. Montalbano¹⁵¹, J. Montejo Berlingen³⁶, M. Montella⁹⁵, F. Monticelli⁸⁹, S. Monzani^{69a}, N. Morange⁶⁵, D. Moreno^{22a}, M. Moreno Llácer¹⁷³, C. Moreno Martinez¹⁴, P. Morettini^{55b}, M. Morgenstern¹⁵⁹, S. Morgenstern⁴⁸, D. Mori¹⁵¹, M. Morii⁵⁹, M. Morinaga¹⁷⁸, V. Morisbak¹³³, A. K. Morley³⁶, G. Mornacchi³⁶, A. P. Morris⁹⁵, L. Morvaj¹⁵⁴, P. Moschovakos³⁶, B. Moser¹²⁰, M. Mosidze^{158b}, T. Moskalets¹⁴⁴, H. J. Moss¹⁴⁸, J. Moss^{31,m}, E. J. W. Moyses¹⁰³, S. Muanza¹⁰², J. Mueller¹³⁸, R. S. P. Mueller¹¹⁴, D. Muenstermann⁹⁰, G. A. Mullier⁹⁷, D. P. Mungo^{69a,69b}, J. L. Munoz Martinez¹⁴, F. J. Munoz Sanchez¹⁰¹, P. Murin^{28b}, W. J. Murray^{143,177}, A. Murrone^{69a,69b}, J. M. Muse¹²⁸, M. Muškinja¹⁸, C. Mwewa^{33a}, A. G. Myagkov^{123,ag}, A. A. Myers¹³⁸, J. Myers¹³¹, M. Myska¹⁴¹, B. P. Nachman¹⁸, O. Nackenhorst⁴⁷, A. Nag Nag⁴⁸, K. Nagai¹³⁴, K. Nagano⁸², Y. Nagasaka⁶², J. L. Nagle²⁹, E. Nagy¹⁰², A. M. Nairz³⁶, Y. Nakahama¹¹⁷, K. Nakamura⁸², T. Nakamura¹⁶², H. Nanjo¹³², F. Napolitano^{61a}, R. F. Naranjo Garcia⁴⁶, R. Narayan⁴², I. Naryshkin¹³⁷, T. Naumann⁴⁶, G. Navarro^{22a}, P. Y. Nechaeva¹¹¹, F. Nechansky⁴⁶, T. J. Neep²¹, A. Negri^{71a,71b}, M. Negrini^{23b}, C. Nellist¹¹⁹, C. Nelson¹⁰⁴, M. E. Nelson^{45a,45b}, S. Nemecek¹⁴⁰, M. Nessi^{36,e}, M. S. Neubauer¹⁷², F. Neuhaus¹⁰⁰, M. Neumann¹⁸¹, R. Newhouse¹⁷⁴, P. R. Newman²¹, C. W. Ng¹³⁸, Y. S. Ng¹⁹, Y. W. Y. Ng¹⁷⁰, B. Ngair^{35e}, H. D. N. Nguyen¹⁰², T. Nguyen Manh¹¹⁰, E. Nibigira³⁸, R. B. Nickerson¹³⁴, R. Nicolaidou¹⁴⁴, D. S. Nielsen⁴⁰, J. Nielsen¹⁴⁵, M. Niemeyer⁵³, N. Nikiforou¹¹, V. Nikolaenko^{123,ag}, I. Nikolic-Audit¹³⁵, K. Nikolopoulos²¹, P. Nilsson²⁹, H. R. Nindhito⁵⁴, Y. Ninomiya⁸², A. Nisati^{73a}, N. Nishu^{60c}, R. Nisius¹¹⁵, I. Nitsche⁴⁷, T. Nitta¹⁷⁸, T. Nobe¹⁶², D. L. Noel³², Y. Noguchi⁸⁶, I. Nomidis¹³⁵, M. A. Nomura²⁹, M. Nordberg³⁶, J. Novak⁹², T. Novak⁹², O. Novgorodova⁴⁸, R. Novotny¹⁴¹, L. Nozka¹³⁰, K. Ntekas¹⁷⁰, E. Nurse⁹⁵, F. G. Oakham^{34,al}, H. Oberlack¹¹⁵, J. Ocariz¹³⁵, A. Ochi⁸³, I. Ochoa³⁹, J. P. Ochoa-Ricoux^{146a}, K. O'Connor²⁶, S. Oda⁸⁸, S. Odaka⁸², S. Oerdek⁵³, A. Ogrodnik^{84a}, A. Oh¹⁰¹, S. H. Oh⁴⁹, C. C. Ohm¹⁵³, H. Oide¹⁶⁴, M. L. Ojeda¹⁶⁶, H. Okawa¹⁶⁸, Y. Okazaki⁸⁶, M. W. O'Keefe⁹¹, Y. Okumura¹⁶², T. Okuyama⁸², A. Olariu^{27b}, L. F. Oleiro Seabra^{139a}, S. A. Olivares Pino^{146a}, D. Oliveira Damazio²⁹, J. L. Oliver¹, M. J. R. Olsson¹⁷⁰, A. Olszewski⁸⁵, J. Olszowska⁸⁵, Ö. Ö. Öncel²⁴, D. C. O'Neil¹⁵¹, A. P. O'Neill¹³⁴, A. Onofre^{139a,139e}, P. U. E. Onyisi¹¹, H. Oppen¹³³, R. G. Oreamuno Madriz¹²¹, M. J. Oreglia³⁷, G. E. Orellana⁸⁹, D. Orestano^{75a,75b}, N. Orlando¹⁴, R. S. Orr¹⁶⁶, V. O'Shea⁵⁷, R. Ospanov^{60a}, G. Otero y Garzon³⁰, H. Otono⁸⁸, P. S. Ott^{61a}, G. J. Ottino¹⁸, M. Ouchrif^{35d}, J. Ouellette²⁹, F. Ould-Saada¹³³, A. Ouraou¹⁴⁴, Q. Ouyang^{15a}, M. Owen⁵⁷, R. E. Owen¹⁴³, V. E. Ozcan^{12c}, N. Ozturk⁸, J. Pacalt¹³⁰, H. A. Pacey³², K. Pachal⁴⁹, A. Pacheco Pages¹⁴, C. Padilla Aranda¹⁴, S. Pagan Griso¹⁸, G. Palacino⁶⁶,

S. Palazzo⁵⁰, S. Palestini³⁶, M. Palka^{84b}, P. Palni^{84a}, C. E. Pandini⁵⁴, J. G. Panduro Vazquez⁹⁴, P. Pani⁴⁶, G. Panizzo^{67a,67c}, L. Paolozzi⁵⁴, C. Papadatos¹¹⁰, K. Papageorgiou^{9,g}, S. Parajuli⁴², A. Paramonov⁶, C. Paraskevopoulos¹⁰, D. Paredes Hernandez^{63b}, S. R. Paredes Saenz¹³⁴, B. Parida¹⁷⁹, T. H. Park¹⁶⁶, A. J. Parker³¹, M. A. Parker³², F. Parodi^{55a,55b}, E. W. Parrish¹²¹, J. A. Parsons³⁹, U. Parzefall⁵², L. Pascual Dominguez¹³⁵, V. R. Pascuzzi¹⁸, J. M. P. Pasner¹⁴⁵, F. Pasquali¹²⁰, E. Pasqualucci^{73a}, S. Passaggio^{55b}, F. Pastore⁹⁴, P. Pasuwan^{45a,45b}, S. Pataria¹⁰⁰, J. R. Pater¹⁰¹, A. Pathak^{180,i}, J. Patton⁹¹, T. Pauly³⁶, J. Pearkes¹⁵², B. Pearson¹¹⁵, M. Pedersen¹³³, L. Pedraza Diaz¹¹⁹, R. Pedro^{139a}, T. Peiffer⁵³, S. V. Peleganchuk^{122a,122b}, O. Penc¹⁴⁰, H. Peng^{60a}, B. S. Peralva^{81a}, M. M. Perego⁶⁵, A. P. Pereira Peixoto^{139a}, L. Pereira Sanchez^{45a,45b}, D. V. Perepelitsa²⁹, E. Perez Codina^{167a}, F. Peri¹⁹, L. Perini^{69a,69b}, H. Pernegger³⁶, S. Perrella³⁶, A. Perrevoort¹²⁰, K. Peters⁴⁶, R. F. Y. Peters¹⁰¹, B. A. Petersen³⁶, T. C. Petersen⁴⁰, E. Petit¹⁰², V. Petousis¹⁴¹, A. Petridis¹, C. Petridou¹⁶¹, F. Petrucci^{75a,75b}, M. Pettee¹⁸², N. E. Pettersson¹⁰³, K. Petukhova¹⁴², A. Peyaud¹⁴⁴, R. Pezoa^{146d}, L. Pezzotti^{71a,71b}, T. Pham¹⁰⁵, F. H. Phillips¹⁰⁷, P. W. Phillips¹⁴³, M. W. Phipps¹⁷², G. Piacquadio¹⁵⁴, E. Pianori¹⁸, A. Picazio¹⁰³, R. H. Pickles¹⁰¹, R. Piegaia³⁰, D. Pietreanu^{27b}, J. E. Pilcher³⁷, A. D. Pilkington¹⁰¹, M. Pinamonti^{67a,67c}, J. L. Pinfold³, C. Pitman Donaldson⁹⁵, M. Pitt¹⁶⁰, L. Pizzimento^{74a,74b}, M.-A. Pleier²⁹, V. Pleskot¹⁴², E. Plotnikova⁸⁰, P. Podberezko^{122a,122b}, R. Poettgen⁹⁷, R. Poggi⁵⁴, L. Poggioli¹³⁵, I. Pogrebnnyak¹⁰⁷, D. Pohl²⁴, I. Pokharel⁵³, G. Polesello^{71a}, A. Poley¹⁵¹, A. Policicchio^{73a,73b}, R. Polifka¹⁴², A. Polini^{23b}, C. S. Pollard⁴⁶, V. Polychronakos²⁹, D. Ponomarenko¹¹², L. Pontecorvo³⁶, S. Popa^{27a}, G. A. Popeneciu^{27d}, L. Portales⁵, D. M. Portillo Quintero⁵⁸, S. Pospisil¹⁴¹, K. Potamianos⁴⁶, I. N. Potrap⁸⁰, C. J. Potter³², H. Potti¹¹, T. Poulos⁹⁷, J. Poveda¹⁷³, T. D. Powell¹⁴⁸, G. Pownall⁴⁶, M. E. Pozo Astigarraga³⁶, P. Pralavorio¹⁰², S. Prell⁷⁹, D. Price¹⁰¹, M. Primavera^{68a}, M. L. Proffitt¹⁴⁷, N. Proklova¹¹², K. Prokofiev^{63c}, F. Prokoshin⁸⁰, S. Protopopescu²⁹, J. Proudfoot⁶, M. Przybycien^{84a}, D. Pudzha¹³⁷, A. Puri¹⁷², P. Puzo⁶⁵, D. Pyatizbyantseva¹¹², J. Qian¹⁰⁶, Y. Qin¹⁰¹, A. Quadt⁵³, M. Queitsch-Maitland³⁶, A. Qureshi¹, M. Racko^{28a}, F. Ragusa^{69a,69b}, G. Rahal⁹⁸, J. A. Raine⁵⁴, S. Rajagopalan²⁹, A. Ramirez Morales⁹³, K. Ran^{15a,15d}, D. M. Rauch⁴⁶, F. Rauscher¹¹⁴, S. Rave¹⁰⁰, B. Ravina¹⁴⁸, I. Ravinovich¹⁷⁹, J. H. Rawling¹⁰¹, M. Raymond³⁶, A. L. Read¹³³, N. P. Readoff⁵⁸, M. Reale^{68a,68b}, D. M. Rebuffi^{71a,71b}, G. Redlinger²⁹, K. Reeves⁴³, J. Reichert¹³⁶, D. Reikher¹⁶⁰, A. Reiss¹⁰⁰, A. Rej¹⁵⁰, C. Remser³⁶, A. Renardi⁴⁶, M. Renda^{27b}, M. B. Rendel¹¹⁵, S. Resconi^{69a}, E. D. Resseguie¹⁸, S. Rettie⁹⁵, B. Reynolds¹²⁷, E. Reynolds²¹, O. L. Rezanova^{122a,122b}, P. Reznicek¹⁴², E. Ricci^{76a,76b}, R. Richter¹¹⁵, S. Richter⁴⁶, E. Richter-Was^{84b}, M. Ridel¹³⁵, P. Rieck¹¹⁵, O. Rifki⁴⁶, M. Rijssenbeek¹⁵⁴, A. Rimoldi^{71a,71b}, M. Rimoldi⁴⁶, L. Rinaldi^{23b}, T. T. Rinn¹⁷², G. Ripellino¹⁵³, I. Riu¹⁴, P. Rivadeneira⁴⁶, J. C. Rivera Vergara¹⁷⁵, F. Rizatdinova¹²⁹, E. Rizvi⁹³, C. Rizzi³⁶, S. H. Robertson^{104,ab}, M. Robin⁴⁶, D. Robinson³², C. M. Robles Gajardo^{146d}, M. Robles Manzano¹⁰⁰, A. Robson⁵⁷, A. Rocchi^{74a,74b}, E. Rocco¹⁰⁰, C. Roda^{72a,72b}, S. Rodriguez Bosca¹⁷³, A. M. Rodríguez Vera^{167b}, S. Roe³⁶, J. Roggel¹⁸¹, O. Røhne¹³³, R. Røhrig¹¹⁵, R. A. Rojas^{146d}, B. Roland⁵², C. P. A. Roland⁶⁶, J. Roloff²⁹, A. Romaniouk¹¹², M. Romano^{23a,23b}, N. Rompotis⁹¹, M. Ronzani¹²⁵, L. Roos¹³⁵, S. Rosati^{73a}, G. Rosin¹⁰³, B. J. Rosser¹³⁶, E. Rossi⁴⁶, E. Rossi^{75a,75b}, E. Rossi^{70a,70b}, L. P. Rossi^{55b}, L. Rossini^{69a,69b}, R. Rosten¹⁴, M. Rotaru^{27b}, B. Rottler⁵², D. Rousseau⁶⁵, G. Rovelli^{71a,71b}, A. Roy¹¹, D. Roy^{33e}, A. Rozanov¹⁰², Y. Rozen¹⁵⁹, X. Ruan^{33e}, F. Rühr⁵², A. Ruiz-Martinez¹⁷³, A. Rummler³⁶, Z. Rurikova⁵², N. A. Rusakovich⁸⁰, H. L. Russell¹⁰⁴, L. Rustige^{38,47}, J. P. Rutherford⁷, E. M. Rüttinger¹⁴⁸, M. Rybar³⁹, G. Rybkin⁶⁵, E. B. Rye¹³³, A. Ryzhov¹²³, J. A. Sabater Iglesias⁴⁶, P. Sabatini⁵³, L. Sabetta^{73a,73b}, S. Sacerdoti⁶⁵, H. F.-W. Sadrozinski¹⁴⁵, R. Sadykov⁸⁰, F. Safai Tehrani^{73a}, B. Safarzadeh Samani¹⁵⁵, M. Safdari¹⁵², P. Saha¹²¹, S. Saha¹⁰⁴, M. Sahinsoy¹¹⁵, A. Sahu¹⁸¹, M. Saimpert³⁶, M. Saito¹⁶², T. Saito¹⁶², H. Sakamoto¹⁶², D. Salamani⁵⁴, G. Salamanna^{75a,75b}, A. Salnikov¹⁵², J. Salt¹⁷³, A. Salvador Salas¹⁴, D. Salvatore^{41a,41b}, F. Salvatore¹⁵⁵, A. Salvucci^{63a,63b,63c}, A. Salzburger³⁶, J. Samarati³⁶, D. Sammel⁵², D. Sampsonidis¹⁶¹, D. Sampsonidou¹⁶¹, J. Sánchez¹⁷³, A. Sanchez Pineda^{36,67a,67c}, H. Sandaker¹³³, C. O. Sander⁴⁶, I. G. Sanderswood⁹⁰, M. Sandhoff¹⁸¹, C. Sandoval^{22a}, D. P. C. Sankey¹⁴³, M. Sannino^{55a,55b}, Y. Sano¹¹⁷, A. Sansoni⁵¹, C. Santoni³⁸, H. Santos^{139a,139b}, S. N. Santpur¹⁸, A. Santra¹⁷³, K. A. Saoucha¹⁴⁸, A. Sapronov⁸⁰, J. G. Saraiva^{139a,139d}, O. Sasaki⁸², K. Sato¹⁶⁸, F. Sauerburger⁵², E. Sauvan⁵, P. Savard^{166,al}, R. Sawada¹⁶², C. Sawyer¹⁴³, L. Sawyer^{96,af}, I. Sayago Galvan¹⁷³, C. Sbarra^{23b}, A. Sbrizzi^{67a,67c}, T. Scanlon⁹⁵, J. Schaarschmidt¹⁴⁷, P. Schacht¹¹⁵, D. Schaefer³⁷, L. Schaefer¹³⁶, S. Schaepe³⁶, U. Schäfer¹⁰⁰, A. C. Schaffer⁶⁵, D. Schaile¹¹⁴, R. D. Schamberger¹⁵⁴, E. Schanet¹¹⁴, N. Scharmberg¹⁰¹, V. A. Schegelsky¹³⁷, D. Scheirich¹⁴², F. Schenck¹⁹, M. Schernau¹⁷⁰, C. Schiavi^{55a,55b}, L. K. Schildgen²⁴, Z. M. Schillaci²⁶

T. T. Tulbure^{27a}, A. N. Tuna⁵⁹, S. Turchikhin⁸⁰, D. Turgeman¹⁷⁹, I. Turk Cakir^{4b,s}, R. J. Turner²¹, R. Turra^{69a}, P. M. Tuts³⁹, S. Tzamarias¹⁶¹, E. Tzovara¹⁰⁰, K. Uchida¹⁶², F. Ukegawa¹⁶⁸, G. Unal³⁶, M. Unal¹¹, A. Undrus²⁹, G. Unel¹⁷⁰, F. C. Ungaro¹⁰⁵, Y. Unno⁸², K. Uno¹⁶², J. Urban^{28b}, P. Urquijo¹⁰⁵, G. Usai⁸, Z. Uysal^{12d}, V. Vacek¹⁴¹, B. Vachon¹⁰⁴, K. O. H. Vadla¹³³, T. Vafeiadis³⁶, A. Vaidya⁹⁵, C. Valderanis¹¹⁴, E. Valdes Santurio^{45a,45b}, M. Valente⁵⁴, S. Valentini^{23a,23b}, A. Valero¹⁷³, L. Valéry⁴⁶, R. A. Vallance²¹, A. Vallier³⁶, J. A. Valls Ferrer¹⁷³, T. R. Van Daalen¹⁴, P. Van Gemmeren⁶, I. Van Vulpen¹²⁰, M. Vanadia^{74a,74b}, W. Vandelli³⁶, M. Vandenbroucke¹⁴⁴, E. R. Vandewall¹²⁹, A. Vaniachine¹⁶⁵, D. Vannicola^{73a,73b}, R. Vari^{73a}, E. W. Varnes⁷, C. Varni^{55a,55b}, T. Varol¹⁵⁷, D. Varouchas⁶⁵, K. E. Varvell¹⁵⁶, M. E. Vasile^{27b}, G. A. Vasquez¹⁷⁵, F. Vazeille³⁸, D. Vazquez Furelos¹⁴, T. Vazquez Schroeder³⁶, J. Veatch⁵³, V. Vecchio¹⁰¹, M. J. Veen¹²⁰, L. M. Veloce¹⁶⁶, F. Veloso^{139a,139c}, S. Veneziano^{73a}, A. Ventura^{68a,68b}, A. Verbitskiy¹¹⁵, V. Vercesi^{71a}, M. Verducci^{72a,72b}, C. M. Vergel Infante⁷⁹, C. Vergis²⁴, W. Verkerke¹²⁰, A. T. Vermeulen¹²⁰, J. C. Vermeulen¹²⁰, C. Vernieri¹⁵², M. C. Vetterli^{151,al}, N. Viaux Maira^{146d}, T. Vickey¹⁴⁸, O. E. Vickey Boeriu¹⁴⁸, G. H. A. Viehhauser¹³⁴, L. Vigani^{61b}, M. Villa^{23a,23b}, M. Villaplana Perez³, E. M. Villhauer⁵⁰, E. Vilucchi⁵¹, M. G. Vincker³⁴, G. S. Virdee²¹, A. Vishwakarma⁵⁰, C. Vittori^{23a,23b}, I. Vivarelli¹⁵⁵, M. Vogel¹⁸¹, P. Vokac¹⁴¹, S. E. von Buddenbrock^{33c}, E. Von Toerne²⁴, V. Vorobel¹⁴², K. Vorobev¹¹², M. Vos¹⁷³, J. H. Vosseveld⁹¹, M. Vozak¹⁰¹, N. Vranjes¹⁶, M. Vranjes Milosavljevic¹⁶, V. Vrba¹⁴¹, M. Vreeswijk¹²⁰, R. Vuillermet³⁶, I. Vukotic³⁷, S. Wada¹⁶⁸, P. Wagner²⁴, W. Wagner¹⁸¹, J. Wagner-Kuhr¹¹⁴, S. Wahdan¹⁸¹, H. Wahlberg⁸⁹, R. Wakasa¹⁶⁸, V. M. Walbrecht¹¹⁵, J. Walder⁹⁰, R. Walker¹¹⁴, S. D. Walker⁹⁴, W. Walkowiak¹⁵⁰, V. Wallangen^{45a,45b}, A. M. Wang⁵⁹, A. Z. Wang¹⁸⁰, C. Wang^{60a}, C. Wang^{60c}, F. Wang¹⁸⁰, H. Wang¹⁸, H. Wang³, J. Wang^{63a}, P. Wang⁴², Q. Wang¹²⁸, R.-J. Wang¹⁰⁰, R. Wang^{60a}, R. Wang⁶, S. M. Wang¹⁵⁷, W. T. Wang^{60a}, W. Wang^{15c}, W. X. Wang^{60a}, Y. Wang^{60a}, Z. Wang¹⁰⁶, C. Wanotayaroj⁴⁶, A. Warburton¹⁰⁴, C. P. Ward³², D. R. Wardrope⁹⁵, N. Warrack⁵⁷, A. T. Watson²¹, M. F. Watson²¹, G. Watts¹⁴⁷, B. M. Waugh⁹⁵, A. F. Webb¹¹, C. Weber²⁹, M. S. Weber²⁰, S. A. Weber³⁴, S. M. Weber^{61a}, A. R. Weidberg¹³⁴, J. Weingarten⁴⁷, M. Weirich¹⁰⁰, C. Weiser⁵², P. S. Wells³⁶, T. Wenaus²⁹, B. Wendland⁴⁷, T. Wengler³⁶, S. Wenig³⁶, N. Wermes²⁴, M. Wessels^{61a}, T. D. Weston²⁰, K. Whalen¹³¹, N. L. Whallon¹⁴⁷, A. M. Wharton⁹⁰, A. S. White¹⁰⁶, A. White⁸, M. J. White¹, D. Whiteson¹⁷⁰, B. W. Whitmore⁹⁰, W. Wiedenmann¹⁸⁰, C. Wiel⁴⁸, M. Wielders¹⁴³, N. Wieseotte¹⁰⁰, C. Wiglesworth⁴⁰, L. A. M. Wiik-Fuchs⁵², H. G. Wilkens³⁶, L. J. Wilkins⁹⁴, H. H. Williams¹³⁶, S. Williams³², S. Willocq¹⁰³, P. J. Windischhofer¹³⁴, I. Wingerter-Seez⁵, E. Winkels¹⁵⁵, F. Winklmeier¹³¹, B. T. Winter⁵², M. Wittgen¹⁵², M. Wobisch⁹⁶, A. Wolf¹⁰⁰, R. Wölker¹³⁴, J. Wollrath⁵², M. W. Wolter⁸⁵, H. Wolters^{139a,139c}, V. W. S. Wong¹⁷⁴, N. L. Woods¹⁴⁵, S. D. Worm⁴⁶, B. K. Wosiek⁸⁵, K. W. Woźniak⁸⁵, K. Wraight⁵⁷, S. L. Wu¹⁸⁰, X. Wu⁵⁴, Y. Wu^{60a}, J. Wuerzinger¹³⁴, T. R. Wyatt¹⁰¹, B. M. Wynne⁵⁰, S. Xella⁴⁰, L. Xia¹⁷⁷, J. Xiang^{63c}, X. Xiao¹⁰⁶, X. Xie^{60a}, I. Xioidis¹⁵⁵, D. Xu^{15a}, H. Xu^{60a}, H. Xu^{60a}, L. Xu²⁹, T. Xu¹⁴⁴, W. Xu¹⁰⁶, Z. Xu^{60b}, Z. Xu¹⁵², B. Yabsley¹⁵⁶, S. Yacoub^{33a}, K. Yajima¹³², D. P. Yallup⁹⁵, N. Yamaguchi⁸⁸, Y. Yamaguchi¹⁶⁴, A. Yamamoto⁸², M. Yamatani¹⁶², T. Yamazaki¹⁶², Y. Yamazaki⁸³, J. Yan^{60c}, Z. Yan²⁵, H. J. Yang^{60c,60d}, H. T. Yang¹⁸, S. Yang^{60a}, T. Yang^{63c}, X. Yang^{58,60b}, Y. Yang¹⁶², Z. Yang^{60a}, W.-M. Yao¹⁸, Y. C. Yap⁴⁶, Y. Yasu⁸², E. Yatsenko^{60c}, H. Ye^{15c}, J. Ye⁴², S. Ye²⁹, I. Yeletsikh⁸⁰, M. R. Yexley⁹⁰, E. Yigitbasi²⁵, P. Yin³⁹, K. Yorita¹⁷⁸, K. Yoshihara⁷⁹, C. J. S. Young³⁶, C. Young¹⁵², J. Yu⁷⁹, R. Yuan^{60b,h}, X. Yue^{61a}, M. Zaazoua^{35e}, B. Zabinski⁸⁵, G. Zacharis¹⁰, E. Zaffaroni⁵⁴, J. Zahreddine¹³⁵, A. M. Zaitsev^{123,ag}, T. Zakareishvili^{158b}, N. Zakharchuk³⁴, S. Zambito³⁶, D. Zanzi³⁶, D. R. Zaripovas⁵⁷, S. V. Zeißner⁴⁷, C. Zeitnitz¹⁸¹, G. Zemaityte¹³⁴, J. C. Zeng¹⁷², O. Zenin¹²³, T. Ženiš^{28a}, D. Zerwas⁶⁵, M. Zgubić¹³⁴, B. Zhang^{15c}, D. F. Zhang^{15b}, G. Zhang^{15b}, J. Zhang⁶, Kaili. Zhang^{15a}, L. Zhang^{15c}, L. Zhang^{60a}, M. Zhang¹⁷², R. Zhang¹⁸⁰, S. Zhang¹⁰⁶, X. Zhang^{60c}, X. Zhang^{60b}, Y. Zhang^{15a,15d}, Z. Zhang^{63a}, Z. Zhang⁶⁵, P. Zhao⁴⁹, Z. Zhao^{60a}, A. Zhemchugov⁸⁰, Z. Zheng¹⁰⁶, D. Zhong¹⁷², B. Zhou¹⁰⁶, C. Zhou¹⁸⁰, H. Zhou⁷, M. S. Zhou^{15a,15d}, M. Zhou¹⁵⁴, N. Zhou^{60c}, Y. Zhou⁷, C. G. Zhu^{60b}, C. Zhu^{15a,15d}, H. L. Zhu^{60a}, H. Zhu^{15a}, J. Zhu¹⁰⁶, Y. Zhu^{60a}, X. Zhuang^{15a}, K. Zhukov¹¹¹, V. Zhulanov^{122a,122b}, D. Zieminska⁶⁶, N. I. Zimine⁸⁰, S. Zimmermann⁵², Z. Zinonos¹¹⁵, M. Ziolkowski¹⁵⁰, L. Živković¹⁶, G. Zobernig¹⁸⁰, A. Zoccoli^{23a,23b}, K. Zoch⁵³, T. G. Zorbas¹⁴⁸, R. Zou³⁷, L. Zwalinski³⁶

¹ Department of Physics, University of Adelaide, Adelaide, Australia

² Physics Department, SUNY Albany, Albany, NY, USA

³ Department of Physics, University of Alberta, Edmonton, AB, Canada

- ⁴ (a)Department of Physics, Ankara University, Ankara, Turkey; (b)Application and Research Center for Advanced Studies, Istanbul Aydin University, Istanbul, Turkey; (c)Division of Physics, TOBB University of Economics and Technology, Ankara, Turkey
- ⁵ LAPP, Université Grenoble Alpes, Université Savoie Mont Blanc, CNRS/IN2P3, Annecy, France
- ⁶ High Energy Physics Division, Argonne National Laboratory, Argonne, IL, USA
- ⁷ Department of Physics, University of Arizona, Tucson, AZ, USA
- ⁸ Department of Physics, University of Texas at Arlington, Arlington, TX, USA
- ⁹ Physics Department, National and Kapodistrian University of Athens, Athens, Greece
- ¹⁰ Physics Department, National Technical University of Athens, Zografou, Greece
- ¹¹ Department of Physics, University of Texas at Austin, Austin, TX, USA
- ¹² (a)Faculty of Engineering and Natural Sciences, Bahcesehir University, Istanbul, Turkey; (b)Faculty of Engineering and Natural Sciences, Istanbul Bilgi University, Istanbul, Turkey; (c)Department of Physics, Bogazici University, Istanbul, Turkey; (d)Department of Physics Engineering, Gaziantep University, Gaziantep, Turkey
- ¹³ Institute of Physics, Azerbaijan Academy of Sciences, Baku, Azerbaijan
- ¹⁴ Institut de Física d'Altes Energies (IFAE), Barcelona Institute of Science and Technology, Barcelona, Spain
- ¹⁵ (a)Institute of High Energy Physics, Chinese Academy of Sciences, Beijing, China; (b)Physics Department, Tsinghua University, Beijing, China; (c)Department of Physics, Nanjing University, Nanjing, China; (d)University of Chinese Academy of Science (UCAS), Beijing, China
- ¹⁶ Institute of Physics, University of Belgrade, Belgrade, Serbia
- ¹⁷ Department for Physics and Technology, University of Bergen, Bergen, Norway
- ¹⁸ Physics Division, Lawrence Berkeley National Laboratory and University of California, Berkeley, CA, USA
- ¹⁹ Institut für Physik, Humboldt Universität zu Berlin, Berlin, Germany
- ²⁰ Albert Einstein Center for Fundamental Physics and Laboratory for High Energy Physics, University of Bern, Bern, Switzerland
- ²¹ School of Physics and Astronomy, University of Birmingham, Birmingham, UK
- ²² (a)Facultad de Ciencias y Centro de Investigaciones, Universidad Antonio Nariño, Bogotá, Colombia; (b)Departamento de Física, Universidad Nacional de Colombia, Bogotá, Colombia
- ²³ (a)Dipartimento di Fisica, INFN Bologna and Università di Bologna, Bologna, Italy; (b)INFN Sezione di Bologna, Bologna, Italy
- ²⁴ Physikalisches Institut, Universität Bonn, Bonn, Germany
- ²⁵ Department of Physics, Boston University, Boston, MA, USA
- ²⁶ Department of Physics, Brandeis University, Waltham, MA, USA
- ²⁷ (a)Transilvania University of Brasov, Brasov, Romania; (b)Horia Hulubei National Institute of Physics and Nuclear Engineering, Bucharest, Romania; (c)Department of Physics, Alexandru Ioan Cuza University of Iasi, Iasi, Romania; (d)Physics Department, National Institute for Research and Development of Isotopic and Molecular Technologies, Cluj-Napoca, Romania; (e)University Politehnica Bucharest, Bucharest, Romania; (f)West University in Timisoara, Timisoara, Romania
- ²⁸ (a)Faculty of Mathematics, Physics and Informatics, Comenius University, Bratislava, Slovakia; (b)Department of Subnuclear Physics, Institute of Experimental Physics of the Slovak Academy of Sciences, Kosice, Slovak Republic
- ²⁹ Physics Department, Brookhaven National Laboratory, Upton, NY, USA
- ³⁰ Departamento de Física, Universidad de Buenos Aires, Buenos Aires, Argentina
- ³¹ California State University, Long Beach, CA, USA
- ³² Cavendish Laboratory, University of Cambridge, Cambridge, UK
- ³³ (a)Department of Physics, University of Cape Town, Cape Town, South Africa; (b)iThemba Labs, Cape Town, Western Cape, South Africa; (c)Department of Mechanical Engineering Science, University of Johannesburg, Johannesburg, South Africa; (d)University of South Africa, Department of Physics, Pretoria, South Africa; (e)School of Physics, University of the Witwatersrand, Johannesburg, South Africa
- ³⁴ Department of Physics, Carleton University, Ottawa, ON, Canada
- ³⁵ (a)Faculté des Sciences Ain Chock, Réseau Universitaire de Physique des Hautes Energies-Université Hassan II, Casablanca, Morocco; (b)Faculté des Sciences, Université Ibn-Tofail, Kenitra, Morocco; (c)Faculté des Sciences Semlalia, Université Cadi Ayyad, LPHEA-Marrakech, Marrakech, Morocco; (d)Faculté des Sciences, Université Mohamed Premier and LTPM, Oujda, Morocco; (e)Faculté des sciences, Université Mohammed V, Rabat, Morocco
- ³⁶ CERN, Geneva, Switzerland

- 37 Enrico Fermi Institute, University of Chicago, Chicago, IL, USA
- 38 LPC, Université Clermont Auvergne, CNRS/IN2P3, Clermont-Ferrand, France
- 39 Nevis Laboratory, Columbia University, Irvington, NY, USA
- 40 Niels Bohr Institute, University of Copenhagen, Copenhagen, Denmark
- 41 (a)Dipartimento di Fisica, Università della Calabria, Rende, Italy; (b)INFN Gruppo Collegato di Cosenza, Laboratori Nazionali di Frascati, Frascati, Italy
- 42 Physics Department, Southern Methodist University, Dallas, TX, USA
- 43 Physics Department, University of Texas at Dallas, Richardson, TX, USA
- 44 National Centre for Scientific Research “Demokritos”, Agia Paraskevi, Greece
- 45 (a)Department of Physics, Stockholm University, Stockholm, Sweden; (b)Oskar Klein Centre, Stockholm, Sweden
- 46 Deutsches Elektronen-Synchrotron DESY, Hamburg and Zeuthen, Germany
- 47 Lehrstuhl für Experimentelle Physik IV, Technische Universität Dortmund, Dortmund, Germany
- 48 Institut für Kern- und Teilchenphysik, Technische Universität Dresden, Dresden, Germany
- 49 Department of Physics, Duke University, Durham, NC, USA
- 50 SUPA-School of Physics and Astronomy, University of Edinburgh, Edinburgh, UK
- 51 INFN e Laboratori Nazionali di Frascati, Frascati, Italy
- 52 Physikalisches Institut, Albert-Ludwigs-Universität Freiburg, Freiburg, Germany
- 53 II. Physikalisches Institut, Georg-August-Universität Göttingen, Göttingen, Germany
- 54 Département de Physique Nucléaire et Corpusculaire, Université de Genève, Genève, Switzerland
- 55 (a)Dipartimento di Fisica, Università di Genova, Genoa, Italy; (b)INFN Sezione di Genova, Genoa, Italy
- 56 II. Physikalisches Institut, Justus-Liebig-Universität Giessen, Giessen, Germany
- 57 SUPA-School of Physics and Astronomy, University of Glasgow, Glasgow, UK
- 58 LPSC, Université Grenoble Alpes, CNRS/IN2P3, Grenoble INP, Grenoble, France
- 59 Laboratory for Particle Physics and Cosmology, Harvard University, Cambridge, MA, USA
- 60 (a)Department of Modern Physics and State Key Laboratory of Particle Detection and Electronics, University of Science and Technology of China, Hefei, China; (b)Institute of Frontier and Interdisciplinary Science and Key Laboratory of Particle Physics and Particle Irradiation (MOE), Shandong University, Qingdao, China; (c)School of Physics and Astronomy, Shanghai Jiao Tong University, KLPPAC-MoE, SKLPPC, Shanghai, China; (d)Tsung-Dao Lee Institute, Shanghai, China
- 61 (a)Kirchhoff-Institut für Physik, Ruprecht-Karls-Universität Heidelberg, Heidelberg, Germany; (b)Physikalisches Institut, Ruprecht-Karls-Universität Heidelberg, Heidelberg, Germany
- 62 Faculty of Applied Information Science, Hiroshima Institute of Technology, Hiroshima, Japan
- 63 (a)Department of Physics, Chinese University of Hong Kong, Shatin, N.T., Hong Kong; (b)Department of Physics, University of Hong Kong, Pok Fu Lam, Hong Kong; (c)Department of Physics and Institute for Advanced Study, Hong Kong University of Science and Technology, Clear Water Bay, Kowloon, Hong Kong, China
- 64 Department of Physics, National Tsing Hua University, Hsinchu, Taiwan
- 65 IJCLab, Université Paris-Saclay, CNRS/IN2P3, 91405 Orsay, France
- 66 Department of Physics, Indiana University, Bloomington, IN, USA
- 67 (a)INFN Gruppo Collegato di Udine, Sezione di Trieste, Udine, Italy; (b)ICTP, Trieste, Italy; (c)Dipartimento Politecnico di Ingegneria e Architettura, Università di Udine, Udine, Italy
- 68 (a)INFN Sezione di Lecce, Lecce, Italy; (b)Dipartimento di Matematica e Fisica, Università del Salento, Lecce, Italy
- 69 (a)INFN Sezione di Milano, Milan, Italy; (b)Dipartimento di Fisica, Università di Milano, Milan, Italy
- 70 (a)INFN Sezione di Napoli, Naples, Italy; (b)Dipartimento di Fisica, Università di Napoli, Naples, Italy
- 71 (a)INFN Sezione di Pavia, Pavia, Italy; (b)Dipartimento di Fisica, Università di Pavia, Pavia, Italy
- 72 (a)INFN Sezione di Pisa, Pisa, Italy; (b)Dipartimento di Fisica E. Fermi, Università di Pisa, Pisa, Italy
- 73 (a)INFN Sezione di Roma, Rome, Italy; (b)Dipartimento di Fisica, Sapienza Università di Roma, Rome, Italy
- 74 (a)INFN Sezione di Roma Tor Vergata, Rome, Italy; (b)Dipartimento di Fisica, Università di Roma Tor Vergata, Rome, Italy
- 75 (a)INFN Sezione di Roma Tre, Rome, Italy; (b)Dipartimento di Matematica e Fisica, Università Roma Tre, Rome, Italy
- 76 (a)INFN-TIFPA, Povo, Italy; (b)Università degli Studi di Trento, Trento, Italy
- 77 Institut für Astro- und Teilchenphysik, Leopold-Franzens-Universität, Innsbruck, Austria
- 78 University of Iowa, Iowa City, IA, USA
- 79 Department of Physics and Astronomy, Iowa State University, Ames, IA, USA

- 80 Joint Institute for Nuclear Research, Dubna, Russia
- 81 (a) Departamento de Engenharia Elétrica, Universidade Federal de Juiz de Fora (UFJF), Juiz de Fora, Brazil; (b) Universidade Federal do Rio De Janeiro COPPE/EE/IF, Rio de Janeiro, Brazil; (c) Universidade Federal de São João del Rei (UFSJ), São João del Rei, Brazil; (d) Instituto de Física, Universidade de São Paulo, São Paulo, Brazil
- 82 KEK, High Energy Accelerator Research Organization, Tsukuba, Japan
- 83 Graduate School of Science, Kobe University, Kobe, Japan
- 84 (a) AGH University of Science and Technology, Faculty of Physics and Applied Computer Science, Kraków, Poland; (b) Marian Smoluchowski Institute of Physics, Jagiellonian University, Kraków, Poland
- 85 Institute of Nuclear Physics Polish Academy of Sciences, Kraków, Poland
- 86 Faculty of Science, Kyoto University, Kyoto, Japan
- 87 Kyoto University of Education, Kyoto, Japan
- 88 Research Center for Advanced Particle Physics and Department of Physics, Kyushu University, Fukuoka, Japan
- 89 Instituto de Física La Plata, Universidad Nacional de La Plata and CONICET, La Plata, Argentina
- 90 Physics Department, Lancaster University, Lancaster, UK
- 91 Oliver Lodge Laboratory, University of Liverpool, Liverpool, UK
- 92 Department of Experimental Particle Physics, Jožef Stefan Institute and Department of Physics, University of Ljubljana, Ljubljana, Slovenia
- 93 School of Physics and Astronomy, Queen Mary University of London, London, UK
- 94 Department of Physics, Royal Holloway University of London, Egham, UK
- 95 Department of Physics and Astronomy, University College London, London, UK
- 96 Louisiana Tech University, Ruston, LA, USA
- 97 Fysiska institutionen, Lunds universitet, Lund, Sweden
- 98 Centre de Calcul de l'Institut National de Physique Nucléaire et de Physique des Particules (IN2P3), Villeurbanne, France
- 99 Departamento de Física Teórica C-15 and CIAFF, Universidad Autónoma de Madrid, Madrid, Spain
- 100 Institut für Physik, Universität Mainz, Mainz, Germany
- 101 School of Physics and Astronomy, University of Manchester, Manchester, UK
- 102 CPPM, Aix-Marseille Université, CNRS/IN2P3, Marseille, France
- 103 Department of Physics, University of Massachusetts, Amherst, MA, USA
- 104 Department of Physics, McGill University, Montreal, QC, Canada
- 105 School of Physics, University of Melbourne, Victoria, Australia
- 106 Department of Physics, University of Michigan, Ann Arbor, MI, USA
- 107 Department of Physics and Astronomy, Michigan State University, East Lansing, MI, USA
- 108 B.I. Stepanov Institute of Physics, National Academy of Sciences of Belarus, Minsk, Belarus
- 109 Research Institute for Nuclear Problems of Byelorussian State University, Minsk, Belarus
- 110 Group of Particle Physics, University of Montreal, Montreal, QC, Canada
- 111 P.N. Lebedev Physical Institute of the Russian Academy of Sciences, Moscow, Russia
- 112 National Research Nuclear University MEPhI, Moscow, Russia
- 113 D.V. Skobel'syn Institute of Nuclear Physics, M.V. Lomonosov Moscow State University, Moscow, Russia
- 114 Fakultät für Physik, Ludwig-Maximilians-Universität München, Munich, Germany
- 115 Max-Planck-Institut für Physik (Werner-Heisenberg-Institut), Munich, Germany
- 116 Nagasaki Institute of Applied Science, Nagasaki, Japan
- 117 Graduate School of Science and Kobayashi-Maskawa Institute, Nagoya University, Nagoya, Japan
- 118 Department of Physics and Astronomy, University of New Mexico, Albuquerque, NM, USA
- 119 Institute for Mathematics, Astrophysics and Particle Physics, Radboud University Nijmegen/Nikhef, Nijmegen, The Netherlands
- 120 Nikhef National Institute for Subatomic Physics and University of Amsterdam, Amsterdam, The Netherlands
- 121 Department of Physics, Northern Illinois University, DeKalb, IL, USA
- 122 (a) Budker Institute of Nuclear Physics and NSU, SB RAS, Novosibirsk, Russia; (b) Novosibirsk State University Novosibirsk, Novosibirsk, Russia
- 123 Institute for High Energy Physics of the National Research Centre Kurchatov Institute, Protvino, Russia
- 124 Institute for Theoretical and Experimental Physics named by A.I. Alikhanov of National Research Centre "Kurchatov Institute", Moscow, Russia

- 125 Department of Physics, New York University, New York, NY, USA
126 Ochanomizu University, Otsuka, Bunkyo-ku, Tokyo, Japan
127 Ohio State University, Columbus, OH, USA
128 Homer L. Dodge Department of Physics and Astronomy, University of Oklahoma, Norman, OK, USA
129 Department of Physics, Oklahoma State University, Stillwater, OK, USA
130 Palacký University, RCPTM, Joint Laboratory of Optics, Olomouc, Czech Republic
131 Institute for Fundamental Science, University of Oregon, Eugene, OR, USA
132 Graduate School of Science, Osaka University, Osaka, Japan
133 Department of Physics, University of Oslo, Oslo, Norway
134 Department of Physics, Oxford University, Oxford, UK
135 LPNHE, Sorbonne Université, Université de Paris, CNRS/IN2P3, Paris, France
136 Department of Physics, University of Pennsylvania, Philadelphia, PA, USA
137 Konstantinov Nuclear Physics Institute of National Research Centre “Kurchatov Institute”, PNPI, St. Petersburg, Russia
138 Department of Physics and Astronomy, University of Pittsburgh, Pittsburgh, PA, USA
139 (a) Laboratório de Instrumentação e Física Experimental de Partículas - LIP, Lisbon, Portugal; (b) Departamento de Física, Faculdade de Ciências, Universidade de Lisboa, Lisbon, Portugal; (c) Departamento de Física, Universidade de Coimbra, Coimbra, Portugal; (d) Centro de Física Nuclear da Universidade de Lisboa, Lisbon, Portugal; (e) Departamento de Física, Universidade do Minho, Braga, Portugal; (f) Departamento de Física Teórica y del Cosmos, Universidad de Granada, Granada, Spain; (g) Dep Física and CEFITEC of Faculdade de Ciências e Tecnologia, Universidade Nova de Lisboa, Caparica, Portugal; (h) Instituto Superior Técnico, Universidade de Lisboa, Lisbon, Portugal
140 Institute of Physics of the Czech Academy of Sciences, Prague, Czech Republic
141 Czech Technical University in Prague, Prague, Czech Republic
142 Charles University, Faculty of Mathematics and Physics, Prague, Czech Republic
143 Particle Physics Department, Rutherford Appleton Laboratory, Didcot, UK
144 IRFU, CEA, Université Paris-Saclay, Gif-sur-Yvette, France
145 Santa Cruz Institute for Particle Physics, University of California Santa Cruz, Santa Cruz, CA, USA
146 (a) Departamento de Física, Pontificia Universidad Católica de Chile, Santiago, Chile; (b) Department of Physics, Universidad Andres Bello, Santiago, Chile; (c) Instituto de Alta Investigación, Universidad de Tarapacá, Arica, Chile; (d) Departamento de Física, Universidad Técnica Federico Santa María, Valparaiso, Chile
147 Department of Physics, University of Washington, Seattle, WA, USA
148 Department of Physics and Astronomy, University of Sheffield, Sheffield, UK
149 Department of Physics, Shinshu University, Nagano, Japan
150 Department Physik, Universität Siegen, Siegen, Germany
151 Department of Physics, Simon Fraser University, Burnaby, BC, Canada
152 SLAC National Accelerator Laboratory, Stanford, CA, USA
153 Physics Department, Royal Institute of Technology, Stockholm, Sweden
154 Departments of Physics and Astronomy, Stony Brook University, Stony Brook, NY, USA
155 Department of Physics and Astronomy, University of Sussex, Brighton, UK
156 School of Physics, University of Sydney, Sydney, Australia
157 Institute of Physics, Academia Sinica, Taipei, Taiwan
158 (a) E. Andronikashvili Institute of Physics, Iv. Javakhishvili Tbilisi State University, Tbilisi, Georgia; (b) High Energy Physics Institute, Tbilisi State University, Tbilisi, Georgia
159 Department of Physics, Technion, Israel Institute of Technology, Haifa, Israel

- 160 Raymond and Beverly Sackler School of Physics and Astronomy, Tel Aviv University, Tel Aviv, Israel
 161 Department of Physics, Aristotle University of Thessaloniki, Thessaloniki, Greece
 162 International Center for Elementary Particle Physics and Department of Physics, University of Tokyo, Tokyo, Japan
 163 Graduate School of Science and Technology, Tokyo Metropolitan University, Tokyo, Japan
 164 Department of Physics, Tokyo Institute of Technology, Tokyo, Japan
 165 Tomsk State University, Tomsk, Russia
 166 Department of Physics, University of Toronto, Toronto, ON, Canada
 167 ^(a)TRIUMF, Vancouver, BC, Canada; ^(b)Department of Physics and Astronomy, York University, Toronto, ON, Canada
 168 Division of Physics and Tomonaga Center for the History of the Universe, Faculty of Pure and Applied Sciences, University of Tsukuba, Tsukuba, Japan
 169 Department of Physics and Astronomy, Tufts University, Medford, MA, USA
 170 Department of Physics and Astronomy, University of California Irvine, Irvine, CA, USA
 171 Department of Physics and Astronomy, University of Uppsala, Uppsala, Sweden
 172 Department of Physics, University of Illinois, Urbana, IL, USA
 173 Instituto de Física Corpuscular (IFIC), Centro Mixto Universidad de Valencia-CSIC, Valencia, Spain
 174 Department of Physics, University of British Columbia, Vancouver, BC, Canada
 175 Department of Physics and Astronomy, University of Victoria, Victoria, BC, Canada
 176 Fakultät für Physik und Astronomie, Julius-Maximilians-Universität Würzburg, Würzburg, Germany
 177 Department of Physics, University of Warwick, Coventry, UK
 178 Waseda University, Tokyo, Japan
 179 Department of Particle Physics and Astrophysics, Weizmann Institute of Science, Rehovot, Israel
 180 Department of Physics, University of Wisconsin, Madison, WI, USA
 181 Fakultät für Mathematik und Naturwissenschaften, Fachgruppe Physik, Bergische Universität Wuppertal, Wuppertal, Germany
 182 Department of Physics, Yale University, New Haven, CT, USA
- ^a Also at Borough of Manhattan Community College, City University of New York, New York NY, USA
^b Also at Centro Studi e Ricerche Enrico Fermi, Italy
^c Also at CERN, Geneva, Switzerland
^d Also at CPPM, Aix-Marseille Université, CNRS/IN2P3, Marseille, France
^e Also at Département de Physique Nucléaire et Corpusculaire, Université de Genève, Geneva, Switzerland
^f Also at Departament de Física de la Universitat Autònoma de Barcelona, Barcelona, Spain
^g Also at Department of Financial and Management Engineering, University of the Aegean, Chios, Greece
^h Also at Department of Physics and Astronomy, Michigan State University, East Lansing MI, USA
ⁱ Also at Department of Physics and Astronomy, University of Louisville, Louisville, KY, USA
^j Also at Department of Physics, Ben Gurion University of the Negev, Beer Sheva, Israel
^k Also at Department of Physics, California State University, East Bay, USA
^l Also at Department of Physics, California State University, Fresno, USA
^m Also at Department of Physics, California State University, Sacramento, USA
ⁿ Also at Department of Physics, King's College London, London, UK
^o Also at Department of Physics, St. Petersburg State Polytechnical University, St. Petersburg, Russia
^p Also at Department of Physics, University of Fribourg, Fribourg, Switzerland
^q Also at Dipartimento di Matematica, Informatica e Fisica, Università di Udine, Udine, Italy
^r Also at Faculty of Physics, M.V. Lomonosov Moscow State University, Moscow, Russia
^s Also at Giresun University, Faculty of Engineering, Giresun, Turkey
^t Also at Graduate School of Science, Osaka University, Osaka, Japan
^u Also at Hellenic Open University, Patras, Greece
^v Also at IJCLab, Université Paris-Saclay, CNRS/IN2P3, 91405, Orsay, France
^w Also at Institutio Catalana de Recerca i Estudis Avancats, ICREA, Barcelona, Spain
^x Also at Institut für Experimentalphysik, Universität Hamburg, Hamburg, Germany
^y Also at Institute for Mathematics, Astrophysics and Particle Physics, Radboud University Nijmegen/Nikhef, Nijmegen, The Netherlands

- ^z Also at Institute for Nuclear Research and Nuclear Energy (INRNE) of the Bulgarian Academy of Sciences, Sofia, Bulgaria
- ^{aa} Also at Institute for Particle and Nuclear Physics, Wigner Research Centre for Physics, Budapest, Hungary
- ^{ab} Also at Institute of Particle Physics (IPP), Canada
- ^{ac} Also at Institute of Physics, Azerbaijan Academy of Sciences, Baku, Azerbaijan
- ^{ad} Also at Instituto de Fisica Teorica, IFT-UAM/CSIC, Madrid, Spain
- ^{ae} Also at Joint Institute for Nuclear Research, Dubna, Russia
- ^{af} Also at Louisiana Tech University, Ruston LA, USA
- ^{ag} Also at Moscow Institute of Physics and Technology State University, Dolgoprudny, Russia
- ^{ah} Also at National Research Nuclear University MEPhI, Moscow, Russia
- ^{ai} Also at Physics Department, An-Najah National University, Nablus, Palestine
- ^{aj} Also at Physikalisches Institut, Albert-Ludwigs-Universität Freiburg, Freiburg, Germany
- ^{ak} Also at The City College of New York, New York NY, USA
- ^{al} Also at TRIUMF, Vancouver BC, Canada
- ^{am} Also at Universita di Napoli Parthenope, Naples, Italy
- ^{an} Also at University of Chinese Academy of Sciences (UCAS), Beijing, China
- * Deceased

Minerva Access is the Institutional Repository of The University of Melbourne

Author/s:

Aad, G; Abbott, B; Abbott, DC; Abud, A; Abeling, K; Abhayasinghe, DK; Abidi, SH; AbouZeid, OS; Abraham, NL; Abramowicz, H; Abreu, H; Abulaiti, Y; Acharya, BS; Achkar, B; Adachi, S; Adam, L; Bourdarios, AC; Adamczyk, L; Adamek, L; Adelman, J; Adersberger, M; Adiguzel, A; Adorni, S; Adye, T; Affolder, AA; Afik, Y; Agapopoulou, C; Agaras, MN; Aggarwal, A; Agheorghiesei, C; Aguilar-Saavedra, JA; Ahmadov, F; Ahmed, WS; Ai, X; Aielli, G; Akatsuka, S; Akesson, TPA; Akilli, E; Akimov, AV; Al Khoury, K; Alberghi, GL; Albert, J; Alconada Verzini, MJ; Alderweireldt, S; Aleksa, M; Aleksandrov, IN; Alexa, C; Alexandre, D; Alexopoulos, T; Alfonsi, A; Alfonsi, F; Alhroob, M; Ali, B; Alimonti, G; Alison, J; Alkire, SP; Allaire, C; Allbrooke, BMM; Allen, BW; Allport, PP; Aloisio, A; Alonso, A; Alonso, F; Alpigiani, C; Alshehri, AA; Alvarez Estevez, M; Alvarez Piqueras, D; Alviggi, MG; Amaral Coutinho, Y; Ambler, A; Ambroz, L; Amelung, C; Amidei, D; Amor Dos Santos, SP; Amoroso, S; Amrouche, CS; An, F; Anastopoulos, C; Andari, N; Andeen, T; Anders, CF; Anders, JK; Andrezza, A; Andrei, V; Anelli, CR; Angelidakis, S; Angerami, A; Anisenkov, AV; Annovi, A; Antel, C; Anthony, MT; Antonelli, M; Antrim, DJA; Anulli, F; Aoki, M; Aparisi Pozo, JA; Aperio Bella, L; Arabidze, G; Araque, JP; Araujo Ferraz, V; Araujo Pereira, R; Arcangeletti, C; Arce, ATH; Arduh, FA; Arguin, J-F; Argyropoulos, S; Arling, J-H; Armbruster, AJ; Armstrong, A; Arnaez, O; Arnold, H; Arrubarrena Tame, ZP; Artamonov, A; Artoni, G; Artz, S; Asai, S; Asbah, N; Asimakopoulou, EM; Asquith, L; Assahsah, J; Assamagan, K; Astalos, R; Atkin, RJ; Atkinson, M; Atlay, NB; Atmani, H; Augsten, K; Avolio, G; Avramidou, R; Ayoub, MK; Azoulay, AM; Azuelos, G; Bachacou, H; Bachas, K; Backes, M; Backman, F; Bagnaia, P; Bahmani, M; Bahrasemani, H; Bailey, AJ; Bailey, VR; Baines, JT; Bajic, M; Bakalis, C; Baker, OK; Bakker, PJ; Bakshi Gupta, D; Balaji, S; Baldin, EM; Balek, P; Balli, F; Balunas, WK; Balz, J; Banas, E; Bandyopadhyay, A; Banerjee, S; Bannoura, AAE; Barak, L; Barbe, WM; Barberio, EL; Barberis, D; Barbero, M; Barbour, G; Barillari, T; Barisits, M-S; Barkeloo, J; Barklow, T; Barnea, R; Barnes, SL; Barnett, BM; Barnett, RM; Barnovska-Blenessy, Z; Baroncelli, A; Barone, G; Barr, AJ; Navarro, BL; Barreiro, F; da Costa, JBG; Barsov, S; Bartoldus, R; Bartolini, G; Barton, AE; Bartos, P; Basalae, A; Bassalat, A; Basso, MJ; Bates, RL; Batlamous, S; Batley, JR; Batool, B; Battaglia, M; Bauce, M; Bauer, F; Bauer, KT; Bawa, HS; Beacham, JB; Beau, T; Beauchemin, PH; Becherer, F; Bechtle, P; Beck, HC; Beck, HP; Becker, K; Becker, M; Becot, C; Beddall, A; Beddall, AJ; Bednyakov, VA; Bedognetti, M; Bee, CP; Beerermann, TA; Begalli, M; Begel, M; Behera, A; Behr, JK; Beisiegel, F; Bell, AS; Bella,